Funktionsmorphologische Untersuchungen abdominaler Infrarot-Rezeptoren von Insekten

Dissertation

zur

Erlangung des Doktorgrades (Dr. rer. nat.)

der

Mathematisch-Naturwissenschaftlichen Fakultät

der

Rheinischen Friedrich-Wilhelms-Universität Bonn

vorgelegt von

Erik Sebastian Schneider

aus

Köln

Bonn, Juni 2014

Angefertigt mit Genehmigung der Mathematisch-Naturwissenschaftlichen Fakultät der Rheinischen Friedrich-Wilhelms-Universität Bonn

1. Gutachter: PD Dr. Helmut Schmitz
Institut für Zoologie
Universität Bonn

2. Gutachter: Prof. Dr. Horst Bleckmann
Institut für Zoologie
Universität Bonn

Tag der Promotion: 03.12.2014
Erscheinungsjahr: 2014

Zusammenfassung

Infrarot (IR) -Rezeptoren sind innerhalb der Insekten offensichtlich mehrfach unabhängig voneinander entstanden. Bei den Vertretern der Gattung *Melanophila*, einigen Rindenwanzen der Gattung *Aradus* und bei dem australischen Käfer *Acanthocnemus nigricans* sind diese aus unterschiedlichen Vorläuferstrukturen in verschiedenen Bereichen des Thorax entstanden. Abdominale IR-Rezeptoren hingegen sind bisher nur beim australischen Feuerkäfer *Merimna atrata* und der Wanze *Leptoglossus occidentalis* beschrieben worden und sind Gegenstand der vorliegenden Arbeit.

Der australische Feuerkäfer *Merimna atrata* (Buprestidae, Coleoptera) zeigt ein ausgeprägtes pyrophiles („Feuer liebendes“) Verhalten. Käfer dieser Spezies suchen gezielt frische Brandflächen auf, die durch offenes Feuer, heiße Asche und Rauch gekennzeichnet sind. Grund für dieses ungewöhnliche Verhalten ist die Abhängigkeit ihres Reproduktionszyklus von Waldbränden. Die IR-Organe von *Merimna atrata* befinden sich paarig angeordnet auf den abdominalen Sterniten. Sie bestehen aus einem spezialisierten Cuticula-Bereich, der rundlichen absorbierenden Fläche, und einem sensorischen Komplex, der diesen Bereich innerviert. Der sensorische Komplex beinhaltet ein thermosensitives, multipolares Neuron mit einer spezialisierten dendritischen Region, der sog. terminalen dendritischen Masse (TDM). In direkter Nähe zu diesem multipolaren Neuron befinden sich zusätzlich mechanorezeptive Strukturen (Skolopidien), deren genaue Morphologie und Funktion im IR-Organ jedoch zu Beginn der Arbeit weitgehend unbekannt waren.

Leptoglossus occidentalis (Coreidae, Hemiptera) ist die einzige Insektenspezies ohne pyrophile Lebensweise, für die ebenfalls extra-antennale IR-Rezeptoren beschrieben wurden. Es handelt sich um eine, ursprünglich in Nordamerika beheimatete, mittlerweile kosmopolitisch verbreitete Spezies, die sich phytophag von sich entwickelnden Samen verschiedener Koniferen ernährt. Basierend auf Verhaltensexperimenten und elektrophysiologischen Untersuchungen wurde beschrieben, dass *L. occidentalis* ebenfalls über abdominale IR-Rezeptoren verfügt. Der IR-Sinn soll dazu dienen, die Samen tragenden Zapfen aufzuspüren. Morphologische Daten über die dafür notwendigen Rezeptorstrukturen fehlten bisher jedoch.

Im Rahmen der vorliegenden Arbeit sollten auch die vermeintlichen IR-rezeptiven Strukturen von *L. occidentalis* morphologisch charakterisiert werden. Die gewonnenen Ergebnisse widerlegen aufgrund mangelnder Innervation eine mögliche Funktion der in der Literatur beschriebenen abdominalen Strukturen als IR-Rezeptoren. Es konnten jedoch unterschied-

liche Typen epidermaler Drüsenzellen in hoher Zahl identifiziert werden, die eine sekretorische Funktion der besagten Bereiche nahelegen.

Das Vorkommen von IR-Rezeptoren bei Insekten ist somit nach aktuellem Kenntnisstand beschränkt auf Spezies mit pyrophiler Lebensweise. Abdominale IR-Rezeptoren existieren bisher nur bei *Merimna atrata*.

Im Vordergrund der Arbeiten lag die funktionsmorphologische Charakterisierung der im IR-Organ von *Merimna* identifizierten Skolopidien im Hinblick auf eine mögliche Beteiligung bei der IR-Rezeption. Die gewonnenen Ergebnisse belegen eine zusätzliche Innervation des IR-Organs durch ein einzelnes Chordotonalorgan. Dieses befindet sich in direkter Nachbarschaft zu dem bereits beschriebenen thermosensitiven multipolaren Neuron. Das Chordotonalorgan besteht aus zwei einzelnen nebeneinander liegenden mononematischen, monodynalen Skolopidien. Ihre Dendriten erstrecken sich in anteriorer Richtung und sind über Kappenzellen unterhalb der Cuticula im Zentrum der absorbierenden Fläche befestigt. Die relative Position und Lagebeziehung der sensorischen Komponenten im Verhältnis zur absorbierenden Fläche konnte über die Kombination neuroanatomischer Färbetechniken und dreidimensionale Rekonstruktion eindeutig bestimmt werden. Vergleichende Untersuchungen an abdominaler Cuticula offenbarten weitere strukturelle Spezialisierungen der absorbierenden Fläche, insbesondere im Bereich des sensorischen Komplexes und der Anheftungsstellen der Skolopidien. So ist die Dicke der Cuticula im Zentrum der absorbierenden Fläche im Vergleich zu gewöhnlicher abdominaler Cuticula um durchschnittlich 47% reduziert. Auch der relative Anteil der unterschiedlichen Cuticula-Schichten sowie ihre Materialeigenschaften (Elastizitätsmodul und Härte) weisen signifikante Unterschiede auf.

Basierend auf den gewonnen Daten zur dreidimensionalen Morphologie der absorbierenden Fläche und ihrer Materialeigenschaften wurden mit Hilfe von Finite Element Simulationen ihre thermomechanischen Eigenschaften analysiert. Die Ergebnisse weisen darauf hin, dass bei Erwärmung deutliche thermische Deformationen der absorbierenden Fläche auftreten. Eine potentielle Funktion der Skolopidien als thermo-, bzw. photomechanische IR-Rezeptoren ist daher denkbar. Des Weiteren deuten die Ergebnisse darauf hin, dass die Skolopidien als potentielle IR-Rezeptoren möglicherweise keine höhere Sensitivität aufweisen als das multipolare Neuron. Eine potentielle Funktion der zusätzlichen Innervation des IR-Organs durch ein Chordotonalorgan ist somit eher in der Erweiterung des generellen Funktionsumfangs, z.B. durch die Vergrößerung des Dynamikbereichs, einer Verringerung der Ansprechzeiten, einer höheren Ausfallsicherheit oder verbesserten Filtereigenschaften zu erwarten.

Abstract

In insects, infrared (IR) -receptors have evolved several times independently. IR-receptors can be found in buprestid beetles of the genus *Melanophila*, in several flat bug species belonging to the genus *Aradus*, and in the Australian beetle *Acanthocnemus nigricans* on different regions of the thoracic segments, respectively. Abdominal IR-receptors, so far have been described only in the Australian 'fire-beetle', *Merimna atrata*, and in the western conifer seed bug, *Leptoglossus occidentalis*. The abdominal IR-receptors in the two mentioned species are the subject of the present thesis.

As the name already indicates, the 'fire-beetle' *Merimna atrata* (Buprestidae, Coleoptera) shows a pronounced pyrophilous ("fire-loving") behavior. Beetles of this species approach freshly burnt areas that are characterized by open flames, hot ash and smoke. A reason for this unusual behavior is the dependency of the reproductive cycle of *Merimna atrata* on the occurrence of forest fires.

IR-organs are located in pairs on the abdominal sternites. They consist of a specialized cuticular portion, the roundish absorbing area, and a sensory complex innervating this area. The sensory complex comprises a thermosensitive, multipolar neuron with a specialized dendritic region, the so-called terminal dendritic mass (TDM). In direct vicinity to the multipolar neuron additional mechanoreceptive units (scolopidia) have been identified, but their specific morphology and function within the IR-organ, so far were unknown.

Leptoglossus occidentalis (Coreidae, Hemiptera) is the only non-pyrophilous insect species, for which extra-antennal IR-receptors have been described. Originally native to North-America, *L. occidentalis* became a cosmopolitan in the recent years. The species feeds on developing seeds of different conifers. Based on behavioral and electrophysiological experiments it has been proposed that *L. occidentalis* is equipped with abdominal IR-receptors used for the localization of cones. Morphological data on the underlying IR-receptors, however, are missing. In the present thesis an attempt was made to characterize the putative IR-receptors of *L. occidentalis* morphologically. Due to missing innervation the results clearly disprove the existence of abdominal IR-receptors in *L. occidentalis*. Instead, the identification of different types of epidermal glandular cells, occurring in high numbers, indicates a secretory function of the proposed regions. According to these results, the existence of IR-receptors in insects is still restricted to pyrophilous beetles. Abdominal IR-receptors can be found, so far, only in *Merimna atrata*.

Investigations on the IR-organ of *Merimna atrata* confirmed a bimodal innervation by an additional mechanosensory unit, represented by a single chordotonal organ situated in close proximity to the thermosensitive multipolar neuron. The chordotonal organ houses two single mononematic, monodynal scolopidia. They are located approximately in the center of the absorbing area. Their dendrites extend in anterior direction and are attached to the cuticle apically via a cap cell. The relative position and orientation of the sensory cells in relation to the absorbing area was determined by combining neuroanatomical staining techniques with three-dimensional reconstructions. Comparative studies on the abdominal cuticle revealed further structural specializations of the absorbing area, especially at the region of the sensory complex and the attachment sites of the scolopidia. Accordingly, cuticular thickness at the center of the absorbing area is reduced on average by 47% in comparison to normal abdominal cuticle. Furthermore, the relative proportion of the different cuticular layers and their respective material properties exhibit significant differences at both regions.

Based on these findings, the thermomechanical properties of the absorbing area were analyzed by using finite element simulations. The results indicate that a distinct thermal deformation of the absorbing area takes place in response to heating of the exterior cuticle. Therefore, a function of the scolopidia as putative thermo- or photomechanical IR-receptors seems possible. The findings further indicate that the scolopidia, if acting as IR-receptors, probably do not exhibit higher sensitivities as the multipolar neuron. Other probable benefits provided by the additional mechanoreceptive innervation of the IR-organ could include e.g. faster response times, a larger dynamic range, higher reliability or improved filter properties. In summary, this could increase the overall performance of the whole IR-organ.

Inhaltsverzeichnis

Kapitel 4

Kapitel 5

Kapitel 1

Einleitung

1.1 Infrarotstrahlung

Als Infrarot (IR) -strahlung wird elektromagnetische Strahlung mit einer Wellenlänge zwischen 780 nm und 1 mm bezeichnet. Im Gesamtspektrum elektromagnetischer Strahlung liegt sie damit zwischen dem kürzerwelligen, für uns Menschen sichtbaren Licht, und der längerwelligen Mikrowellenstrahlung. Das Spektrum der IR-Strahlung wird oft weiterhin unterteilt in nahes (NIR), mittleres (MIR), fernes (FIR) und ultrafernes IR (UFIR). Diese Einteilung ergibt sich aus der Transmission unserer Atmosphäre. Aufgrund der Absorptionseigenschaften der in unserer Luft befindlichen Moleküle, insbesondere der von Wasser und Kohlendioxid, ergeben sich bestimmte Wellenlängenbereiche, sog. atmosphärische Fenster, in denen IR-Strahlung erst über weitere Strecken übertragen werden kann (Budzier and Gerlach, 2010). Für das MIR befindet sich ein solches Fenster im Bereich zwischen 3 - 5 µm und für das FIR im Bereich zwischen 8 - 13 µm.

Jedes Objekt mit einer Temperatur über dem absoluten Nullpunkt (-273,15°C) emittiert elektromagnetische Strahlung über einen großen Wellenlängenbereich. Dieser Zusammenhang ist durch das Planck'sche Gesetz (Gleichung 1.1) gegeben. Es beschreibt die Intensitätsverteilung der elektromagnetischen Energie in Abhängigkeit von der Wellenlänge (λ) und der Oberflächentemperatur (T) eines Objektes. Das Gesetz gilt allerdings nur für einen perfekten Emitter, einen sog. schwarzen Strahler, der abhängig von seiner Temperatur maximal emittiert (Emissivität (ε) =1). Das Planck'sche Gesetz gibt an, welche Strahlungsleistung (M) ein Objekt mit gegebener Temperatur bei einer bestimmten Wellenlänge (λ) in den Halbraum abstrahlt (Budzier and Gerlach, 2010).

$$M_\lambda = \frac{2\pi hc^2}{\lambda^5} \cdot \frac{1}{e^{\frac{hc}{\lambda k_B T}} - 1} \; [W \cdot m^{-2} \cdot \mu m^{-1}] \qquad (1.1)$$

Dabei ist h das Planck'sche Wirkungsquantum (6,62606957 · 10^{-34} J·s), c die Lichtgeschwindigkeit (299792458 m·s^{-1}) und k_B die Boltzmann Konstante (1,3806488 · 10^{-23} J·K^{-1}).

Integration über den gesamten Spektralbereich ergibt den durch das Stefan-Boltzmann-Gesetz (Gleichung 1.2) beschriebenen Zusammenhang, wonach die emittierte Strahlungsleistung

eines schwarzen Strahlers (M_S) proportional zur vierten Potenz seiner Oberflächentemperatur (T) ist (Budzier and Gerlach, 2010).

$$M_S = \varepsilon \cdot \sigma \cdot T^4 \ [W \cdot m^{-2}] \qquad (1.2)$$

σ stellt hierbei die Stefan-Boltzmann Konstante (5,670373 · 10^{-8} $W \cdot m^{-2} \cdot K^{-4}$) dar. Die Strahlungsleistung nimmt näherungsweise mit der zweiten Potenz zur Entfernung des jeweiligen Strahlers ab. Berücksichtigt man diesen Zusammenhang, so kann das Stefan-Boltzmann-Gesetz entsprechend der Gleichung 3.6 (siehe Abschnitt 3.3.7) erweitert werden. Mit dieser Gleichung (3.6) lässt sich die in einer Entfernung r resultierende Strahlungsleistung eines Strahlers mit der Temperatur T und einer Fläche A_{rad} berechnen.
Innerhalb des Emissionsspektrums eines Objektes kann die Wellenlänge mit der höchsten Leistungsdichte (λ_{max}) für eine gegebene Temperatur (T) mit Hilfe des Wienschen Verschiebungsgesetzes (Gleichung 1.3) berechnet werden (Budzier and Gerlach, 2010).

$$\lambda_{max} = \frac{2{,}898 \cdot 10^{-3} \ [m \cdot K]}{T \ [K]} \qquad (1.3)$$

Die Absorption elektromagnetischer Strahlung im IR-Bereich ist im Allgemeinen abhängig von der Materialbeschaffenheit des Absorbers und dem Frequenzspektrum der einfallenden Strahlung. In Abhängigkeit von der Bandstruktur der Moleküle im Absorber werden verschiede Frequenzbereiche der elektromagnetischen Strahlung unterschiedlich stark absorbiert. Entspricht die Frequenz der einfallenden Strahlung der natürlichen Vibrationsfrequenz der Absorbermoleküle (Resonanzbedingung), werden Letztere durch kurzzeitige Erhöhung ihrer Vibrationsamplitude die Energie der Photonen absorbieren (Colthup et al., 1990). Daraus resultiert eine erhöhte Schwingungsenergie der Absorbermoleküle und somit auch eine höhere Wärmeenergie des gesamten Absorbers. Viele funktionelle Gruppen von organischen Verbindungen weisen charakteristische Schwingungen auf, denen Absorptionsbanden in definierten Bereichen des IR-Spektrums entsprechen (sog. „IR-Fingerprint“). Die stärksten Absorptionsbanden der meisten organischen Verbindungen, sowie die von Wasser, liegen alle im Wellenlängenbereich zwischen 2,7 µm und 14 µm (Hesse et al., 1995). Dieser Bereich deckt sich relativ genau mit den beiden oben erwähnten atmosphärischen Fenstern im MIR- und FIR-Bereich. Die Analyse unterschiedlichster Cuticula-Bereiche von *Melanophila acuminata*, darunter die äußeren Schichten der Augen,

Flügelvene, Hüftgelenkkapsel und Grubenorgan, ergab ähnliche IR-Spektren mit Absorptionsmaxima im Bereich zwischen 2,75 – 3,5 µm (Vondran et al., 1995; Sowards et al., 2001). IR-Strahlung mit dieser Wellenlänge wird nach dem Wienschen Verschiebungsgesetz maximal von Oberflächen mit Temperaturen zwischen 781°C – 555°C emittiert. Dies sind Temperaturen, wie sie vor allem bei Bränden auftreten. Sowohl der spezifische Absorptionsbereich unserer Atmosphäre als auch der der meisten organischen Moleküle stellen demnach Grundvoraussetzungen für die Evolution von biologischen IR-Rezeptoren dar.

1.2 Technische IR-Sensoren

Die Geschichte der technischen IR-Sensorik begann mit der Entdeckung der IR-Strahlung durch William Herschel im Jahre 1800 (Herschel, 1800). Nach mehr als 200 Jahren Forschung und Entwicklung existiert heute eine Vielzahl von IR-Sensoren mit unterschiedlichen Funktionsprinzipien und Anwendungsmöglichkeiten (Rogalski, 2012). Die Natur hat im Laufe der Evolution ebenfalls verschiedene IR-Sensoren hervorgebracht (siehe Abschnitt 1.3). Allerdings kann sie auf einen durch natürliche Selektion bestimmten Entwicklungszeitraum von meist vielen Jahrmillionen Jahren zurückblicken. Im konkreten Falle der Insekten kann aufgrund fossiler Funde sogar von ca. 400 Millionen Jahren ausgegangen werden (Engel and Grimaldi, 2004). Vergleicht man diesen Zeitraum mit der Entfernung zum Mond, so entspricht der Entwicklungszeitraum technischer IR-Sensoren mit nur 200 m noch nicht einmal dem Weg zum nächsten Kiosk. Durch diesen Vorsprung der Natur an Entwicklungsdauer und ständiger Selektion kann generell davon ausgegangen werden, dass biologische Organismen entsprechend der jeweiligen Anforderungen, die ihr Lebensraum an sie stellt, in höchstem Maße optimiert sind. Darüber hinaus ist es sogar möglich, dass die Natur Lösungsansätze hervorgebracht hat, deren Funktionsprinzipien in der Technik bisher unbekannt sind. Dieses Potential der Natur zu nutzen, um bestehende technische Systeme zu verbessern oder neuartige Produkte zu entwickeln, scheint daher ein vielversprechender Ansatz zu sein und ist gleichzeitig das Arbeitsgebiet der Wissenschaftsdisziplin Bionik.

Um jedoch das technische Potential eines biologischen Systems überhaupt einschätzen zu können, bedarf es der Kenntnis über den aktuellen Stand der Forschung und Entwicklung im entsprechenden Fachgebiet. Daher im Folgenden ein kurzer Abriss über technische IR-Sensoren und den aktuellen Stand der Forschung in diesem Bereich.

1.2.1 Quantendetektoren

IR-Sensoren können generell unterteilt werden in Quantendetektoren und thermische Detektoren. Quantendetektoren nutzen den photoelektrischen Effekt; d.h. die Erzeugung freier Ladungsträger durch einfallende elektromagnetische Strahlung zur Generierung eines Ausgangssignals. Sie basieren auf der Verwendung von Halbleitermaterialien mit möglichst schmalen Bandlücken. Damit ein Photon ein Signal generieren kann, muss es genügend Energie besitzen, damit die Elektronen des Halbleitermaterials die Bandlücke überwinden und vom Valenz- ins Halbleiterband wechseln können. Quantendetektoren weisen demnach eine starke Wellenlängenabhängigkeit auf. Vorteile gegenüber thermischen Detektoren liegen in der deutlich höheren Sensitivität und kürzeren Antwortzeiten. Für die beschriebenen Eigenschaften der Quantendetektoren ist jedoch eine extreme Kühlung unter Raumtemperatur notwendig (Rogalski, 2002, 2003). Aufgrund der damit einhergehenden Zunahme an Größe, Gewicht und Kosten sind sie nur für vergleichsweise wenige Spezialanwender, Militär, Grenzüberwachung, o.Ä. geeignet (Budzier and Gerlach, 2010).

1.2.2 Thermische IR-Detektoren

Thermische IR-Detektoren wandeln mit Hilfe eines Absorbers einfallende elektromagnetische Strahlungsenergie zunächst in Wärme um. Die resultierende Temperaturänderung des Absorbers führt dann wiederum zur Erzeugung eines elektrischen Signals. Die Temperaturänderung des Absorbers ist dabei direkt proportional zur Leistung der absorbierten Strahlung. Die Empfindlichkeit von thermischen IR-Sensoren ist prinzipiell wellenlängen-unabhängig (Rogalski, 2002, 2003, 2012). Praktisch resultiert jedoch durch die Absorptionseigenschaften von Linsen- und Absorbermaterialien trotzdem eine Wellen-längenabhängigkeit, die zu einer Begrenzung des spektralen Arbeitsbereichs führen (Budzier and Gerlach, 2010). Abhängig von der Art und Weise, wie die Temperatur des Absorbers in ein elektrisches Signal umgewandelt wird, kann man die in den folgenden Abschnitten vorgestellten Typen thermischer IR-Sensoren unterscheiden. Großer Vorteil der thermischen IR-Sensoren ist, dass sie generell ohne Kühlung betrieben werden können. Sie bieten sich daher speziell für kleine, leichte und portable Anwendungen, gerade auch im Bereich der IR-Thermografie, an.

1.2.2.1 Pyroelektrische Sensoren

Pyroelektrische Sensoren nutzen den sog. pyroelektrischen Effekt, d.h. die spontane Polarisation (Ladungstrennung) bestimmter dielektrischer Materialien, den Pyroelektrika (Rogalski, 2011). Pyroelektrika sind piezoelektrische Kristalle, die sowohl durch mechanische als auch durch thermische Effekte eine Änderung ihrer Feldstärke erfahren. Die resultierende Spannungsdifferenz an den gegenüberliegenden Kristalloberflächen wird mit Hilfe von Elektroden abgegriffen und gemessen. Da die am Kristall entstehenden Oberflächenladungen relativ schnell durch freie Elektronen aus der Umgebung neutralisiert werden, antworten pyroelektrische Sensoren nur auf relativ schnelle transiente Änderungen des Strahlungsflusses (Budzier and Gerlach, 2010). Pyroelektrische Sensoren finden daher häufig Anwendung als passive Bewegungsmelder. Für Anwendungen bei denen auch konstante oder sich langsam ändernde Strahlungsintensitäten auftreten (z.B. in der Thermographie), müssen die Sensoren gechoppert werden.

1.2.2.2 Thermoelektrische Sensoren

Thermoelektrische Sensoren werden technisch in Form von Thermoelementen (*engl.: thermocouple*) umgesetzt. Sie nutzen als Messprinzip den thermoelektrischen Effekt, auch Seebeck-Effekt genannt. Dieser beschreibt die Entstehung einer Spannung (Thermospannung) zwischen zwei Punkten eines elektrischen Leiters, wenn diese unterschiedliche Temperaturen aufweisen (Rogalski, 2011). Die Thermospannung entsteht dabei durch Thermodiffusion von Ladungsträgern, auch Thermodiffusionsstrom genannt. Die Thermospannung ist dabei direkt proportional zur Temperaturdifferenz der beiden Punkte (Budzier and Gerlach, 2010). Ein Thermoelement besteht aus zwei unterschiedlich elektrisch leitenden Materialien, die in einem Punkt miteinander verbunden werden. Dabei entstehen eine Kontakt- oder Messstelle und eine Vergleichsstelle, die unterschiedliche Temperaturen aufweisen müssen. Eine Kenntnis der Temperatur an der Vergleichsstelle ist für die Signalauswertung notwendig. Diese wird mit Hilfe eines integrierten Temperaturfühlers, meist ein Heißleiter- (NTC-) Widerstand, gemessen (Budzier and Gerlach, 2010). In der technischen Praxis werden meist mehrere Thermoelemente zu einer Thermosäule (*engl.: thermopile*) in Reihe geschaltet, was zu einer Erhöhung der Ausgangsspannung führt.

1.2.2.3 Mikrobolometer

Mikrobolometer sind IR-Sensoren, die als Absorber einen temperaturabhängigen Widerstand, meist aus amorphem Silizium oder Vanadiumoxid bestehend, besitzen. Absorbierte elektromagnetische Strahlung führt zu einer Temperatur- und damit verbundenen Widerstandsänderung des Bolometerwiderstandes (Budzier and Gerlach, 2010). Beim Betrieb des Sensors mit einer konstanten Arbeitsspannung führt die Widerstandsänderung zu einer Spannungsänderung, die als Ausgangssignal verwendet wird. Die Bolometerwiderstände bedürfen für ihre Funktion als IR-Sensoren einer ausreichenden thermischen Isolation. Hierfür werden sie meist in Form von Mikrobrücken gefertigt, die sich im Vakuum befinden. Mikrobolometer werden überwiegend als Arrays mit mittlerweile bis zu 2048 x 1536 Einzelbolometern (Pixeln) und Pixelabständen (von der Mitte des einen bis zur Mitte des nächsten Pixels) von unter 17µm (Rogalski, 2012) für bildgebende Verfahren (IR-Kameras) verwendet. Kommerziell erhältliche Mikrobolometerarrays können derzeit Temperaturunterschiede von 0,03 K auflösen und besitzen Antwortgeschwindigkeiten von 15 – 20 ms (Rogalski, 2012).

1.2.2.4 Golay-Zelle

Eine Golay-Zelle ist eine mit Gas gefüllte, thermisch isolierte, abgeschlossene Kammer. Im Zellinneren absorbierte elektromagnetische Strahlung führt zu einer Temperaturerhöhung und damit verbundenen thermischen Ausdehnung des sich in der Kammer befindlichen Gases. Die resultierende Druckerhöhung verursacht dann die Auslenkung einer deformierbaren Kammerwand oder Membran (Budzier and Gerlach, 2010; Rogalski, 2011). Die Stärke der Membranauslenkung wird dann meist optisch oder, im Falle von miniaturisierten Golay-Zellen, piezoresistiv oder kapazitiv ausgelesen. Bei Letzterem muss zumindest die äußere Oberfläche der deformierbaren Membran elektrisch leitend sein, da sie eine von zwei Kondensatorplatten darstellt. Innerhalb der thermischen IR-Sensoren weisen Golay-Zellen nach wie vor die höchsten Sensitivitäten auf. Sie sind jedoch vergleichsweise groß und reagieren empfindlich gegenüber mechanischen Störungen. Eine weitere technologische Herausforderung, die bis heute nicht in befriedigendem Maße gelungen ist, stellt die Entwicklung von miniaturisierten Mikro-Golay-Zellen dar.

1.2.2.5 Mikrotragarm-IR-Sensoren

Bimorphe oder Bimetalle sind Streifen aus zwei Schichten unterschiedlicher Materialien, meist Metalle. Diese weisen unterschiedliche thermische Ausdehnungskoeffizienten auf und dehnen sich daher infolge von Temperaturänderungen unterschiedlich stark aus. Dies bewirkt eine Verbiegung des gesamten Bimorphs oder Bimetalls. Man spricht hierbei auch vom sog. Bimetall-Effekt. In der IR-Sensorik wird dieser Effekt bei Mikrotragarm-Sensoren (*engl.: microcantilever detectors*) ausgenutzt. Bei diesen Sensoren führt die Absorption von elektromagnetischer Strahlung durch einen Absorber zu einer Temperaturerhöhung. Diese Temperaturerhöhung wiederum bewirkt eine Verbiegung von dünnen Bimaterialarmen, die den Absorber tragen (Budzier and Gerlach, 2010; Rogalski, 2011). Die Auslenkung des gesamten Sensorelements kann schließlich optisch, piezoresistiv oder kapazitiv gemessen werden. Mikrotragarm-Sensoren können Temperaturunterschiede von nur 0,005 K registrieren (Amantea et al., 1997). Ihre Antwortgeschwindigkeiten liegen bei 5 – 10 ms (Rogalski, 2011). Kommerziell erhältliche Mikrotragarm-Sensoren zur IR-Detektion sind jedoch nicht bekannt. Gründe hierfür sind unter anderem eine hohe Störanfälligkeit gegenüber diversen mechanischen Reizen wie z.B. Erschütterungen oder Beschleunigungskräften.

1.3 IR-Rezeptoren im Tierreich

1.3.1 Vertebraten

1.3.1.1 Schlangen

Innerhalb der Schlangen gibt es drei Gruppen, die IR-Rezeptoren in Form von Gruben- oder Lippenorganen besitzen. Hierzu gehören die Familien der Boidae, der Pythonidae und innerhalb der Viperidae die Unterfamilie der Crotalinae (Grubenottern). Grubenorgane (*engl.: pit organs*) findet man bei allen Vertretern der Grubenottern, bei den meisten Pythons und bei einigen Boas. Auch bei den Schlangen innerhalb der genannten Gruppen, die keine Grubenorgane besitzen, konnten spezialisierte IR-Rezeptoren identifiziert werden (Bullock and Barrett, 1968; De Cock Buning et al., 1981; De Cock Buning, 1983; Goris, 2011). Grubenottern besitzen ein einzelnes Paar hoch entwickelter Grubenorgane, die sich jeweils in der lorealen Region zwischen Auge und Nasenloch befinden (Lynn, 1931). Bei Pythons und Boas befinden sich die Grubenorgane, wenn vorhanden, im Bereich der rostralen und labialen (supralabiale und/ oder sublabiale) Schuppen. Bei Boas sind die Gruben stets als Einstülpungen zwischen zwei benachbarten Schuppen ausgebildet. Die IR-Rezeptoren

befinden sich hier jeweils im hinteren Bereich der vorderen Schuppe und im vorderen Bereich der hinteren Schuppe (Fig. 1.1 a, b) (Ebert, 2007). Bei Pythons hingegen sind die Grubenorgane immer als Einstülpungen innerhalb einer Schuppe ausgebildet (Fig. 1.1 c). Die IR-Rezeptoren befinden sich am Grund der Grube (*engl.: pit fundus*) (Noble and Schmidt, 1937; Warren and Proske, 1968; Ebert, 2007). Die am stärksten spezialisierte Grubenmorphologie besitzen jedoch die Grubenottern. Bei ihnen kann das Grubenorgan generell in drei Teile gegliedert werden: eine äußere und eine innere Kammer, die von einer sehr dünnen Membran (*engl.: pit membrane*) getrennt werden (Lynn, 1931; Bullock and Fox, 1957) (vgl. Fig. 1.1 d).

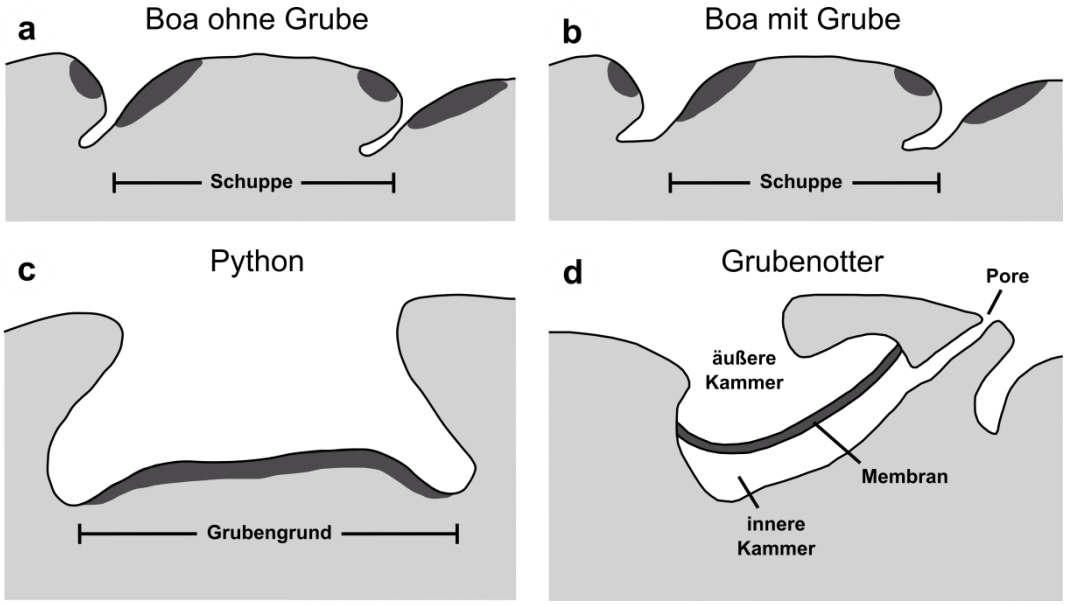

Fig. 1.1 IR-Organe bei Schlangen (Querschnitte, schematisch). Dunkelgraue Bereiche zeigen die Position der IR-Rezeptorendigungen an. Abbildung geändert nach Goris (2011). **a)** Boa ohne Grubenorgan. **b)** Boa mit Grubenorgan. **c)** Grubenorgan einer Python. **d)** Grubenorgan einer Grubenotter.

Die Membran wird von den IR-Rezeptoren innerviert und besitzt aufgrund ihrer geringen Stärke im Gegensatz zu den anderen Grubenorganen, denen eine solche Membran fehlt, eine viel geringere thermische Masse. Die IR-Rezeptoren sind bei allen drei genannten Gruppen freie Nervenendigungen des Nervus trigeminus. Die einzelnen Nervenfasern verjüngen sich bis zu Durchmessern von ca. 1 µm und verlieren schließlich ihre Myelinscheide. Danach dehnen sich die Nervenfasern aus und bilden breite, flache handförmige Strukturen mit einem Durchmesser von 4 - 6 µm (Bullock and Fox, 1957). Diesen präterminalen Verdickungen entspringen sekundäre und tertiäre Verzweigungen, die als außerordentlich feine, freie Nervenendigungen terminieren und eng mit Schwann-Zellen assoziiert sind. Des Weiteren

enthalten die Nervenendigungen viele dicht gepackte, große Mitochondrien, sowie hohe Konzentrationen oxidativer Enzyme (Molenaar, 1992). Die Gesamtheit der gerade beschriebenen Struktur aus freien Nervenendigungen mit Mitochondrien und Schwann-Zellen wird als terminale Nervenmasse (TNM, *engl.: terminal nerve mass*) bezeichnet (Bleichmar and Robertis, 1962; Terashima et al., 1970). Jede TNM ist mit einer einzelnen Nervenfaser verbunden. Die Größe der TNMs stimmt mit der Größe der rezeptiven Fläche der peripheren Einheiten überein, so dass jede TNM im Prinzip einem Pixel entspricht (Molenaar, 1992). Innerhalb der Grubenmembran sind die IR-Rezeptoren in einem einschichtigen Array angeordnet und liegen einem dichten Netzwerk aus Blutkapillaren auf. Dieses kapillare Netzwerk dient zum einen der Energieversorgung der TNMs und zum anderen dem Wärmeaustausch. Letzterer ermöglicht die Aufrechterhaltung einer relativ stabilen Temperatur der Rezeptoren und reduziert den Nachbild-Effekt eines beweglichen Stimulus auf ein Minimum. Der Blutfluss wird dabei direkt von den einzelnen TNMs und nicht vom ZNS gesteuert (Goris et al., 2000).

Die Rezeptoren sind spontanaktiv, antworten jedoch besonders stark und äußerst empfindlich auf Temperaturänderungen. So können bereits Temperaturänderungen von nur 0,001°C wahrgenommen werden (Bullock and Diecke, 1956; Ebert and Westhoff, 2006), was einer Empfindlichkeitsschwelle von $3{,}35 \cdot 10^{-2}$ $W \cdot m^{-2}$ entspricht. Die Rezeptorantwort ist am stärksten bei Reizen mit Wellenlängen zwischen 8 - 12 µm (Grace et al., 1999). IR-Strahlung mit einer Wellenlänge in diesem Bereich wird entsprechend dem Wienschen Verschiebungs-gesetz (Gleichung 1.3, Abschnitt 1.1) maximal von Oberflächen mit Temperaturen zwischen 89°C und -32°C emittiert.

Eine weitere Besonderheit der IR-sensitiven Schlangen ist, dass sie eine bestimmte Gehirnstruktur in der Medulla zur Verarbeitung von IR-Reizen besitzen, die in nicht IR-sensitiven Schlangen fehlt. Diese Struktur wird „lateraler absteigender Ast und Kern des Nervus trigeminus“ oder kurz LTTD genannt. Dendriten der IR-sensitiven Neurone aus dem Trigeminalganglion terminieren im LTTD. Von dort werden die Informationen weiter ins kontralaterale Tectum opticum geleitet. Bei den Grubenottern nehmen die Informationen einen Umweg über den ipsilateralen Reticularis caloris, einen Relaiskern, der nur bei dieser Gruppe von Schlangen existiert (Goris, 2011).

Elektrophysiologische Untersuchungen haben weiterhin gezeigt, dass sowohl das rezeptive Feld der Augen als auch das des Grubenorgans eine somatotope Repräsentation im optischen Tectum besitzen und dass beide Felder überlappen. So findet man im Tectum opticum hauptsächlich folgende drei Neuronen-Typen: solche die nur auf IR-Reize antworten, solche

die nur auf visuelle Reize antworten, und solche die auf beide Stimuli antworten. Man könnte also sagen, dass bereits auf der Ebene des Tectum opticum ein Bild konstruiert wird, welches zusätzlich zu den drei Primärfarben auch die Farbe „IR“ enthält (Goris, 2011). Zusammengenommen deuten die bisherigen Ergebnisse daraufhin, dass der IR-Sinn bei Schlangen einen integralen Teil des visuellen Sinnessystems darstellt.

1.3.1.2 Fledermäuse

Vampirfledermäuse der Art *Desmodus rotundus* sind die einzigen Vertreter der Gruppe der Säugetiere für die IR-Rezeptoren bisher nachgewiesen wurden. Thermische Reize werden in den drei Gruben wahrgenommen, die das zentrale Nasenblatt im Gesicht der Vampirfledermäuse umgeben. Die Haut an dieser Stelle ist besonders dünn, Haare und Drüsen fehlen. Unter der Haut befindet sich dichtes Bindegewebe mit verhältnismäßig wenigen Blutgefäßen, was in Verbindung mit der blattartigen äußeren Form zu einer guten thermischen Isolierung des Nasenblattes vom restlichen Körper führt. Als Folge weist das Nasenblatt eine um 9°C niedrigere Temperatur auf als die nur wenige Millimeter entfernten Bereiche der Augen und Wangen (Kürten and Schmidt, 1982). Das Nasenblatt wird von sehr feinen Ausläufern des infraorbitalen Nervenastes des Nervus trigeminus innerviert. Elektrophysiologische Ableitungen an einzelnen Nervenfasern dieses Nervenastes haben gezeigt, dass sich insbesondere im Bereich des zentralen Nasenblattes und dem rostralen Teil der Oberlippe viele (77) Thermorezeptoren in Form freier Nervenendigungen befinden. Davon sind ca. 70% Kalt- und 30% Warmrezeptoren (Kürten et al., 1984). Die Analyse des Aktivitätsbereiches der Warmrezeptoren zeigte, dass dieser mit einem Arbeitsbereich zwischen 20 - 40°C im Vergleich zu anderen Säugetieren deutlich zu niedrigeren Temperaturen hin verschoben ist. Warmrezeptoren mit konstanten Entladungsraten unterhalb von 28°C konnten bei Säugetieren bisher nicht beschrieben werden. Dafür scheinen sie jedoch ein typisches Merkmal der Thermorezeptoren IR-sensitiver Schlangen und eine Anpassung an das Auffinden von endothermen Beutetieren zu sein. Eine weitere Gemeinsamkeit zu IR-sensitiven Schlangen ist das Vorhandensein eines spezifischen Kerns im Hirnstamm der Vampirfledermäuse, der anderen Fledermausarten fehlt. Dieser entspricht sowohl bezüglich seiner Lage als auch seiner histologischen Eigenschaften dem LTTD bei IR-sensitiven Schlangen (Kishida et al., 1984). Die Empfindlichkeit des IR-Organs von *Desmodus rotundus* ermöglicht die Detektion gut durchbluteter menschlicher Haut aus einer Entfernung von 13 cm. Diese Ergebnisse wurden anhand von Verhaltensversuchen gewonnen bei der eine

Sensitivitätsschwelle von 0,5 $W \cdot m^{-2}$ ermittelt wurde (Kürten and Schmidt, 1982). Dies ist in etwa um einen Faktor 15 unempfindlicher als die IR-Rezeptoren einiger Schlangen (siehe Abschnitt 1.3.1.1). Die ermittelten Sensitivitäten deuten auf die Verwendung des IR-Sinns bei Vampirfledermäusen als Nah-Sinn hin, der eher dazu geeignet scheint, eine gut durchblutete Bissstelle ausfindig zu machen als der Ortung von Beute aus größeren Entfernungen zu dienen.

1.3.2 Invertebraten

Bei Invertebraten, besonders innerhalb der Insekten, findet man mitunter sehr empfindliche Thermorezeptoren an verschiedenen Körperanhängen, insbesondere jedoch an den Antennen (Altner and Loftus, 1985; Gingl and Tichy, 2001; Ruchty et al., 2010). Diese Thermorezeptoren können abhängig von ihrer Lage und Morphologie sowohl von Konvektionswärme als auch von Strahlungsenergie (IR-Strahlung) erregt werden. Ursache dafür ist, dass beide physikalischen Parameter letztendlich in einer Temperaturänderung der Rezeptormembran und der Aktivierung darin befindlicher thermosensitiver Ionenkanäle resultieren (Bandell et al., 2007; Caterina, 2007; Gracheva et al., 2010; Gracheva et al., 2011). Die Rezeptorantwort in Hinblick auf die Quelle der Temperaturänderung ist somit nicht eindeutig und kann entweder durch Wärmestrahlung, Konvektion oder eine Kombination aus beiden hervorgerufen werden. Die Ergebnisse von Gingl & Tichy (2001) deuten darauf hin, dass die Strahlungsenergie, die benötigt wird um die Entladungsrate der von ihnen untersuchten antennalen Thermorezeptoren von Heuschrecken, Schaben und Zecken zu modulieren, sehr hoch ist und außerhalb des biologisch relevanten Bereichs liegt. Dennoch gilt es, die gerade erwähnte potentielle Mehrdeutigkeit der Rezeptorantwort in Hinblick auf die Reizquelle zu berücksichtigen. Dies gilt insbesondere für das Design von Verhaltensversuchen zur Untersuchung von potentiellen IR-Rezeptoren. Gefahren liegen in der Verwendung von nicht eindeutigen Reizquellen aufgrund des Versuchsaufbaus oder der Verwendung von Reizintensitäten außerhalb des biologisch relevanten Bereichs.

Eine einheitliche oder zufriedenstellende Definition zur Abgrenzung von IR-Rezeptoren gegenüber Thermorezeptoren existiert in der bisherigen Literatur nicht. Der Übersichtlichkeit halber werden im weiteren Verlauf dieses Kapitels alle antennalen Thermorezeptoren, die ebenfalls auf IR-Strahlung antworten, wenn offensichtlich auch nicht im Bereich der biologischen Relevanz, von der Betrachtung ausgeschlossen. Es wird sich ausschließlich auf

extra-antennale IR-Rezeptoren beschränkt, für welche nach bisherigem Erkenntnisstand eine Sensitivität gegenüber IR-Strahlung als adäquaten Reiz bestätigt wurde.

1.3.2.1 Melanophila

Prachtkäfer der Gattung *Melanophila* sind seit langem bekannt für ihr pyrophiles („Feuer liebendes“) Verhalten (Ricksecker, 1885). Um sich zu paaren und ihre Eier unter die verbrannte Borke ihrer Wirtsbäume zu legen, fliegen sie gezielt noch andauernde Waldbrände an, deren frische Brandflächen durch offenes Feuer, heiße Asche und Rauch gekennzeichnet sind. Grund für dieses ausgeprägte pyrophile Verhalten ist die Abhängigkeit ihres Reproduktionszyklus vom Auftreten solcher Brände. Erst der durch starke Hitze zumindest partiell abgetötete Baum stellt ein geeignetes Substrat für die xylophagen Larven dar, die sich vom Kambium und Holz verschiedener Nadel- und Laubbäume ernähren und sonst nicht in der Lage sind, gegen die natürlichen Abwehrmechanismen eines intakten Baumes anzukommen (Horion, 1955; Schmitz and Bleckmann, 1997; Wikars, 1997). Als besondere Anpassung an die pyrophile Lebensweise haben *Melanophila*-Käfer IR-Organe (auch Grubenorgane genannt; *engl.: pit organs*) entwickelt (Evans, 1964; Schmitz and Bleckmann, 1997; Schmitz et al., 1997). Diese werden wahrscheinlich sowohl zur Nah- und Ferndetektion von Waldbränden, als auch zur Orientierung auf den Brandflächen genutzt. Von den nach Bellamy (2008) beschriebenen dreizehn rezenten *Melanophila*-Arten wurde in der bestehenden Fachliteratur für acht Spezies pyrophiles Verhalten (Ricksecker, 1885; Manee, 1913; Champion, 1918; Sharp, 1918; VanDyke, 1926; Linsley, 1933, 1943; Wikars, 1997) und für elf Spezies das Vorhandensein von Grubenorganen (Sloop, 1937; Evans, 1964, 1966) beschrieben (vgl. Tab. 1.1). Die Grubenorgane der einzelnen Spezies sind bezüglich ihres Grundbauplans und ihrer Funktionsweise wahrscheinlich ähnlich, eine detaillierte vergleichende Beschreibung existiert jedoch bisher nicht. Die folgende Beschreibung der Gruben-/ IR-Organe basiert auf Ergebnissen zur am besten untersuchten Art, *Melanophila acuminata*.

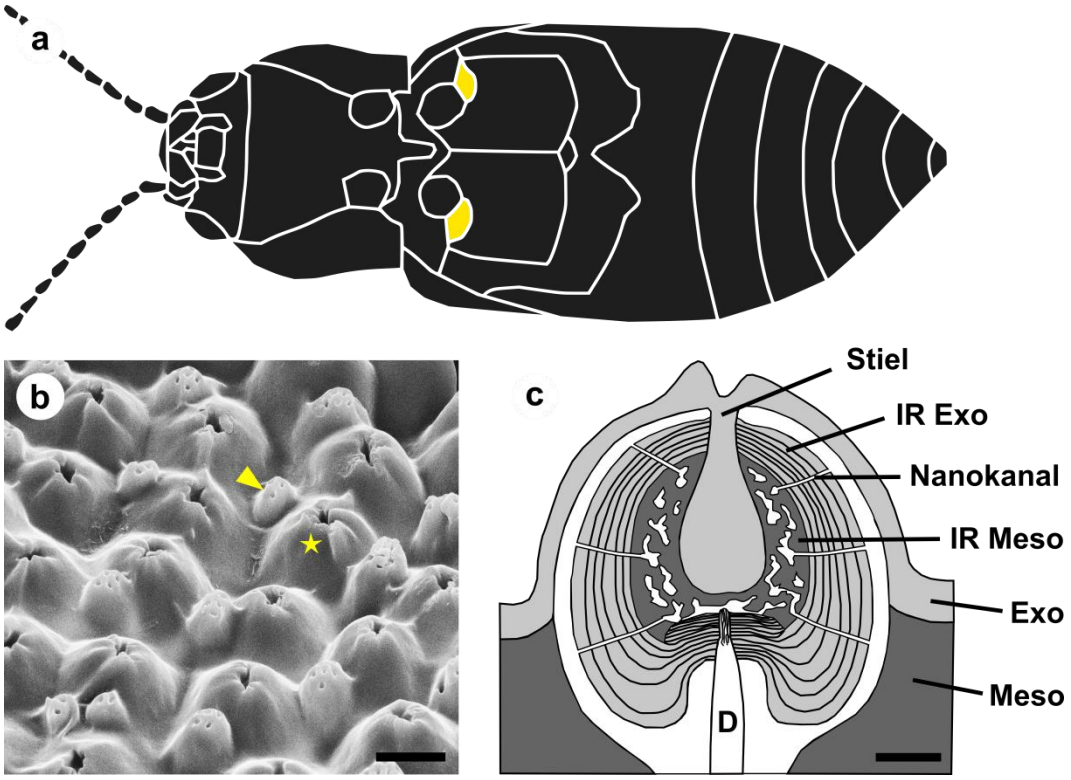

Fig. 1.2 IR-Rezeptoren von *Melanophila acuminata*. **a)** Habitus, schematisch. Beine weggelassen. Die IR- oder Grubenorgane (gelbe Markierung) befinden sich am Metathorax neben den mesothorakalen Coxen. Länge des Käfers ca. 1,3 cm. Bild geändert nach Vondran et al. (1995). **b)** IR-Rezeptoren (Stern) mit assoziierten Wachsdrüsen (Pfeil) am Grund des Grubenorgans. Maßstab: 10 µm. **c)** Schematischer Querschnitt durch einzelnen IR-Rezeptor. Die innere Cuticula-Kugel eines IR-Rezeptors setzt sich aus einem äußeren Mantel (IR Exo) und einem mikrofluidischen Kern (IR Meso) zusammen. Sie ist apikal über einen Stiel mit der Exocuticula der äußeren Kuppel (Exo) verbunden und wird basal vom Dendriten (D) eines Mechanorezeptors innerviert. Meso = Mesocuticula. Maßstab: 3 µm. Bild geändert nach Schmitz et al. (2007) und Klocke et al. (2011).

Die Organe befinden sich am Metathorax neben den mesothorakalen Coxen (Fig. 1.2 a) und haben einen Durchmesser von ungefähr 450 µm x 200 µm (Evans, 1964). Am Grund jedes Grubenorgans liegen zwischen 50 – 100 einzelne IR-Rezeptoren (auch Sensillen genannt) (Vondran et al., 1995). Jedes Sensillum hat von außen betrachtet eine halbkugelförmige kuppelartige Gestalt mit einem Durchmesser von 12 – 15 µm und wird von einer Wachsdrüse begleitet (Fig. 1.2 b) (Vondran et al., 1995). Die Kuppel besteht aus einer dünnen Cuticula-Schicht, hauptsächlich unmelanisierte Exocuticula (Schmitz et al., 2007), und stellt die äußere Hülle eines innen gelegenen kugelförmigen Hohlraumes dar. Dieser wird wiederum nahezu vollständig von einer inneren Cuticula-Kugel mit einem Durchmesser von ungefähr 10 µm ausgefüllt, die über einen kleinen apikalen Stiel (*engl.: stalk*) an der Cuticula der äußeren Kuppel aufgehängt ist (Fig. 1.2 c). Zwischen der inneren Kugel und der Cuticula der äußeren Kuppel befindet sich eine schmale Kluft (protoplasmatische Schicht) von 300 – 400 nm Dicke. Diese wird von apikalen Ausläufern zweier Hüllzellen gebildet (Vondran et al., 1995).

Die innere Cuticula-Kugel besteht aus mindestens zwei voneinander unterscheidbaren Bereichen: i) ein äußerer Mantel bestehend aus harter Exocuticula und ii) ein innerer mikrofluidischer Kern aus weicher schwammartiger Mesocuticula, die durchzogen ist von vielen kleinen Mikrokanälen und Kavitäten (Fig. 1.2 c) (Klocke et al., 2011; Klocke and Schmitz, 2012). Letztere sind mit einem Fluid von unbekannter Zusammensetzung gefüllt. Sie konzentrieren sich vor allem im basalen Teil der inneren Cuticula-Kugel und bilden dort eine Art fluidgefüllte sog. innere Druckkammer (Schmitz et al., 2007). Von unten wird die innere Kugel vom Dendriten eines Mechanorezeptors innerviert, dessen Spitze bis in den fluidischen Kern und die innere Druckkammer vordringt (Fig. 1.2 c) (Vondran et al., 1995; Schmitz et al., 1997). Das Funktionsprinzip des *Melanophila*-IR-Rezeptors entsprach keinem der in der Technik bis dahin bekannten Modellen (vgl. Abschnitt 1.2) und wurde photomechanisches Prinzip genannt (Schmitz and Bleckmann, 1997; Schmitz et al., 1997). Beim photo-mechanischen Prinzip wird IR-Strahlung von den Proteinen und Chitinfasern der Cuticula absorbiert, die Cuticula-Kugel und das Fluid erwärmen und dehnen sich in Folge dessen aus. Der innere mikrofluidische Kern wird sich auf Grund seiner thermomechanischen Eigenschaften wahrscheinlich stärker ausdehnen als der härtere und steifere exocuticuläre äußere Mantel (Klocke et al., 2011; Klocke and Schmitz, 2012). Die einzig nachgiebige Stelle innerhalb der Cuticula-Kugel, an welcher der sich aufbauende Druck abgegeben werden kann, ist die Dendritenspitze des Mechanorezeptors. Der Zellkörper des Rezeptors wird ungefähr Umgebungsdruck aufweisen. Ein Druckanstieg innerhalb der Kugel wird daher in einer Kompression der Dendritenspitze resultieren. Dies führt dann zur Öffnung mechanisch gesteuerter Ionenkanäle und letztlich zur Generierung von Aktionspotentialen (Schmitz and Bleckmann, 1998). Langsame Druckänderungen, z.B. durch langsame Änderungen der Umgebungstemperatur, können wohlmöglich durch feine Nanokanäle, die durch den äußeren Mantel der Kugel ziehen (Fig. 1.2 c), kompensiert werden (Schmitz et al., 2007).

Primäre Afferenzen herkömmlicher Mechanorezeptoren ramifizieren und terminieren für gewöhnlich, in Abhängigkeit von ihrer Lage, entweder nur im zugehörigen Ganglion oder bilden zusätzlich zu diesen lokalen auch noch intersegmentale Projektionen aus (Bräunig et al., 1983). Ganz anders hingegen konnte im Grubenorgan von *Melanophila* eine kleine Gruppe (10%) primärer Afferenzen identifiziert werden, die direkt ins Gehirn projizieren ohne lokale Projektionen im entsprechenden Ganglion auszubilden (Gronenberg and Schmitz, 1999). Dies deutet auf eine komplexere Verarbeitung der IR-Signale hin, bei der wohlmöglich auch Informationen aus verschiedenen Körperarealen und Sinnessystemen (z.B. Geruch) integriert werden (Gronenberg and Schmitz, 1999).

Tab. 1.1 Rezente *Melanophila*-Spezies nach Bellamy (2008), ihre biogeographische Verbreitung und frühe Belege pyrophilen Verhaltens und von IR-Organen.

Rezente *Melanophila* Spezies	Verbreitung	Pyrophiles Verhalten beschrieben durch	IR-Organe vorhanden nach
M. acuminata	afrikanisch; nearktisch; neotropisch; orientalisch; paläarktisch	Ricksecker (1885); Manee (1913); Sharp (1918); Linsley (1933);	Sloop (1937); Evans (1964)
M. atra	neotropisch	-	Evans (1966)
M. atropurpurea	nearktisch	Linsley (1933);	Sloop (1937)
M. caudata	nearktisch	-	Sloop (1937)
M. consputa	nearktisch	Ricksecker (1885); Van Dyke (1926); Linsley (1933);	Sloop (1937)
M. coriacea	orientalisch	Wikars (1997)	Evans (1966)
M. cuspidata (syn.: *M. nigrita*)	afrikanisch; paläarktisch	Wikars (1997)	Evans (1966)
M. gestroi	afrikanisch; paläarktisch	-	-
M. ignicola	orientalisch; paläarktisch	Champion (1918)	Sloop (1937)
M. notata	nearktisch; neotropisch; paläarktisch; orientalisch	Manee (1913); Linsley (1933);	Sloop (1937)
M. obscurata	paläarktisch	-	-
M. occidentalis	nearktisch	Obenberger 1928 in Linsley (1943)	Sloop (1937)
M. unicolor	afrikanisch	-	Evans (1966)

Elektrophysiologische Untersuchungen an *Melanophila acuminata* zeigten ein rein phasisches Antwortverhalten auf IR-Reize (Schmitz and Bleckmann, 1997) mit einer Schwellenempfindlichkeit von ca. 50 $W \cdot m^{-2}$ (Schmitz and Bleckmann, 1998; Schmitz and Trenner, 2003). Antwortzeiten (Latenzen) eines einzelnen Sensillums betrugen bei dieser Schwellenintensität 5 – 6 ms (Schmitz and Bleckmann, 1998). In Verhaltensversuchen wurden von Evans (1966) sogar Schwellenempfindlichkeiten von nur 0,6 $W \cdot m^{-2}$ ermittelt. Auf Grundlage dieser Werte ergibt die Berechnung der Entfernung, bis zu der *Melanophila* in der Lage sein müsste, ein hypothetisches Feuer mit einer Fläche zwischen 100.000 – 200.000 m^2 wahrzunehmen, weniger als 12 km (Schmitz and Bleckmann, 1998). Diese Entfernung ist

deutlich geringer als die, die in vielen der anfangs erwähnten alten Berichte zum pyrophilen Verhalten von *Melanophila* beschrieben wurde (vgl. Tab. 1.1). Schmitz und Bousack (2012) berechneten auf Grundlage historisch belegter Daten die Entfernung, aus der aller Wahrscheinlichkeit nach bei einem großen Öltank-Feuer im Jahre 1924 in Coalinga, Kalifornien, ungeheure Mengen von *Melanophila consputa* angelockt wurden. Die ermittelte Entfernung betrug ihren Berechnungen zufolge 130 km. Dies würde einer Schwellen-empfindlichkeit eines einzelnen Sensillums von $1{,}3 \cdot 10^{-4}$ $W \cdot m^{-2}$ entsprechen (Schmitz and Bousack, 2012). Da derart geringe Intensitäten an IR-Strahlung eigentlich im thermischen Rauschen untergehen, wäre es möglich, dass *Melanophila*-Käfer zusätzlich zu dem bisher beschriebenen Funktionsmodell auch noch eine Art von aktivem Verstärkungsmechanismus oder stochastischer Resonanz bei der Detektion sehr schwacher IR-Strahlung anwenden (Schmitz and Bousack, 2012).

1.3.2.2 Aradus

Die Gattung *Aradus*, innerhalb der Familie der Rindenwanzen (Aradidae), umfasst weltweit ca. 200 Arten. Davon zeigen die Wenigsten, d.h. nur etwa 8 Arten, ein pyrophiles Verhalten (Wikars, 1997; Lappalainen and Simola, 1998; Wyniger et al., 2002; Schmitz et al., 2008; Johansson et al., 2010; Schmitz et al., 2010; Baena and Torres, 2013). Die Larven der pyrophilen *Aradus*-Wanzen sind mycophag und ernähren sich von im Holz lebenden Ascomyceten, die wiederum besser oder teilweise nur auf verbrannten Bäumen wachsen können (Wikars, 1997). Innerhalb dieser pyrophilen Vertreter konnten IR-Rezeptoren bisher bei vier Arten nachgewiesen werden (Schmitz et al., 2008; Schmitz et al., 2010) (vgl. Tab. 1.2). Ungefähr ein Dutzend IR-Rezeptoren (auch IR-Sensillen genannt) befinden sich auf beiden Seiten des Prothorax, auf den sog. Propleurae direkt hinter dem ersten Beinpaar, und zwei bis vier weitere IR-Sensillen auf dem Mesothorax unmittelbar hinter dem zweiten Beinpaar (Fig. 1.3 a). Letztere sind nur bei *A. flavicornis* nicht vorhanden (Schmitz et al., 2010). Die einzelnen IR-Rezeptoren besitzen morphologisch starke Ähnlichkeit zu den IR-Sensillen von *Melanophila* und funktionieren wahrscheinlich ebenfalls nach dem bereits beschriebenen Prinzip eines photomechanischen IR-Rezeptors (Schmitz et al., 2008) (vgl. Abschnitt 1.3.2.1). Trotz der Gemeinsamkeiten gibt es jedoch auch einige strukturelle Unterschiede. So sind die IR-Sensillen bei *Aradus* nicht wie bei *Melanophila* in Form eines Organs zusammengefasst, sondern sie liegen einzeln verstreut zwischen zahlreichen cuticulären Haarmechanorezeptoren (Fig. 1.3 b) (Schmitz et al., 2008). Die einzelnen IR-

Sensillen weisen zwischen den bisher untersuchten *Aradus*-Arten keine auffälligen strukturellen Unterscheide auf (Schmitz et al., 2010). Ein typisches IR-Sensillum (Fig. 1.3 c) besteht von außen betrachtet aus einer kuppelartigen Halbkugel mit einem Durchmesser von 13 – 15 µm und zeichnet sich durch eine apikale Aussparung aus. Die äußere Hülle des Sensillums besteht aus einer dünnen Schicht Exocuticula.

Tab. 1.2 *Aradus*-Spezies mit pyrophilem Verhalten und/oder IR-Rezeptoren.

Aradus-Spezies	Verbreitung	Pyrophiles Verhalten beschrieben durch	IR-Rezeptoren vorhanden (+); nicht vorhanden (-); nicht untersucht (n.u.); nach Schmitz et al. (2010)
A. albicornis	Australien	Schmitz et al. (2008)	+
A. anisotomus = *anullicornis*	Eurasien	Wikars (1997); Wyniger et al. (2002)	n.u.
A. crenaticollis	Eurasien	Wikars (1997); Johansson et al. (2010)	-
A. flavicornis	Eurasien, Afrika	Baena & Torres (2013)	+
A. fuscicornis	Australien	Schmitz et al. (2010)	+
A. laeviusculus	Eurasien	Lappalainen & Simola (1998)	-
A. lugubris	Eurasien, Nord-Amerika	Wyniger et al. (2002); Johansson et al. (2010)	+
A. signaticornis	Eurasien, Nord-Amerika	Wikars (1997); Wyniger et al. (2002)	n.u.

Unmittelbar darunter befindet sich eine Cuticula-Kugel mit einem Durchmesser von ungefähr 10 µm (Schmitz et al., 2008). Diese setzt sich zusammen aus einer äußeren Hülle, die ebenfalls aus Exocuticula besteht, und einem inneren Kern. Letzterer kann wiederum in zwei Bereiche unterteilt werden: i) ein oberer Pfropfen-artiger Bereich aus Exocuticula und ii) ein darunter liegender Bereich aus schwammartiger Mesocuticula, der durch fluidgefüllte Hohlräume gekennzeichnet ist (Schmitz et al., 2010; Klocke and Schmitz, 2012). Von unten wird die Cuticula-Kugel vom Dendriten eines Mechanorezeptors innerviert, dessen Spitze bis in den inneren Kern vordringt und dort von kleinen fluidgefüllten Hohlräumen umgeben wird. Verglichen mit den IR-Sensillen bei *Melanophila* existieren weitere strukturelle Unterschiede i) im Fehlen von Nanokanälen, die die äußere Hülle der Cuticula-Kugel durchziehen, ii) im Fehlen der protoplasmatischen Schicht (vgl. Abschnitt 1.3.2.1) zwischen der äußersten

Exocuticula und dem Mantel der inneren Cuticula-Kugel, was bedingt, dass die Kugel ohne einen Zwischenraum in die umgebende Cuticula eingepasst ist, bzw. iii) in einer aufsitzenden Konformation der Cuticula-Kugel (siehe Fig. 1.3 c) bei *Aradus* im Vergleich zu der in *Melanophila* vorhanden Aufhängung über einen apikalen Stiel (vgl. Fig. 1.2 c), und iv) bezüglich des kleineren und weniger stark differenzierten mikrofluidischen Kerns im *Aradus*-Sensillum (Schmitz et al., 2010).

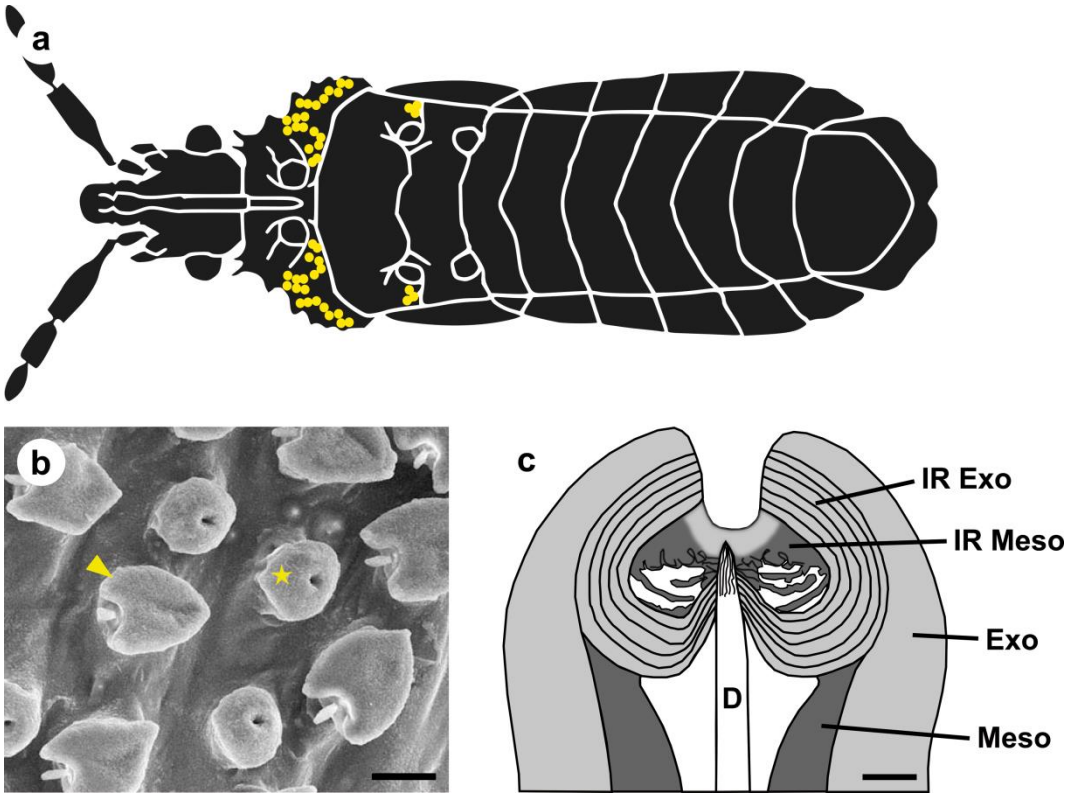

Fig. 1.3 IR-Rezeptoren von *Aradus albicornis*. **a)** Habitus, schematisch. Beine weggelassen. IR-Rezeptoren (gelbe Punkte) befinden sich auf den Propleurae hinter dem ersten Beinpaar und auf dem Mesothorax hinter dem zweiten Beinpaar. Länge der Wanze ca. 5 mm. Bild geändert nach Schmitz et al. (2010). **b)** Die IR-Rezeptoren (Stern) liegen einzeln verstreut zwischen Haarmechanorezeptoren (Pfeil). Maßstab: 10 µm. Bild geändert nach Schmitz et al. (2008). **c)** Schematischer Querschnitt durch einzelnen IR-Rezeptor. Die äußere Hülle des IR-Rezeptors besteht aus einer dünnen Schicht Exocuticula (Exo). Unmittelbar darunter befindet sich eine Cuticula-Kugel, die sich aus einem äußeren Mantel (IR Exo) und einem mikrofluidischen Kern (IR Meso) zusammensetzt. Die Cuticula-Kugel wird basal vom Dendriten (D) eines Mechanorezeptors innerviert. Meso = Mesocuticula. Maßstab: 2 µm. Bild geändert nach Schmitz et al. (2008).

Insbesondere der zuletzt genannte Unterschied in Verbindung mit einer weniger stark ausgeprägten Differenzierung einiger mechanischer Eigenschaften (reduzierter E-Modul und Härte) in den unterschiedlichen Cuticula-Bereichen des *Aradus*-Sensillums (vgl. Klocke and Schmitz, 2012) könnte eine mögliche Ursache für seine mutmaßlich geringere Sensitivität darstellen. So zeigten erste elektrophysiologische Untersuchungen an *Aradus albicornis* ein

phasisch-tonisches Antwortverhalten der Sensillen auf IR-Reize mit einer Schwellenempfindlichkeit von 113 $W \cdot m^{-2}$ (Schmitz et al., 2008). Dies ist in etwa halb so empfindlich wie die IR-Sensillen von *Melanophila acuminata* (vgl. Abschnitt 1.3.2.1).

1.3.2.3 Acanthocnemus nigricans

Acanthocnemus nigricans ist der einzige rezente Vertreter seiner Gattung. Ursprünglich nur in Australien beheimatet, ist die Art mittlerweile jedoch auch durch Einzelfunde in wärmeren Regionen der gesamten alten Welt beschrieben worden (Champion, 1922). Die mit einer Körpergröße von nur 3 – 6 mm sehr kleinen, dunkel gefärbten Käfer zeigen ein ausgeprägtes pyrophiles Verhalten und werden von Waldbränden angelockt. Die Käfer sammeln und paaren sich auf den frischen Brandflächen, insbesondere in direkter Nähe zu noch heißen Stellen, sog. ‚hot-spots' (Schmitz et al., 2002). Nach der Befruchtung legen die Weibchen ihre Eier wahrscheinlich unter die Borke der verbrannten Bäume (Kreiss et al., 2007). Die Nahrungsquelle der sich entwickelnden Larven ist derzeit noch unbekannt (Kreiss et al., 2005), mögliche Kandidaten sind jedoch das Kambium oder Holz des Wirtsbaumes oder holzbewohnende Ascomyceten.

Individuen von *Acanthocnemus* besitzen jeweils ein Paar einzigartiger Sinnesorgane unmittelbar vor den Coxae des Prothorax. Insbesondere durch elektrophysiologische Untersuchungen konnte gezeigt werden, dass es sich dabei um IR-Organe handelt (Kreiss et al., 2007). Diese bestehen aus einer runden cuticulären Scheibe (*engl.: disc*) mit einem Durchmesser von ca. 110 – 185 µm (Kreiss et al., 2005). Die Scheibe wird von einem kleinen Stiel (Durchmesser: 30 µm) über einer halbkreisförmigen mit Luft gefüllten Grube gehalten, die sich in Kontinuität mit der Umgebungsluft befindet, sodass ein Luftaustausch stattfinden kann. Die Oberseite der Scheibe ist leicht konkav nach innen gewölbt, die Unterseite deutlich konvex nach außen. Die eigentlichen IR-Rezeptoren (auch Sensillen genannt) befinden sich vor allem auf der anterioren Hälfte der Scheibenoberfläche. Pro Scheibe findet man ca. 90 dieser bisher nur bei *A. nigricans* gefundenen Sensillen vor (Kreiss et al., 2005). Der von außen sichtbare cuticuläre Apparat eines Sensillums setzt sich zusammen aus einem kleinen, aus massiver Cuticula bestehendem, Zapfen (*engl.: peg*) und einem diesen umgebenden Sockel. Der Zapfen weist weder Poren noch ein Lumen in seinem Inneren auf. Von unten ist ein elektronendichter Stab (*engl.: rod*) mit der Basis des Zapfens verbunden. Der Stab zieht in einem Kanal verlaufend von der Basis des Zapfens durch die Cuticula bis in das Innere der Scheibe. Es wurde vermutet, dass es sich bei dem Stab möglicherweise um die

hypertrophierte Dendritenscheide handelt, die das äußere dendritische Segment der Sinneszelle (DOS) aus dem Kanal verdrängt hat (Kreiss et al., 2005). Im Inneren der Scheibe angekommen, schließt sich das nur noch sehr kurze DOS an den Stab an. Das DOS ist über die ciliäre Konstriktion mit dem inneren dendritischen Segment (DIS) verbunden. Ein Tubularkörper innerhalb des DOS, ein charakteristisches Merkmal aller bekannten Insekten-Mechanorezeptoren, konnte nicht gefunden werden. Eine Besonderheit ist hier jedoch, dass dünne Gliazellfortsätze bis tief in das DIS vordringen und man eine große Anzahl an Mitochondrien vorfindet. Das DIS und der sich anschließende relativ große Zellkörper der Sinneszelle weisen beide die gerade genannten Merkmale auf und sind daher nicht klar voneinander zu unterscheiden (Kreiss et al., 2005).

Die genaue Funktionsweise dieser bisher bei keinem anderen Insekt gefundenen Sensillen ist derzeit unbekannt. Bestätigt werden konnte jedoch über elektrophysiologische Untersuchungen ihre generelle Funktion als IR-Rezeptoren. Dabei konnte ein phasisch-tonisches Antwortverhalten gezeigt werden, welches typische Charakteristika eines Thermorezeptors (Warmzelle) aufwies (Kreiss et al., 2007). Die IR-Sensillen von *Acanthocnemus* wurden daher als Mikrobolometer klassifiziert (vgl. Abschnitt 1.2.2.3). Sie liegen damit sowohl bezüglich ihrer Schwellenempfindlichkeit (110 – 250 $W \cdot m^{-2}$) als auch ihrer Latenzen (20 – 40 ms) (Kreiss et al., 2007) zwischen den empfindlicheren und schneller antwortenden photomechanischen IR-Rezeptoren von *Melanophila* und *Aradus* (siehe Abschnitt 1.3.2.1 und 1.3.2.2), und dem weniger empfindlichen und langsamer antwortenden Mikrobolometer-Rezeptor bei *Merimna* (siehe Abschnitt 1.3.2.4).

1.3.2.4 Merimna atrata

Der „Feuerkäfer“ *Merimna atrata* ist der einzige bekannte Vertreter der Gattung *Merimna* und ist endemisch in Australien (Bellamy, 2002). Diese pyrophile Spezies ist unter normalen Bedingungen nicht anzutreffen, wird jedoch während der Sommermonate in Australien regelmäßig in hohen Aufkommen von Waldbränden angelockt (Tepper, 1887; Froggatt, 1907; Poulton, 1915). Es wurde berichtet, dass *Merimna* für seinen Reproduktionszyklus stark abhängig vom Auftreten solcher Waldbrände ist. So werden Paarung und Eiablage ausschließlich auf frisch verbrannten Waldflächen vollzogen (Hawkeswood and Peterson, 1982). Die Eier werden dabei unter die Borke im Bereich der Stammbasis von Bäumen und Sträuchern insbesondere der Familie der *Myrtaceae* gelegt (Hawkeswood and Peterson, 1982; Hawkeswood, 2007; Kitchin, 2009). Die phytophagen Larven der Käfer ernähren sich vom

Kambium und Holz des verbrannten Baumes (Wikars, 1997). Die neue adulte Generation schlüpft ein, zwei oder sogar erst mehrere Jahre später (Kitchin, 2009). Als besondere Anpassung an die pyrophile Lebensweise hat *Merimna* einzigartige IR-Organe ausgebildet (Schmitz et al., 2000). Beobachtungen legen nahe, dass die IR-Organe dem Käfer wahrscheinlich eine sicherere Navigation auf der frischen Brandfläche, auf der sich immer noch zahlreiche ‚hot spots' befinden können, ermöglichen. Die ‚hot-spots' könnten attraktive Treffpunkte für die Käfer darstellen, in deren Nähe die Paarung geschützt vor Prädatoren stattfinden kann. Die IR-Organe stellen wahrscheinlich ein Frühwarnsystem dar, welches verhindert, dass die Käfer inmitten eines ‚hot-spots' landen und umkommen.

Die IR-Organe von *Merimna* liegen paarig ventrolateral auf dem zweiten, dritten und manchmal auch dem vierten abdominalen Sternit (Mainz et al., 2004). Die IR-Organe bestehen aus einer äußeren cuticulären absorbierenden Fläche (*engl.: absorbing area*) und einem inneren sensorischen Komplex, der diese innerviert (Schmitz et al., 2001). Die absorbierende Fläche ist ein annähernd rundlicher eingesenkter Bereich der Cuticula, der sich darüber hinaus durch die folgenden besonderen Eigenschaften auszeichnet: i) eine honigwabenartige Mikrostrukturierung der Cuticula-Oberfläche (Fig. 1.4 c); ii) ein Verlust dunkler Pigmente innerhalb der äußeren Cuticula-Schicht (Exocuticula), was in einer gelben Färbung des IR-Organs gegenüber der sonst dunkelbraunen Färbung der restlichen Cuticula resultiert (Schmitz et al., 2000) (Fig. 1.4 b). Der sensorische Komplex, der die absorbierende Fläche innerviert, befindet sich ungefähr im Zentrum direkt unterhalb einer leichten konvexen Ausbuchtung (Fig. 1.4 c, d). Die Hauptkomponente des sensorischen Komplexes bildet ein großes, thermosensitives multipolares Neuron (Typ II-Rezeptor) mit einer spezialisierten dendritischen Region, der sog. terminalen dendritischen Masse (TDM) (Schmitz et al., 2000). Diese ist durch sehr feine, dicht gepackte Verzweigungen seiner terminalen Dendriten charakterisiert, die darüber hinaus eine Vielzahl von Mitochondrien enthalten (Fig. 1.4 e). Alle Komponenten des multipolaren Neurons inklusive der TDM werden von Gliazellen umhüllt (Schmitz et al., 2001). Der grundlegende Bauplan dieser speziellen dendritischen Region erinnert stark an die TNM IR-sensitiver Schlangen (siehe Abschnitt 1.3.1.1). Innerhalb der Insekten war dieser spezialisierte Typ eines multipolaren Neurons bislang einzigartig bei *Merimna atrata*. Neueste Untersuchungen konnten jedoch in den Beinen von Heuschrecken Neurone mit sehr ähnlichen ultrastrukturellen Anpassungen identifizieren (Bräunig and Krumpholz, 2013). Diese sind jedoch nicht mit der Cuticula assoziiert, sondern befinden sich tief im Lumen der Beine. Es wurde daher spekuliert, dass es sich möglicherweise um einen besonderen Typ eines internen Thermorezeptors handelt.

Ebenfalls in den sensorischen Komplex von *Merimna* integriert, fand man zwei Somata und einen Skolops (Sinnesstift; *engl.: scolopale*) eines oder zweier Skolopidien (Schmitz et al., 2001). Diese wurden jedoch bisher nicht weiter untersucht (siehe Abschnitt 1.4). Der gesamte sensorische Komplex wird von einem ausgedehnten System, bestehend aus mehreren Luftsäcken, umhüllt. Durch schmale Lücken zwischen den Luftsäcken wird die Versorgung der Neurone des sensorischen Komplexes mit Hämolymphe gewährleistet (Schmitz et al., 2000, 2001).

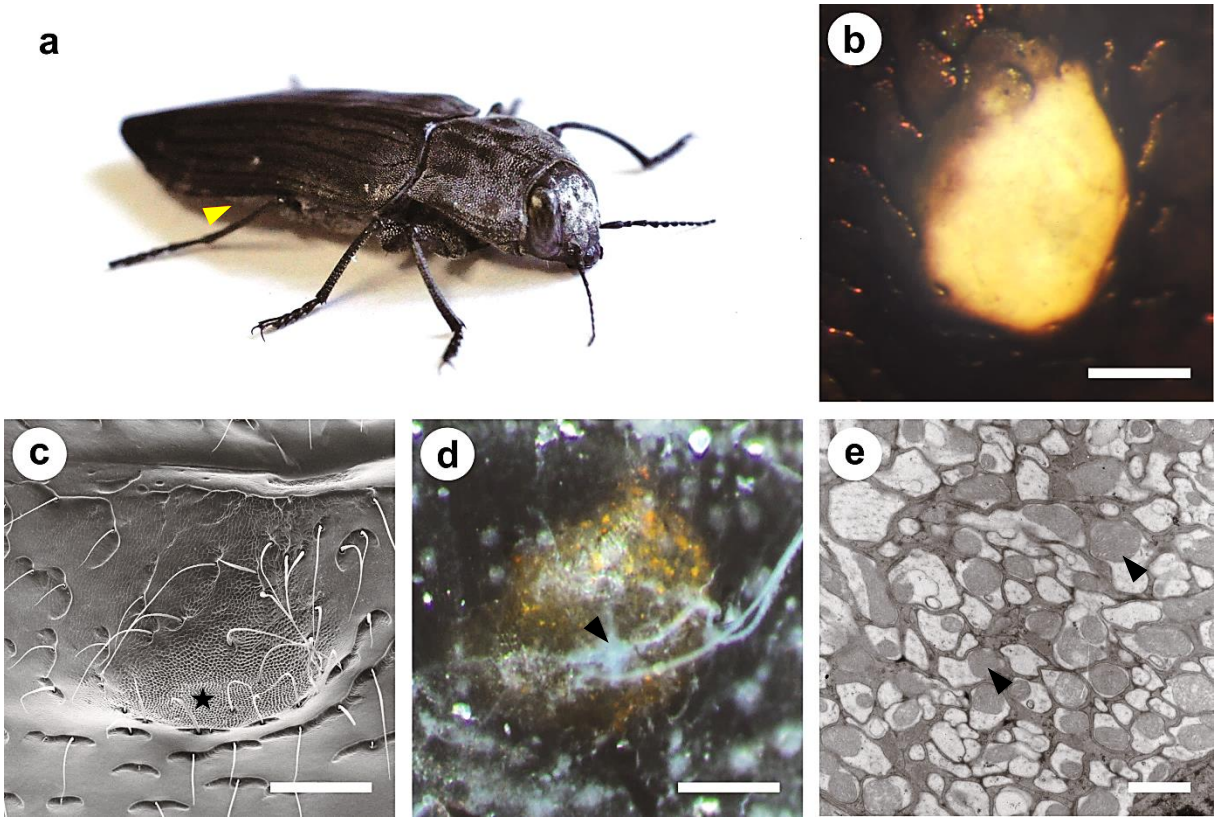

Fig. 1.4 IR-Organe von *Merimna atrata*. **a)** Habitus. Länge des Käfers ca. 2.5 cm. Die IR-Organe befinden sich ventrolateral auf den abdominalen Sterniten (gelber Pfeil). **b)** Lichtmikroskopisches Bild eines IR-Organs; absorbierende Fläche ist anhand ihrer gelblichen Färbung zu erkennen. Maßstab: 250 µm. **c)** REM-Aufnahme der absorbierenden Fläche verdeutlicht die dreidimensionale Form und die honigwabenartige Oberflächenstrukturierung; Stern markiert leichte Ausbuchtung, unterhalb derer sich der sensorische Komplex befindet. Maßstab: 250 µm. **d)** Lichtmikroskopische Aufnahme des IR-Organs; Ansicht von interior (Luftsäcke entfernt). Pfeil markiert den sensorischen Komplex, der von innen dicht an der absorbierenden Fläche angeheftet ist. Maßstab: 250 µm. **e)** TEM-Aufnahme eines Querschnitts durch die TDM des multipolaren Neurons. Pfeile markieren zwei der vielzähligen Mitochondrien. Maßstab: 1 µm. Orientierung in b) - d): oben = anterior; unten = posterior; links = lateral; rechts = medial. Abbildungen b) – e) veröffentlicht in Kahl et al. (2014).

Eine IR-rezeptive Funktionsweise wurde bisher nur für das multipolare Neuron eindeutig belegt. Elektrophysiologische Untersuchungen zeigten einen phasisch-tonischen Anstieg der Spikefrequenz mit einer Sensitivitätsschwelle von 400 $W \cdot m^{-2}$ und einer Latenz von 47 ms als

Antwort auf steigende Temperatur der absorbierenden Fläche (Schmitz et al., 2000; Schmitz and Trenner, 2003). Dies führte zur technischen Klassifizierung des *Merimna*-IR-Organs als Mikrobolometer (vgl. Abschnitt 1.2.2.3): einfallende IR-Strahlung wird von der Cuticula absorbiert und der resultierende Temperaturanstieg von einem Temperatursensor gemessen.

1.3.2.5 Leptoglossus occidentalis

Die zu den Randwanzen (Coreidae) gehörende Gattung *Leptoglossus* ist mit ca. 50 Arten in der Nearktis und Neotropis verbreitet. Einzige Ausnahme bildet die auf den Kanarischen Inseln vorkommende pantropische Art *L. gonagra* (Rabitsch and Heiss, 2005). Die Amerikanische Kiefern- oder Zapfenwanze, *Leptoglossus occidentalis*, ursprünglich im Westen Nordamerikas vorkommend und erstmals in Kalifornien und Utah beschrieben (Heidemann, 1910), wurde 1999 wahrscheinlich zufällig mit Holzlieferungen nach Europa (Nord-Italien) eingeschleppt (Bernardinelli and Zandigiacomo, 2001; Tescari, 2001). In den folgenden Jahren wurde die Art auch in der Schweiz, Österreich und vielen anderen europäischen Ländern beschrieben (Rabitsch and Heiss, 2005; Werner, 2006; Tamburini et al., 2012). Aktuelle Berichte dokumentieren den Fund von *L. occidentalis* sogar in Japan (Ishikawa and Kikuhara, 2009) und Korea (Ahn et al., 2013). In Deutschland wurde die Spezies erstmals 2006 in Berlin (Werner, 2006) und kurze Zeit später auch in anderen Regionen des Landes (z.B. in Köln, NRW; Pérez Vera and Hoffmann, 2007) gefunden.

Individuen von *L. occidentalis* sind phytophag und ernähren sich durch Saugen an jungen Samen verschiedener Koniferen-Arten (Bates et al., 2000; Strong et al., 2001; Bates et al., 2002). In Amerika gilt die Spezies allgemein als Schädling, da die Saugaktivität an den sich entwickelnden Zapfen der Wirtsbäume zu einer geringeren Samenproduktion führt (Bates et al., 2000).

Takács et al. (2009) folgerten aus Verhaltens- und elektrophysiologischen Untersuchungen, dass *L. occidentalis* in der Lage sei, IR-Reize wahrzunehmen. Die Autoren beschrieben vier Paare abdominaler IR-Rezeptoren, die für diese Eigenschaft verantwortlich sein sollen. Sie postulierten weiterhin, dass *L. occidentalis* die von den Zapfen emittierte IR-Strahlung zur Fernortung dieser Nahrungsquelle verwendet. Eine morphologische Charakterisierung der eigentlichen Rezeptoren fehlt jedoch vollständig (siehe Abschnitt 1.4).

1.4 Zielsetzung der Arbeit

Primäres Ziel der vorliegenden Arbeit ist die Identifizierung und morphologische Beschreibung der im IR-Organ von *Merimna atrata* bisher nicht untersuchten sensorischen Komponenten (Skolopidien) und die Aufklärung ihrer potentiellen Funktion bei der IR-Rezeption. Zu diesem Zweck sollen die komplexe Geometrie und charakteristische Materialeigenschaften der cuticulären absorbierenden Fläche bestimmt werden, welche zusammen die thermomechanischen Eigenschaften des IR-Organs maßgeblich beeinflussen. Die gewonnenen Daten sollen schließlich dazu verwendet werden, um mit Hilfe von Finite Element Simulationen, das thermomechanische Verhalten des IR-Organs zu analysieren.
Hierzu wurden folgende konkrete Arbeitsziele formuliert:

- Beschreibung der Anzahl, der exakten Position und, basierend auf der Ultrastruktur, des Typs der vorhandenen Rezeptoren.

- Charakterisierung der dreidimensionalen Geometrie der absorbierenden Fläche

- Materialwissenschaftliche Untersuchungen (Messung von reduziertem E-Modul und Härte) an abdominaler Cuticula, insbesondere der absorbierenden Fläche

- Charakterisierung der thermomechanischen Eigenschaften der absorbierenden Fläche mit Hilfe von Finite Element Simulationen.

Darüber hinaus ergab sich die Gelegenheit, die IR-Rezeptoren von *Leptoglossus occidentalis* näher zu untersuchen. Diese sind, neben denen von *Merima atrata*, die einzigen abdominalen IR-Rezeptoren, die bisher im Tierreich beschrieben wurden. Die Funktionsbeschreibung der genannten Strukturen als potentielle IR-Rezeptoren basiert dabei auf Ergebnissen von Verhaltensversuchen und ersten extrazellulären Ableitungen. Detaillierte morphologische Daten zu den Rezeptorstrukturen fehlen bisher jedoch.
Ein weiteres Ziel der vorliegenden Arbeit soll daher die detaillierte morphologische und ultrastrukturelle Charakterisierung der abdominalen IR-Rezeptoren von *L. occidentalis* sein.

1.5 Literatur

Ahn, S. J., Son, D., Choo, H. Y. and Park, C. G. (2013). "The first record on *Leptoglossus occidentalis* (Hemiptera: Coreidae) in Korea, a potential pest of the pinaceous tree species." *Journal of Asia-Pacific Entomology* **16**(3): 281-284.

Altner, H. and Loftus, R. (1985). "Ultrastructure and function of insect thermo-and hygroreceptors." *Annual Review of Entomology* **30**(1): 273-295.

Amantea, R., Knoedler, C., Pantuso, F. P., Patel, V., Sauer, D. J. and Tower, J. R. (1997). "Uncooled IR imager with 5mK NEDT". *Infrared Technology and Applications XXIII (Proceedings of SPIE), Orlando, Florida, USA*.

Baena, M. and Torres, J. L. (2013). "Notes on the biology and Iberian distribution of *Aradus flavicornis* (Dalmann, 1823) (Hemiptera, Heteroptera, Aradidae)." *Boletin de la Asociacion Espanola de Entomologia* **37**(3-4): 277-284.

Bandell, M., Macpherson, L. J. and Patapoutian, A. (2007). "From chills to chilis: mechanisms for thermosensation and chemesthesis via thermoTRPs." *Current Opinion in Neurobiology* **17**(4): 490-497.

Bates, S. L., Borden, J. H., Kermode, A. R. and Bennett, R. G. (2000). "Impact of *Leptoglossus occidentalis* (Hemiptera: Coreidae) on Douglas-fir seed production." *Journal of Economic Entomology* **93**(5): 1444-1451.

Bates, S. L., Strong, W. B. and Borden, J. H. (2002). "Abortion and seed set in lodgepole and western white pine conelets following feeding by *Leptoglossus occidentalis* (Heteroptera: Coreidae)." *Environmental entomology* **31**(6): 1023-1029.

Bellamy, C. L. (2002). "Zoological Catalogue of Australia, Vol. 29.5 Coleoptera: Buprestoidea". Melbourne, CSIRO Publishing.

Bellamy, C. L. (2008). "A world catalogue and bibliography of the jewel beetles (Coleoptera: Buprestoidea). Volume 3. Buprestinae: Pterobothrini through Agrilinae: Rhaeboscelina". Sofia, Moscow, Pensoft.

Bernardinelli, I. and Zandigiacomo, P. (2001). "*Leptoglossus occidentalis* Heidemann (Heteroptera, Coreidae): a conifer seed bug recently found in northern Italy." *Journal of Forest Science* **47**(2): 56-58.

Bleichmar, H. and Robertis, E. (1962). "Submicroscopic morphology of the infrared receptor of pit vipers." *Zeitschrift für Zellforschung und Mikroskopische Anatomie* **56**(6): 748-761.

Bräunig, P. and Krumpholz, K. (2013). "Internal receptors in insect appendages project directly into a special brain neuropile." *Frontiers in zoology* **10**(1): 54-54.

Bräunig, P., Pflüger, H. J. and Hustert, R. (1983). "The specificity of central nervous projections of locust mechanoreceptors." *The Journal of Comparative Neurology* **218**(2): 197-207.

Budzier, H. and Gerlach, G. (2010). "Thermische Infrarotsensoren: Grundlagen für Anwender". Weinheim, Germany, Wiley-VCH Verlag.

Bullock, T. and Diecke, F. (1956). "Properties of an infra-red receptor." *Journal of Physiology* **134**(1): 47.

Bullock, T. H. and Barrett, R. (1968). "Radiant heat reception in snakes." *Communications in Behavioral Biology* **1**: 19-29.

Bullock, T. H. and Fox, W. (1957). "The anatomy of the infra-red sense organ in the facial pit of pit vipers." *Quarterly Journal of Microscopical Science* **3**(42): 219-234.

Caterina, M. J. (2007). "Transient receptor potential ion channels as participants in thermosensation and thermoregulation." *American journal of physiology - Regulatory Integrative and Comparative Physiology* **292**(1): R64.

Champion, G. C. (1918). "A note on the habits of a *Melanophila* (Buprestidae) and other Indian Coleoptera." *Entomologist's Monthly Magazine* **54**: 199-200.

Champion, G. C. (1922). "The geographical distribution and synonomy of the dasytid-beetle *Acanthocnemus nigricans* Hope (= *ciliatus* Perris)." *Entomologist's Monthly Magazine* **58**: 77-79.

Colthup, N. B., Daly, L. H. and Wiberley, S. E. (1990). "Introduction to infrared and Raman spectroscopy". San Diego, CA, Academic Press.

De Cock Buning, T. (1983). "Thresholds of infrared sensitive tectal neurons in *Python reticulatus, Boa constrictor* and *Agkistrodon rhodostoma*." *Journal of Comparative Physiology. A, Neuroethology, Sensory, Neural, and Behavioral Physiology* **151**(4): 461-467.

De Cock Buning, T., Terashima, S.-i. and Goris, R. (1981). "Python pit organs analyzed as warm receptors." *Cellular and Molecular Neurobiology* **1**(3): 271-278.

Ebert, J. (2007), "Infrared sense in snakes – behavioural and anatomical examinations (*Crotalus atrox, Python regius, Corallus hortulanus*)", Thesis, Rheinische Friedrich Wilhelms Univ. Bonn

Ebert, J. and Westhoff, G. (2006). "Behavioural examination of the infrared sensitivity of rattlesnakes (*Crotalus atrox*)." *Journal of Comparative Physiology A* **192**(9): 941-947.

Engel, M. S. and Grimaldi, D. A. (2004). "New light shed on the oldest insect." *Nature* **427**(6975): 627-630.

Evans, W. G. (1964). "Infra-red Receptors in *Melanophila acuminata* De Geer." *Nature* **202**(4928): 211-211.

Evans, W. G. (1966). "Perception of infrared radiation from forest fires by *Melanophila acuminata* De Geer (Buprestidae, Coleoptera)." *Ecology* **47**(6): 1061-1065.

Froggatt, W. W. (1907). "Australian insects". Sydney, William Brooks & Co.

Gingl, E. and Tichy, H. (2001). "Infrared sensitivity of thermoreceptors." *Journal of Comparative Physiology. A, Neuroethology, Sensory, Neural, and Behavioral Physiology* **187**(6): 467-475.

Goris, R., Nakano, M., Atobe, Y., Kadota, T., Funakoshi, K., Hisajima, T. and Kishida, R. (2000). "Nervous control of blood flow microkinetics in the infrared organs of pit vipers." *Autonomic Neuroscience* **84**(1–2): 98-106.

Goris, R. C. (2011). "Infrared organs of snakes: an integral part of vision." *Journal of Herpetology* **45**(1): 2-14.

Grace, M. S., Church, D. R., Kelly, C. T., Lynn, W. F. and Cooper, T. M. (1999). "The python pit organ: imaging and immunocytochemical analysis of an extremely sensitive natural infrared detector." *Biosensors and Bioelectronics* **14**(1): 53-59.

Gracheva, E. O., Cordero-Morales, J. F., Gonzalez-Carcacia, J. A., Ingolia, N. T., Manno, C., Aranguren, C. I., Weissman, J. S. and Julius, D. (2011). "Ganglion-specific splicing of TRPV1 underlies infrared sensation in vampire bats." *Nature* **476**(7358): 88-91.

Gracheva, E. O., Ingolia, N. T., Kelly, Y. M., Cordero-Morales, J. F., Hollopeter, G., Chesler, A. T., Sanchez, E. E., Perez, J. C., Weissman, J. S. and Julius, D. (2010). "Molecular basis of infrared detection by snakes." *Nature* **464**(7291): 1006-1011.

Gronenberg, W. and Schmitz, H. (1999). "Afferent projections of infrared-sensitive sensilla in the beetle *Melanophila acuminata* (Coleoptera: Buprestidae)." *Cell and Tissue Research* **297**(2): 311-318.

Hawkeswood, T. J. (2007). "Review of the biology of the genus *Merimna* Saunders, 1868 (Coleoptera: Buprestidae)." *Calodema* **9**: 12-13.

Hawkeswood, T. J. and Peterson, M. (1982). "A review of the larval host records for Australian jewel beetels (Coleoptera: Buprestidae)." *Victorian Naturalist (Blackburn)* **99**: 240-251.

Heidemann, O. (1910). "New species of *Leptoglossus* from North America (Hemiptera; Coreidae)." *Proceedings of the Entomological Society of Washington* **12**: 191.

Herschel, W. (1800). "Experiments on the refrangibility of the invisible rays of the sun." *Philosophical Transactions of the Royal Society of London* **90**: 284-292.

Hesse, M., Meier, H. and Zeeh, B. (1995). "Spektroskopische Methoden in der organischen Chemie". Stuttgart, New York, Georg Thieme Verlag.

Horion, A. (1955). "Faunistik der mitteleuropäischen Käfer. 4, Sternoxia (Buprestidæ), Fossipedes, Macrodactylia, Brachymera".

Ishikawa, T. and Kikuhara, Y. (2009). "*Leptoglossus occidentalis* Heidemann (Hemiptera: Coreidae), a presumable recent invader to Japan." *Japanese Journal of Entomology* **12**(3): 115-116.

Johansson, T., Hjältén, J., Stenbacka, F. and Dynesius, M. (2010). "Responses of eight boreal flat bug (Heteroptera: Aradidae) species to clear-cutting and forest fire." *Journal of Insect Conservation* **14**(1): 3-9.

Kishida, R., Goris, R. C., Terashima, S.-I. and Dubbeldam, J. L. (1984). "A suspected infrared-recipient nucleus in the brainstem of the vampire bat, *Desmodus rotundus*." *Brain Research* **322**(2): 351-355.

Kitchin, D. R. (2009). "Notes on the biology of *Merimna atrata*." *Australian Entomologist* **36**(1): 1-2.

Klocke, D., Schmitz, A., Soltner, H., Bousack, H. and Schmitz, H. (2011). "Infrared receptors in pyrophilous ("fire loving") insects as model for new un-cooled infrared sensors." *Beilstein Journal of Nanotechnology* **2**(1): 186-197.

Klocke, D. and Schmitz, H. (2012). "Material properties of photomechanical infrared receptors in pyrophilous *Melanophila* beetles and *Aradus* bugs." *Acta Biomaterialia* **8**(9): 3392-3399.

Kreiss, E.-J., Schmitz, A. and Schmitz, H. (2005). "Morphology of the prothoracic discs and associated sensilla of *Acanthocnemus nigricans* (Coleoptera, Acanthocnemidae)." *Arthropod Structure & Development* **34**(4): 419-428.

Kreiss, E.-J., Schmitz, H. and Gebhardt, M. (2007). "Electrophysiological characterisation of the infrared organ of the Australian "Little Ash Beetle" *Acanthocnemus nigricans* (Coleoptera, Acanthocnemidae)." *Journal of Comparative Physiology. A, Neuroethology, Sensory, Neural, and Behavioral Physiology* **193**(7): 729-739.

Kürten, L. and Schmidt, U. (1982). "Thermoperception in the common vampire bat (*Desmodus rotundus*)." *Journal of comparative physiology* **146**(2): 223-228.

Kürten, L., Schmidt, U. and Schäfer, K. (1984). "Warm and cold receptors in the nose of the vampire bat *Desmodus rotundus*." *Naturwissenschaften* **71**(6): 327-328.

Lappalainen, H. and Simola, H. (1998). "The fire-adapted flatbug *Aradus laeviusculus* Reuter (Heteroptera, Aradidae) rediscovered in Finland (North Karelia, Koli National Park)." *Entomologica Fennica* **9**(1): 3-4.

Linsley, E. G. (1933). "Some observations on the swarming of *Melanophila*." *Pan-Pacific Entomologist* **9**: 138.

Linsley, E. G. (1943). "Attraction of *Melanophila* beetles by fire and smoke." *Journal of Economic Entomology* **36**(2): 341-342.

Lynn, W. G. (1931). "The structure and function of the facial pit of the pit vipers." *American Journal of Anatomy* **49**(1): 97-139.

Mainz, T., Schmitz, A. and Schmitz, H. (2004). "Variation in number and differentiation of the abdominal infrared receptors in the Australian 'fire-beetle' *Merimna atrata* (Coleoptera, Buprestidae)." *Arthropod Structure & Development* **33**(4): 419-430.

Manee, A. H. (1913). "Observations on Buprestidae at Southern Pines, North Carolina." *Entomological News* **24**: 167-171.

Molenaar, G. J. (1992). Anatomy and physiology of infrared sensitivity of snakes. in *Biology of the Reptilia*. C. Gans and P. S. Ulinski. Chicago, University of Chicago. **17:** 367-453.

Noble, G. K. and Schmidt, A. (1937). "The structure and function of the facial and labial pits of snakes." *Proceedings of the American Philosophical Society* **77**(3): 263-288.

Pérez Vera, F. and Hoffmann, H. J. (2007). "*Leptoglossus occidentalis* Heidemann, 1910 (Hemiptera, Heteroptera) nun auch in Köln/Deutschland." *Heteropteron* **25**: 17-18.

Poulton, E. B. (1915). "The habits of the Australian buprestid "fire-beetle" *Merimna atrata*, (Laporte and Gory)." *Transactions of the Entomological Society of London* **Part 1. (Proceedings)**: iii-iv.

Rabitsch, W. and Heiss, E. (2005). "*Leptoglossus occidentalis* Heidemann, 1910, eine amerikanische Adventivart auch in Österreich aufgefunden (Heteroptera: Coreidae)." *Berichte des naturwissenschaftlich-medizinischen Vereins in Innsbruck* **92**: 131.

Ricksecker, L. E. (1885). "Habits of some California beetles." *Entomologica Americana* **1**: 96-98.

Rogalski, A. (2002). "Infrared detectors: an overview." *Infrared Physics & Technology* **43**(3-5): 187-210.

Rogalski, A. (2003). "Infrared detectors: status and trends." *Progress in Quantum Electronics* **27**(2-3): 59-210.

Rogalski, A. (2011). "Infrared detectors". Boca Raton, Florida, USA, CRC Press.

Rogalski, A. (2012). "History of infrared detectors." *Opto-Electronics Review* **20**(3): 279-308.

Ruchty, M., Roces, F. and Kleineidam, C. J. (2010). "Detection of minute temperature transients by thermosensitive neurons in ants." *Journal of neurophysiology* **104**(3): 1249-1256.

Schmitz, A., Gebhardt, M. and Schmitz, H. (2008). "Microfluidic photomechanic infrared receptors in a pyrophilous flat bug." *Naturwissenschaften* **95**(5): 455-460.

Schmitz, A., Schätzel, H. and Schmitz, H. (2010). "Distribution and functional morphology of photomechanic infrared sensilla in flat bugs of the genus *Aradus* (Heteroptera, Aradidae)." *Arthropod Structure & Development* **39**(1): 17-25.

Schmitz, A., Sehrbrock, A. and Schmitz, H. (2007). "The analysis of the mechanosensory origin of the infrared sensilla in *Melanophila acuminata* (Coeloptera; Buprestidae) adduces new insight into the transduction mechanism." *Arthropod Structure & Development* **36**(3): 291-303.

Schmitz, H. and Bleckmann, H. (1997). "Fine structure and physiology of the infrared receptor of beetles of the genus *Melanophila* (Coleoptera: Buprestidae)." *International Journal of Insect Morphology and Embryology* **26**(3–4): 205-215.

Schmitz, H. and Bleckmann, H. (1998). "The photomechanic infrared receptor for the detection of forest fires in the beetle *Melanophila acuminata* (Coleoptera: Buprestidae)." *Journal of Comparative Physiology A* **182**(5): 647-657.

Schmitz, H., Bleckmann, H. and Mürtz, M. (1997). "Infrared detection in a beetle." *Nature* **386**(6627): 773-774.

Schmitz, H. and Bousack, H. (2012). "Modelling a historic oil-tank fire allows an estimation of the sensitivity of the infrared receptors in pyrophilous *Melanophila* beetles." *PLoS ONE* **7**(5): e37627.

Schmitz, H., Schmitz, A. and Bleckmann, H. (2000). "A new type of infrared organ in the Australian" fire-beetle" *Merimna atrata* (Coleoptera: Buprestidae)." *Naturwissenschaften* **87**(12): 542-545.

Schmitz, H., Schmitz, A. and Bleckmann, H. (2001). "Morphology of a thermosensitive multipolar neuron in the infrared organ of *Merimna atrata* (Coleoptera, Buprestidae)." *Arthropod Structure & Development* **30**(2): 99-111.

Schmitz, H., Schmitz, A., Trenner, S. and Bleckmann, H. (2002). "A new type of insect infrared organ of low thermal mass." *Naturwissenschaften* **89**(5): 226-229.

Schmitz, H. and Trenner, S. (2003). "Electrophysiological characterization of the multipolar thermoreceptors in the" fire-beetle" *Merimna atrata* and comparison with the infrared sensilla of *Melanophila acuminata* (both Coleoptera, Buprestidae)." *Journal of Comparative Physiology. A, Neuroethology, Sensory, Neural, and Behavioral Physiology* **189**(9): 715-722.

Sharp, W. E. (1918). "*Melanophila acuminata* in Berkshire." *Entomologist's Monthly Magazine* **54**: 244-245.

Sloop, K. D. (1937). "A revision of the North American buprestid beetles belonging to the genus *Melanophila* (Coleoptera, Buprestidae)", University of California Publications in Entomology.

Sowards, L. A., Schmitz, H., Tomlin, D. W., Naik, R. R. and Stone, M. O. (2001). "Characterization of beetle *Melanophila acuminata* (Coleoptera: Buprestidae) infrared pit organs by high-performance liquid chromatography/mass spectrometry, scanning electron microscope, and Fourier transform-infrared spectroscopy." *Annals of the Entomological Society of America* **94**(5): 686-694.

Strong, W. B., Bates, S. L. and Stoehr, M. U. (2001). "Feeding by *Leptoglossus occidentalis* (Hemiptera: Coreidae) reduces seed set in lodgepole pine (Pinaceae)." *The Canadian Entomologist* **133**(06): 857-865.

Takács, S., Bottomley, H., Andreller, I., Zaradnik, T., Schwarz, J., Bennett, R., Strong, W. and Gries, G. (2009). "Infrared radiation from hot cones on cool conifers attracts seed-feeding insects." *Proceedings of the Royal Society B: Biological Sciences* **276**(1657): 649.

Tamburini, M., Maresi, G., Salvadori, C., Battisti, A., Zottele, F. and Pedrazzoli, F. (2012). "Adaptation of the invasive western conifer seed bug *Leptoglossus occidentalis* to Trentino, an alpine region (Italy)." *Bulletin of insectology* **65**(2): 161-170.

Tepper, J. G. O. (1887). "Common native insects of South Australia: a popular guide to South Australian entomology". Adelaide, E.S. Wigg & Son.

Terashima, S. I., Goris, R. C. and Katsuki, Y. (1970). "Structure of warm fiber terminals in the pit membrane of vipers." *Journal of Ultrastructure Research* **31**(5-6): 494-506.

Tescari, G. (2001). "*Leptoglossus occidentalis*, coreide neartico rinvenuto in Italia (Heteroptera, Coreidae)." *Lavori Società Veneziana di Scienze Naturali* **26**: 3-5.

VanDyke, E. C. (1926). "Buprestid swarming." *Pan-Pacific Entomologist* **3**: 41.

Vondran, T., Apel, K. H. and Schmitz, H. (1995). "The infrared receptor of *Melanophila acuminata* De Geer (Coleoptera: Buprestidae): ultrastructural study of a unique insect thermoreceptor and its possible descent from a hair mechanoreceptor." *Tissue and Cell* **27**(6): 645-658.

Warren, J. W. and Proske, U. (1968). "Infrared receptors in the facial pits of the Australian python *Morelia spilotes*." *Science* **159**(3813): 439-441.

Werner, D. J. (2006). "*Leptoglossus occidentalis* nun auch in Deutschland." *Heteropteron* **23**: 38.

Wikars, L.-O. (1997), "Effects of forest fire and the ecology of fire-adapted insects", Department of Zoology Uppsala University

Wyniger, D., Moretti, M. and Duelli, P. (2002). "*Aradus lugubris* Fallen, 1807 (Hemiptera, Heteroptera, Aradidae) in a chestnut forest of Southern Switzerland after a fire experiment." *Mitteilungen der Schweizerischen Entomologischen Gesellschaft* **75**(1/2): 61-64.

Kapitel 2

Bimodal innervation of the infrared organ of *Merimna atrata* (Coleoptera, Buprestidae) by thermo- and mechanosensory units

Erik S. Schneider and Helmut Schmitz

Published in Arthropod Structure & Development (2013)
Accepted: 7 November 2012

2.1 Abstract

The pyrophilous Australian "fire-beetle" *Merimna atrata* approaches forest fires and possesses abdominal infrared (IR) -organs. Each round IR-organ is centrally innervated by a sensory complex showing two different units: one thermoreceptive multipolar neuron and one mechanosensitive chordotonal organ (CO) consisting of two scolopidia. We investigated the CO and found that the scolopidia are mononematic (the scolopale cap remains below the cuticle) and monodynal (one sensory cell per scolopidium). The dendrites of the scolopidia extend anteriorly and are attached by their caps to the cuticle about in the middle of the absorbing area. Structural features at the site of innervation suggest that the CO measures minute thermal deformations caused by IR-absorption. Therefore, an additional photomechanic component which has been described for the IR-receptors of pyrophilous jewel beetles of the genus *Melanophila* can be proposed for the IR-organ of *Merimna*. Because scolopidia can measure displacements in the subnanometer range, the CO may enhance the sensitivity of the IR-organ. The sensory complex of the *Merimna* IR-organ shows the same units and similar cuticular modifications as the tympanal organs of some noctuid moths. Therefore, a parallel evolution of insect ears and the *Merimna* IR-organ is discussed.

2.2 Introduction

The black-coloured Australian jewel beetle *Merimna atrata* (Coleoptera, Buprestidae) is distributed throughout Australia (Bellamy, 2002; Hawkeswood, 2007). *M. atrata* is the only species within the genus *Merimna* and commonly known as "fire-beetle" because it is attracted by forest fires (Tepper, 1887; Froggatt, 1907; Poulton, 1915). Under normal conditions this beetle is hard to find (Tepper, 1887; Poulton, 1915) but whenever there is a

fire beetles can easily be observed on the freshly burnt area (Tepper, 1887). Moreover, during the last decade one of us (H.S.) has observed this pronounced pyrophilous behaviour every year on freshly burnt areas in Western Australia.

After copulation the females deposit their eggs under the bark of burnt trees or shrubs of the family *Myrtaceae* (Hawkeswood and Peterson, 1982; Hawkeswood, 2007; Kitchin, 2009). Larvae develop inside the fire-killed trees and the next generation of adult beetles hatches one or two years later (Kitchin, 2009). The phenomenon that even small camp fires attract *M. atrata* and after big forest fires sometimes unbelievable numbers of beetles aggregate on the freshly burnt area (own observations) gives rise to the supposition that beetles can detect a fire from large distances. In this context it is of interest that *Merimna* has developed infrared (IR) -organs (Schmitz et al., 2000). Organs are located ventrolaterally in groups of two on the 2., 3., and sometimes also on the 4. abdominal sternite (Schmitz et al., 2001; Mainz et al., 2004). Each IR-organ possesses an amber and round IR-absorbing area which is slightly sunken into the surrounding dark brown cuticle. From inside the innervation of the organ is accomplished by a so-called sensory complex consisting of a single large multiterminal thermoreceptor and two scolopidia (Schmitz et al., 2001, referring to the scolopidia as chordotonal organs).

Up to now electrophysiological recordings have only been obtained from the single multiterminal thermoreceptive neuron which responds to an increase in temperature in a phasic-tonic way (Schmitz and Trenner, 2003). Based on these recordings, the IR-organs of *Merimna* seem not to be very sensitive: a threshold of about 400 $W \cdot m^{-2}$ has been determined (Schmitz and Trenner, 2003) which is much lower than the sensitivity of uncooled technical IR-sensors (e.g. $2 \cdot 10^{-2}$ $W \cdot m^{-2}$ for bolometer arrays, calculated from values given by Niklaus et al. (2007)) and also of thresholds reported for the IR-sensilla of pyrophilous buprestid beetles of the genus *Melanophila*. In *Melanophila* beetles a threshold of 0.6 $W \cdot m^{-2}$ has been determined by behavioural experiments (Evans, 1966) and a theoretical threshold of $1.3 \cdot 10^{-4}$ $W \cdot m^{-2}$ has been calculated based on the simulation of a big oil-tank fire which has attracted untold numbers of *Melanophila consputa* most probably from distances of more than 100 km (VanDyke, 1926; Schmitz and Bousack, 2012).

The much higher sensitivity of the *Melanophila* IR-receptors may be explainable by the innervation of the so-called photomechanic IR-sensilla of *Melanophila* beetles by ciliary mechanoreceptors (Vondran et al., 1995; Schmitz et al., 2007). This class of mechano-receptors shows the highest sensitivities known in the animal kingdom, capable of sensing displacements in the subnanometer range. In filiform hairs of crickets which are specialized

for sensing minute air movements the minimum amount of mechanical energy for the generation of an action potential is in the order of k_BT (k_B: Boltzmann constant, T: temperature), i. e. $4 \cdot 10^{-21}$ J at 300 ° K (Thurm, 1982; Shimozawa et al., 2003).

Because the possible role of the scolopidia in the IR-receptors of *Merimna* has not been further investigated we now made an attempt to characterize their morphology in order to classify them under the categories currently used (Field and Matheson, 1998) and to throw light on the evolutionary origin of the unique sensory complex. Of special interest is the mechanical coupling to the cuticle of the IR-absorbing area. Additionally, possible specializations of the cuticle as well as of the trachea underlying the IR-organs have to be investigated. The aim of the study is to link structural features found to the probable function of the complex. Based on these findings the possible role of the scolopidia in the IR-organ of *M. atrata* is discussed.

2.3 Material and Methods

2.3.1 Axonal in vivo filling of neurons

Male and female adult *Merimna atrata* were collected on freshly burnt areas near Perth, Western Australia in January 2012. For neuroanatomical studies of the innervation of the IR-organs, wings and legs of 16 beetles were removed. Then the ventral sternites bearing the IR-organs were excised and transferred immediately into a Sylgard-lined dish filled with insect saline (140mM NaCl, 5mM KCl, 4mM $CaCl_2$, 28mM Glucose, 5mM Hepes; pH 7.2-7.4; (Trimmer and Weeks, 1989)).

Axonal filling was performed according to Mason (1973): The cut end of the main nerve running to an IR-organ was isolated from the preparation by surrounding it with a little cup of Vaseline (Mason, 1973; Altman and Tyrer, 1980). After a short exposure of the stump to distilled water (1 min.), the Vaseline cup was filled with a drop of either 1M $CoCl_2$ (Pitman et al., 1972) or a 2:3 mixture of 1M $CoCl_2$: 1M $NiCl_2$ (Sakai and Yamaguchi, 1983) and sealed with additional Vaseline to prevent a leakage of the staining solution into the dish. Then the preparations were placed into a moist chamber and incubated for 24 - 48h in a refrigerator at 4°C.

2.3.1.1 Light microscopy

Cobalt/ nickel were precipitated by adding a few drops of concentrated ammonium sulphide (44%) to the insect saline. Afterwards the IR-organs were washed in fresh saline and fixed in Carnoy for 15 min (Mason, 1973; Sandeman and Okajima, 1973; Eibl, 1978; Altman and Tyrer, 1980). Then organs were dehydrated in ascending series of ethanol (30%, 50%, 70%, 80%, 90%, 96%, 100% for 10 min each) and finally cleared and stored in methyl salicylate (Mason, 1973; Honegger and Schürmann, 1975; Mücke and Lakes-Harlan, 1995; Bräunig, 1997) for up to 4 weeks. Whole mount preparations were viewed on depression slides using a Leitz DMRB/R microscope (Leica, Wetzlar Germany). Images of the stained neuronal structures were taken with a Nikon D5000 digital camera.

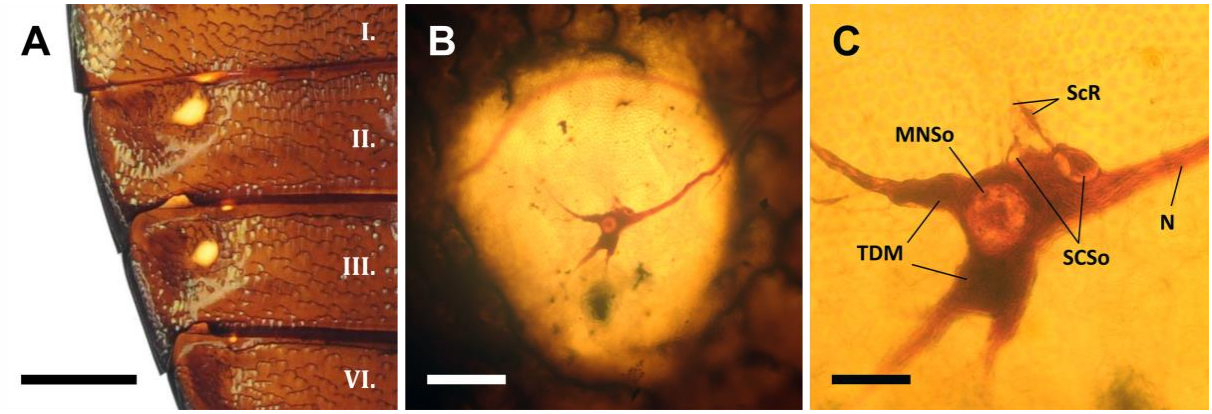

Fig. 2.1 Position and innervation of the abdominal IR-organs. **A)** Ventral view of the right half of the abdomen. IR-organs situated on the second (*II.*) and third (*III.*) sternite show amber IR-absorbing areas. Bar: 1 mm. **B)** Cobalt/nickel stained sensory complex innervating an IR-organ located on a third sternite. Bar: 200 µm. **C)** Sensory complex shown in B at higher magnification. *MNSo*: soma with nucleus of multipolar neuron, *TDM*: terminal dendritic mass of the multipolar neuron, *SCSo*: somata of the sensory cells of two scolopidia, *ScR*: scolopale rods, *N*: nerv. Bar: 50 µm. Orientation in A - C: top = anterior, bottom = posterior, left = lateral, right = medial.

To identify the relative position of the sensory components within the IR-organ, images of the whole mount axonal fillings were transferred into schematic drawings and overlaid with a 10x10 grid (resolution: quarter of a single grid) as template maintaining the original proportion. As reference point we used the center of the respective sensory neuron. Angles between the longitudinal axis of the scolopidium and the sagittal axis of the IR-organ (cf. dotted line in Fig. 2.3) were also measured as well as the dimensions of selected sensory components. It should be mentioned that it was not possible to differentiate between scolopale and ciliary root within a single scolopidium in light microscopical images. For convenience both structures were denoted in their entirety as scolopale/ scolopale rods in all micrographs,

schematic drawings and measurements based on axonal fillings (Figs. 2.1 – 2.3). Furthermore all measured values refer to two-dimensional projections of the sensory components and therefore may deviate from the real conditions. For image processing we used Inkscape 0.48, ImageJ 1.39p and Adobe Photoshop CS3.

For the production of semithin serial sections, whole mount preparations were embedded in Epon 812 resin according to Luft (1961). Semithin sections with a thickness of 0.5 – 1 µm were cut using an Om U3 microtome (C. Reichert, Austria) equipped with a diamond histo knife (Diatome AG, Biel, Switzerland). After mounting onto glass slides, sections were silver intensified according to the light insensitive method introduced by Davis (1982) and improved by Mesce et al. (1993) and counterstained with 0.1% toluidine blue/ borax (von Bohlen und Halbach and Dermietzel, 1999). Sections were investigated with a Leitz DMRB/R microscope (Leica, Wetzlar Germany) and images of relevant sections were taken with a Nikon D5000.

2.3.1.2 Transmission electron microscopy

In order to achieve a better preservation of the ultrastructure of the cobalt/ nickel-filled preparations, in some specimens the sulphide precipitation step was combined with a chemical fixation according to Tyrer and Bell (1974). For that purpose specimens were transferred directly from the moist chamber to glutaraldehyde fixative (4 ml 25% glutaraldehyde, 50ml A. dest, 0.15g KH_2PO_4, 0.87g Na_2HP0_4) to which a few drops of concentrated ammonium sulphide were added. After 5 min the specimens were transferred to fresh fixative for 2h before washing in cooled buffer (50ml A. dest, 0.15g KH_2PO_4, 0,87g Na_2HP0_4). In contrast to the protocol of Tyrer and Bell (1974) a post-fixation with osmium tetroxide (OsO_4) was performed, using a buffered solution of 1.5% OsO_4 for 30 min at 4°C. After washing in buffer specimens were embedded in Epon 812 resin according to Luft (1961). The protocol just mentioned resulted in an inadequate fixation and a very poor preservation of the ultrastructure. Nevertheless, TEM-micrographs are provided only in Figure 2.A1 in the Appendix, because relevant structures for the characterization of scolopidia can be identified anyway.

Ultrathin sections with a thickness of 100 nm were cut using an Om U3 microtome (C. Reichert, Austria) and a diamond histo knife (Diatome AG, Biel, Switzerland). Sections were transferred to single slot copper grids and double stained with uranyl acetate and lead citrate.

Sections were examined using a Zeiss EM 109 transmission electron microscope. Images were taken with an integrated roll-film camera.

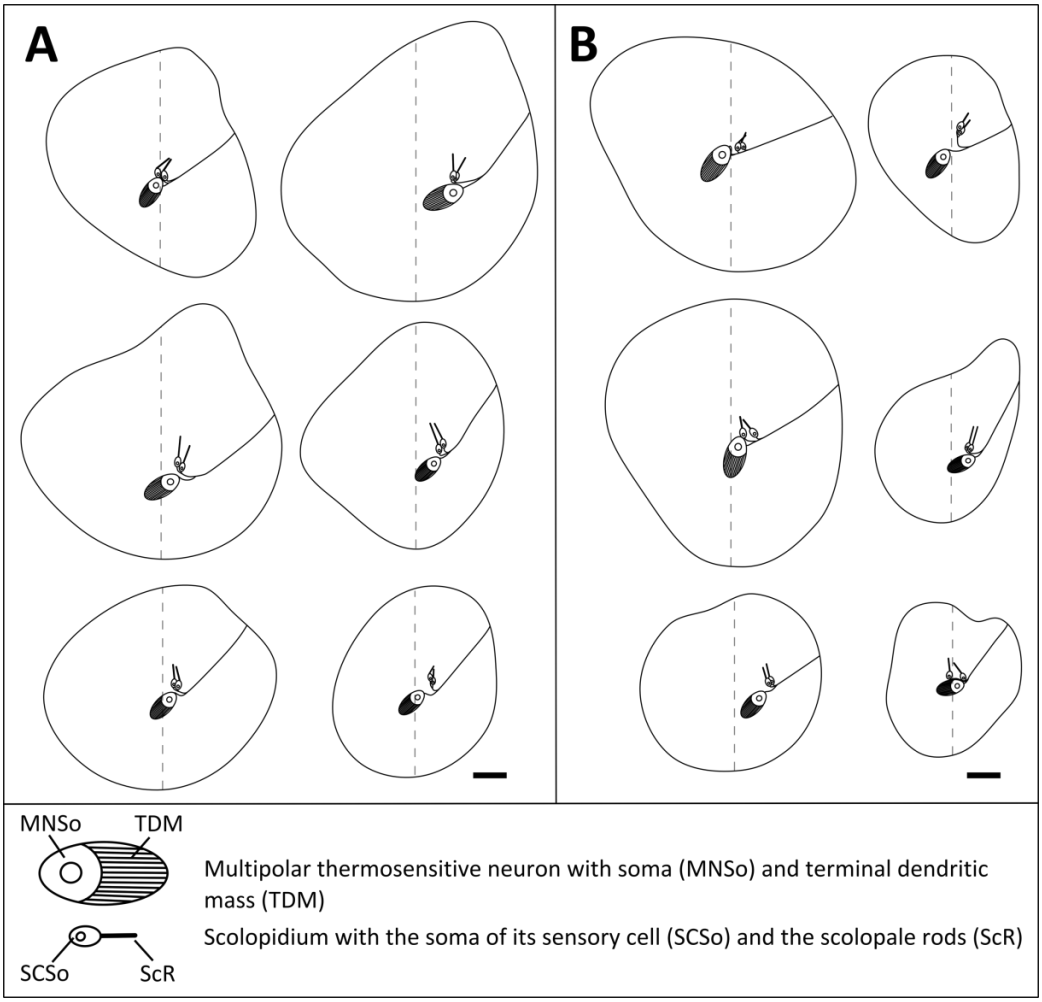

Fig. 2.2 Schematic drawing of the innervation pattern of n = 12 IR-organs from N = 10 beetles. Position of the sensory complexes consisting of a thermosensitive neuron and two scolopidia are indicated by corresponding symbols. Dotted lines represent sagittal axis of the beetles. Organs are located on the second (**A**) and third abdominal sternite (**B**). Bar: 100 µm. Orientation in A and B: top = anterior, bottom = posterior, left = lateral, right = medial.

2.3.2 Micro-computed tomography (micro-CT) and 3D-reconstruction

For three-dimensional reconstruction and morphometric measurements of the IR-organ of *Merimna atrata*, a micro-CT scan of an ethanol-fixed preparation of the second sternite was made. The specimen was fixed with 70% ethanol, stained in 1% iodine metal dissolved in 100% ethanol (Metscher, 2009) and scanned in an ethanol saturated atmosphere mounted in an arrangement according to Metscher (2009). The micro-CT scanner used was a Skyscan

1172 adjusted to 40kV source current resulting in an image pixel size of 0.67 µm (the micro-CT scan was made by RJL Micro & Analytic GmbH, Karlsdorf-Neuthard, Germany).
Image stacks were analysed and processed using the 3D-visualisation and analysis software Avizo (Version 6.0.0 standard edition, Visualization Sciences Group). The cuticular portion (absorbing area) of the IR-organ was labelled in every single image where the electron-dense outer exocuticular layer could be clearly distinguished from the underlying less dense layers of the meso- and endocuticle (results were verified with Mallory trichrome stain according to Weyda 1982). Based on the labeling a 3D model was rendered and morphometric measurements were executed.

2.4 Results

2.4.1 Position and outer morphology of the IR-organs

As already described previously (Schmitz et al., 2000), most beetles have two pairs of circular IR-organs located on the second and third sternite on the abdomen (Fig. 2.1 A). In some beetles a third pair of organs was found on the fourth sternite (Mainz et al., 2004). Organs are located close to the lateral edges of the curved sternites. As a result, in a flying beetle the IR-organs are directed to the ground in an angle of about 45°. Organs can be found in both sexes; so far no sexual dimorphism has been found.
A single organ has a roundish IR-absorbing area. Depending on the size of the beetle the absorbing area has a diameter of 400 - 800 µm. The absorbing area has a concave surface which reveals a honeycomb-like micro-structure at its bottom. As a special feature, the exocuticle of the absorbing area is not pigmented darkly and, therefore, appears in faint amber (Figs. 2.1 A - C).
From inside, each organ is innervated by a sensory complex situated in the center of the absorbing area (Figs. 2.1 B, 2.2; Tabs. 2.1, 2.A1). The sensory complex is tightly attached to the cuticle and is connected by a nerve to the central nervous system. The nerve of each IR-organ runs in an anterior central direction to its corresponding abdominal ganglion (Figs. 2.1 B - C, 2.2). The sensory complex consists of two different components: a thermoreceptive multipolar neuron and a chordotonal organ (CO, Figs. 2.1 C, 2.2, 2.3). Both components are aligned in a fixed manner. The soma and the terminal dendritic mass (TDM) of the multipolar neuron are arranged in continuation of the nerve. Therefore, an average angle of - 130 ° between the sagittal axis of the beetle and the longitudinal axis of the multipolar neuron was measured in the 12 organs investigated (Fig. 2.3 and Tab. 2.A1). Close to the basal region of

the soma of the multipolar neuron a small chordotonal organ (CO) was found. Each CO houses two scolopidia. Basically, the longitudinal axes of the scolopales of both scolopidia are aligned in anterior direction (Figs. 2.1 C, 2.2, 2.3).

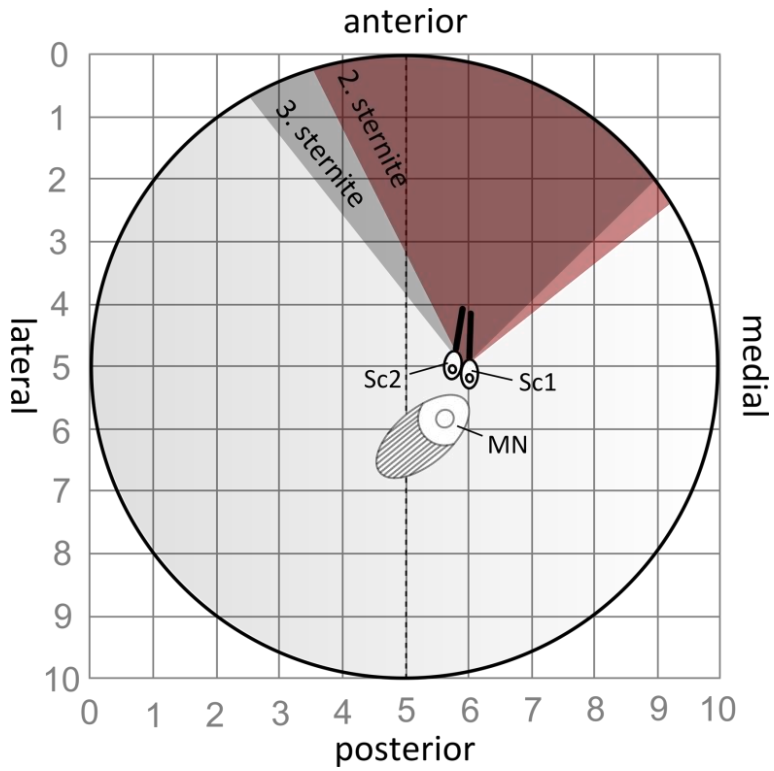

Fig. 2.3 General scheme of the innervation pattern of an IR-organ. Idealized IR-absorbing area superimposed by a 10 x 10 grid. Based on a total of 12 organs, mean values of the relative position, dimension and orientation of the two scolopidia (*Sc*) and the multipolar neuron (*MN*) are indicated (data shown in Tab. 2.1 and also in Tab. 2.A1 provided in the Appendix). Dotted line represents sagittal axis of the beetle. Red and gray areas indicate sectors in which the longitudinal axes of the scolopidia were oriented in the organs of the second and third sternites respectively.

Angles between the longitudinal axes of the scolopales of both scolopidia located on the 2. and 3. sternite and the sagittal axis of the beetle are given in Tab. 2.1 and Tab. 2.A1. Mean angle for the medial scolopidium 1 (cf. Fig. 2.3) was 7.5° in the IR-organ on the second sternite and -1.8° in the IR-organ on the third sternite (mean for all No. 1 scolopidia was 2.9°). Corresponding angles were 9.9° (2. sternite) and 10.1° (3. sternite) for the lateral scolopidium 2 (mean for all No. 2 scolopidia was 10.0°). Sectors containing all angles found are indicated in Figure 2.3 for the 2. and 3. sternite. A broad overlap between these two sectors exists.

Large air sacs enfold the whole sensory complex. This arrangement provides thermal isolation of the absorbing area and the attached sensory complex from the haemolymph in the abdominal cavity (cf. Fig. 2.5).

Tab. 2.1 Mean values (± standard deviation) of relative position and orientation of scolopidia related to the IR-absorbing area. The sagittal axis served as a reference line; angles between the sagittal axis and longitudinal axes of the scolopales are given. Positive angles turn clockwise; negative angles counterclockwise. Measurements based on the analysis of n = 12 organs shown in Fig. 2.2.

Position of IR-organ	Scolopidium 1 (Sc1)					Scolopidium 2 (Sc2)				
	Relative position of scolopidium (on a 10 x 10 grid)		Angle between longitudinal axis of scolopale and sagittal axis [degree]			Relative position of scolopidium (on a 10 x 10 grid)		Angle between longitudinal axis of scolopale and sagittal axis [degree]		
	x-axis	y-axis	min	max	mean ± stdv	x-axis	y-axis	min	max	mean ± stdv
2. sternite (n=6)	6.0 ± 0.47	5.5 ± 0.62	-26.9	33.9	7.5 ± 24.6	5.8 ± 0.54	5.2 ± 0.51	-20.9	51.5	9.9 ± 26.5
3. sternite (n=6)	6.0 ± 0.66	4.8 ± 0.47	-38.4	37.8	-1.8 ± 32.3	5.7 ± 0.77	4.8 ± 0.61	-16.0	45.7	10.1 ± 25.0
total (n=12)	6.0 ± 0.55	5.1 ± 0.62	-38.4	37.8	2.9 ± 27.8	5.8 ± 0.64	5.0 ± 0.59	-20.9	51.5	10.0 ± 24.6

2.4.2 Cuticular specialization of the innervation site

The cuticle above the sensory complex reveals some specializations. First, the soma of the multipolar neuron and the basal part of the TDM are situated beneath a shallow convex bulge (Figs. 2.4 A - C). Based on our morphometric measurements by means of the 3D reconstruction of the IR-absorbing area, it was found that the cuticle around the bulged area is about 35% thinner than the reference cuticle outside the IR-organ (cf. Fig. 2.4 C). However thinning is mainly related to a reduction in thickness of the endocuticle; the exocuticle generally retained its original thickness.

The CO spans the area where the bulge recurves to the central bottom of the absorbing area. Here, the largest curvature of the whole IR-absorbing area could be observed (Figs. 2.4 B, C).

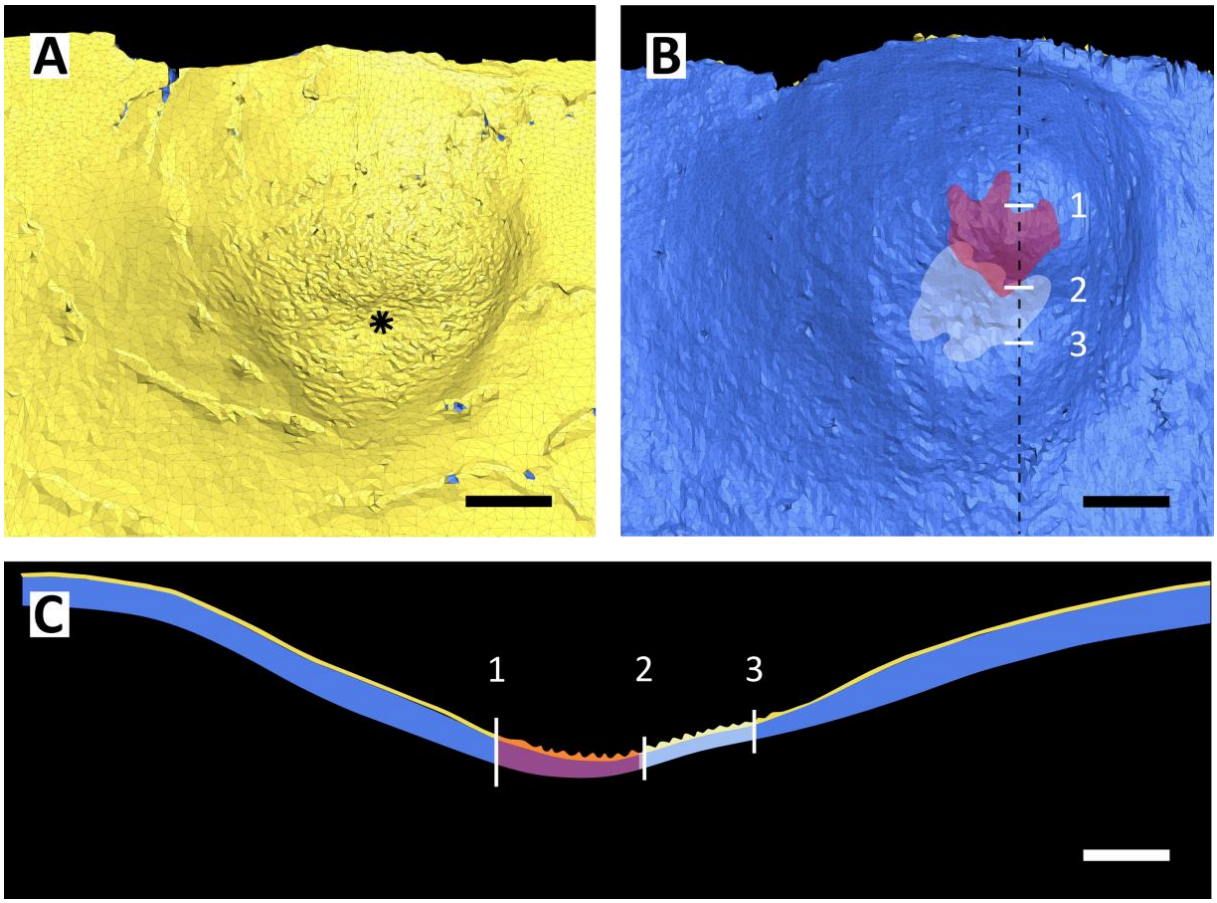

Fig. 2.4 IR-absorbing area (cuticular portion) of the *Merimna* IR-organ. 3D reconstruction based on micro-CT images. Exocuticle = yellow; meso-/endocuticle = blue. **A)** Exterior view. The curvature of the absorbing area is not uniform; it is steeper at the median and posterior edges. Approximately in the center of the absorbing area asterisk marks a slight elevation under which the sensory complex is attached to the cuticle. **B)** Interior view. White area indicates the area where the multipolar neuron has been identified in the organs examined (n=12); red area indicates the area where the chordotonal organ was located in n=12 IR-organs respectively (cf. Fig. 2.2, Tab. 2.1 and Tab 2.*A1*). Dotted line marks position of schematic cross-section shown in C. Bars: 100 µm. Orientation: top = anterior, bottom = posterior, left = lateral, right = medial. **C)** Schematic cross-section based on LM-micrographs. Region between point 2 and 3 shows the smallest thickness of the cuticle. This region is coincident with the bulged area under which the multipolar neuron is situated (white area). Red area marks the region spanned by the scolopidia of the CO. The scolopidia are attached to the inner cuticle in anterior position (point 1) with their somata situated under the cuticle near point 2. This region also exhibits the largest curvature of the absorbing area. Bar: 50 µm. Orientation: top = exterior, bottom = interior, left = anterior, right = medial.

2.4.3 Morphology of the scolopidia

In Figure 2.5, a reconstruction based on the ultrastructural findings (cf. Fig. 2.A1) is given. The vacuolar but otherwise electron dense scolopale cap and the scolopale rods are arranged in parallel and very close to the inner surface of the cuticle. Together they exhibit a total length of about 20 µm (Fig. 2.5). Fastening to the thin epidermal layer is accomplished by an attachment cell (Fig. 2.5; Fig. 2.A1 A - C). The long dendrite is subdivided by a ciliary constriction into a dendritic outer segment or cilium (cf. Figs. 2.A1 B, C) and an inner

dendritic segment (DIS, Figs. 2.A1 D - F); at the distal end of the DIS, two basal bodies arranged in tandem were identified (Fig. 2.5; Fig. 2.A1 D). Most of the dendrite is enclosed by the scolopale cell (Fig. 2.5; Fig. 2.A1 D). Ciliary rootlets originate from the basal bodies and extend inside the DIS to the soma region of the sensory cell (Fig. 2.5; Fig. 2.A1 D - F). The ciliary root possesses an overall length of about 30 µm (Fig. 2.5). Findings revealed that - according to the classification scheme of Moulins, 1976 (see also Field and Matheson, 1998) - the scolopidia can be classified as mononematic (a well-visible scolopale cap remains below the cuticle) and monodynal (only one sensory cell in a given scolopidium; cf. Fig. 2.5 and Tab. 2.2).

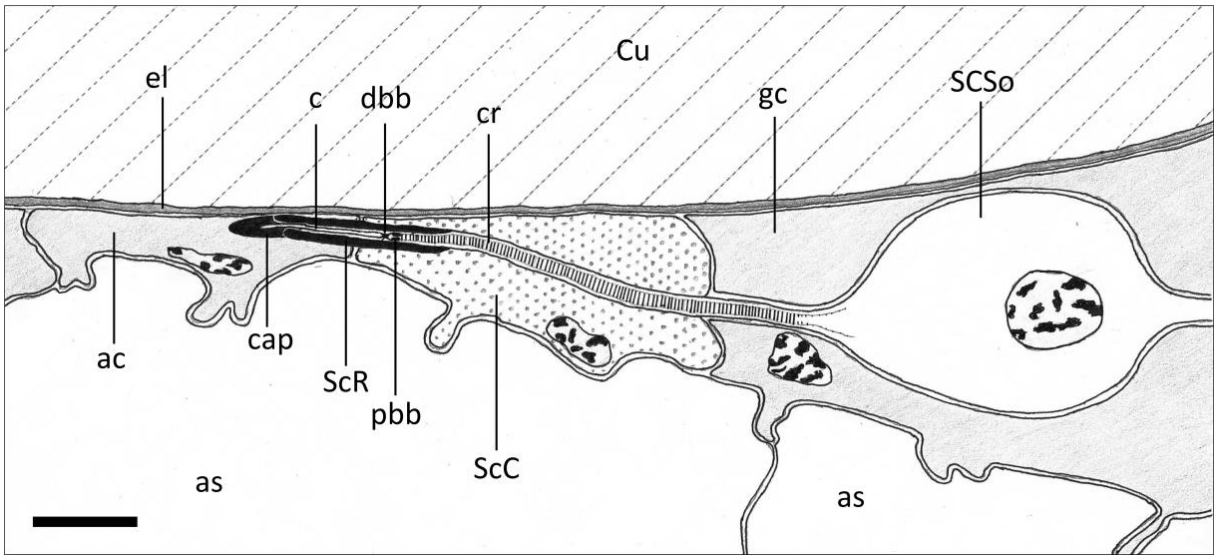

Fig. 2.5 Schematic drawing of a longitudinal section through a scolopidium in the *Merimna* IR-organ based on TEM-micrographs (cf. Fig. 2.A1). Bar: 10 µm. Orientation: top = exterior, bottom = interior, left = anterior, right = posterior. Abbreviations: *ac*: attachment cell, *as*: air sac, *c*: dendritic cilium, *cap*: scolopale cap, *cr*: ciliary rootlets, *Cu*: cuticle, *dbb*: distal basal body, *el*: epidermal layer, *gc*: glial cell, *pbb*: proximal basal body, *ScC*: scolopale cell, *ScR*: scolopale rods, *SCSo*: soma of the sensory cell.

2.5 Discussion

2.5.1 Bimodal innervation of the *Merimna* IR-organ

In previous work we already have described the innervation of the *Merimna* IR-organ by a multiterminal neuron and two COs. In these publications, however, the focus was on the structure and the possible function of the multiterminal thermoreceptive neuron. The presence of additional scolopidia has only been demonstrated by TEM-micrographs showing sections through the soma and the scolopale rods. Additional information relevant for the possible

function of the scolopidia like the type of the scolopidia, their spatial arrangement, and especially the exact locations and positions where the dendritic tips are attached was not available. Therefore, it remained doubtful whether the scolopidia are involved in the sensory surveillance of the IR-absorbing area because dendritic tips also could have been connected to structures below the cuticle like ligaments, muscles, or air sacs.

Our results show that the scolopidia can be classified as monomematic as well as monodynal scolopidia most probably with a Type 1 ciliary segment (cf. Tab. 2.2). The two scolopidia are tightly arranged in a parallel manner, in this way forming a simple CO. The attachment of the dendritic tips to the cuticle in the middle of the absorbing area makes it very probable that the CO serves for the measurement of mechanical events (Schmitz and Trenner, 2003) of the absorbing area. Accordingly, a role in IR-detection can be proposed (see below).

As an important outcome of our work it now can be stated that there is a bimodal innervation of the IR-organ of *Merimna atrata* by one thermoreceptive (the multiterminal neuron) and one mechanoreceptive unit (the CO).

Tab. 2.2 Classification scheme of chordotonal scolopidia based upon ultrastructural features (according to Moulins 1976 and Field & Matheson 1998). Features found in the present study are grayed out (cf. Fig. 2.5 and Fig. 2.A1).

non-connective	**connective**
• attachment cell(s) attach directly (or via intermediate cell) to hypodermis	• attachment cell(s) insert into connective tissue strand
monodynal	**heterodynal**
• single sensory cell	• more than one sensory cell
mononematic	**amphinematic**
• cap as apical extracellular structure; insertion site always subepidermal	• tube as apical extracellular structure; insertion site epidermal or subepidermal
Type 1 cilium	**Type 2 cilium**
• cilium of uniform diameter (except for ciliary dilation)	• diameter of cilium increases progressively into distal segment
• ciliary dilation (increase in diameter; containing electron dense material; 9x2+0 axoneme from base to apex)	• no ciliary dilation
• no distal segment	• distal segment (without 9x2+0 axoneme)
• cap as apical extracellular structure (rarely a tube)	• tube as apical extracellular structure

2.5.2 Possible IR-receptive function of the thermo- and mechanosensitive units

Electrophysiological experiments have shown that the large multiterminal neuron in the IR-organ of *Merimna* monitors the temperature of the absorbing area. An increase of the temperature caused by IR-absorption is coded by a phasic-tonic increase in the firing rate of this thermosensitive neuron (Schmitz and Trenner, 2003). This is in line with the morphological feature that the soma of the neuron and most of its dendritic region is situated under a little convex bulge in the center of the absorbing area where the cuticle reveals its lowest thickness (about 10 µm). The reduced thermal mass of the cuticle of the bulge ensures a larger increase in temperature.

In one of our previous publications we already have discussed a role of the scolopidia in IR-reception (Schmitz et al., 2001). However, due to the lack of important structural information, this remained very speculative. Based on the results of our current study a function of the CO in IR-reception becomes very likely. It can be proposed that heating of the IR-absorbing area will result in thermal expansion of the cuticle which causes mechanical strain and, therefore, minute deformations in the center of the absorbing area. As already pointed out in section *2.4.3 Cuticular specialization of the innervations site*, the CO spans the area where the largest curvature of the IR-absorbing area could be observed (cf. Figs. 2.4 B, C). Although it is not trivial to predict how the three-dimensional absorbing area will deform during a temperature increase, we suppose that deformation will be maximal at the spot where the CO is situated. Theoretically, the whole absorbing area will slightly sink in whereas the region of the little convex elevation will bulge out a little bit. In this case a length measurement at the bent transition zone between the bulge and the bottom of the absorbing area would be advantageous. Of course this has to be demonstrated by computer simulations and, ideally, also by direct measurements e.g. with a micro laser vibrometer.

Moreover it is well known that COs are especially sensitive to vibrations capable of measuring displacements of atomic dimensions. This has been impressively shown e.g. in subgenual organs in the proximal tibia of the cockroach leg (Shaw, 1994) and hearing organs in various insect species (Hoy and Robert, 1996). In spite of the fact that there is no experimental evidence that IR-absorption causes vibrations in the cuticle of the absorbing area we nevertheless want to mention this possibility. In principle heating of the cuticle could result in minute vibrations caused by a thermoacoustic effect (Dowling, 1995). However whether the increase in temperature is high enough to induce measurable acoustic waves and

the resulting frequencies are in an appropriate range to be perceived by the COs needs to be investigated further.

The question how the two sensory units are used in IR-perception is primarily related to the sensitivity of the units. Up to now no electrophysiological recordings from the COs have been obtained. One starting point of discussion would be that the two units cover two measurement ranges: one range with a high sensitivity and one with a lower sensitivity. In insect ears scolopidia are housed in chordotonal organs which act as "elaborate micromechanical transducers" (Field and Matheson, 1998) in some species capable of measuring displacements down to 0.6 nm (Michelsen and Larsen, 1985). Electrophysiological experiments have shown that the smallest temperature difference which can be resolved by the thermosensitive neuron in the IR-organ of *Merimna* is 0.08 °C. Therefore it has been proposed that the IR-receptive system of *Merimna* is not very sensitive and is mainly used when beetles have arrived at the fire. On freshly burnt areas the IR-organs enable the beetles to locate hot surfaces already in flight preventing to land on such a hot spot (Schmitz and Trenner, 2003). However, we propose that minute thermal expansions and/or thermoacoustically induced vibrations of the absorbing area in the sub-nanometer range most probably would already occur at rises in temperature below 0.08 °C. This would imply that there is an additional highly sensitive so-called photomechanic component in the IR-organ of *Merimna*. Photomechanic IR-sensilla have been described in the IR-organ of buprestid beetles of the genus *Melanophila* (Schmitz and Bleckmann, 1997; Klocke and Schmitz, 2012) and in some pyrophilous flat bug species of the genus *Aradus* (Schmitz et al., 2010). In brief, these IR-sensilla consist of tiny cuticular spheres with a diameter of about 12 µm which are innervated by single ciliary mechanoreceptive cells. IR-radiation absorbed by the sphere causes a small increase in internal pressure inside the fluidic core of the sphere which stimulates the outermost tip of the mechanosensitive cell. Because of the ultrahigh sensitivity of mechanosensitive cells mentioned in section *2.2. Introduction, Melanophila* beetles may be able to detect large fires by their IR-organs from distances of 130 km. At these distances radiation intensities have declined to $1.3 \cdot 10^{-4}$ $W \cdot m^{-2}$ corresponding to an energy level at a single IR-sensillum of only $1.3 \cdot 10^{-17}$ J (Schmitz and Bousack, 2012). If the CO inside the sensory complex of the IR-organ of *Merimna* should allow for a similar sensitivity, this beetle also could use its abdominal IR-receptors for the localization of remote fires.

2.5.3 Parallel evolution of insect ears (tympanal organs) and the *Merimna* IR-organ

In two of our previous publications we already have discussed the evolutionary scenario that the sensory complex of the *Merimna* IR-organ may have evolved from common proprioceptive mechanosensory systems (Schmitz et al., 2001; Mainz et al., 2004). This hypothesis becomes further corroborated by our recent study. In general, chordotonal organs (COs) are internal Type 1 mechanoreceptors distributed all over the insect body. They function as proprioreceptors between joints within limbs and body segments or as specialized mechanoreceptor organs (McIver, 1985; Field and Matheson, 1998). Examples for the latter are the hearing organs of many insects, where COs accomplish highly sensitive reception of airborne vibrations (Ewing, 1978; Boyan, 1993; Stumpner and von Helversen, 2001; Göpfert and Robert, 2002). One method to investigate the evolutionary origin of structures in segmented animals is to search for segmentally homologous structures in different segments of the same animal (Meier and Reichert, 1990). In consideration of this the second sternite of *Merimna* and in the majority of cases (98%) also the third sternite house a pair of fully developed IR-organs (see Mainz et al., 2004) consisting of a sensory complex and an IR-absorbing area. On the first sternite no cuticular specialization is present but in a previous work (Mainz et al., 2004) at least one multipolar neuron and two scolopidia have been identified also on the first and fourth sternite at the same position where the sensory complex of a fully developed IR-organ is situated. Additionally for the fourth sternite different transitional stages of cuticular specializations towards a fully developed IR-absorbing area have been described (Mainz et al., 2004). Considering these findings we propose that the IR-organ of *Merimna* has derived from a proprioceptive receptor complex consisting of a multipolar neuron and a chordotonal organ housing two single scolopidia.

For insect hearing organs the evolution from pre-existing proprioceptive chordotonal organs has been widely accepted. Examples are reviewed by Fullard & Yack (1993). One of the most prominent examples is the tympanic hearing organ of moths of the superfamily Noctuoidea which exhibits the same set of neuronal units which we have found in the IR-organ of *Merimna*. It consists of two uniterminal Type I sensory cells (A1 and A2) which are both monodynal and mononematic Type 1 scolopidia and one large multipolar (Type II) neuron (the B cell) (Spangler, 1988; Yack, 1992). It has been proposed that this tympanic organ derived from a proprioceptive complex (the wing-hinge complex) that monitors flight-induced movements of the thorax. In the course of peripheral modifications the chordotonal organ became sensitive to airborne vibrations whereas the multipolar neuron remained unmodified

and can still be found as ancestral remnant in the complex (Yack, 1992). The peripheral modifications that occurred during the evolution of the tympanic organ included i) thinning of the cuticle, ii) enlargement of tracheal sacs and iii) mechanical isolation from non-acoustic stimuli by the development of rigid supporting structures (Van Staaden et al., 2003; Yack, 2004).

Compared to the IR-organ of *Merimna* both sensory organs not only share the same components but also have undergone similar changes of their peripheral structures during their transition from proprioceptive stretch or vibration receptors into far-field exteroreceptors; one organ became sensitive to airborne vibrations the other to thermo-mechanical effects caused by the absorption of IR-radiation. However one difference is, that the multipolar neuron in the noctuid ear seems to remained unmodified while the multipolar neuron in the IR-organ of *Merimna* became thermosensitive (e.g. through the development of a TDM) and thus a basic functional component for the perception of IR-radiation. Concluding, an interesting parallel evolution of insect ears and the abdominal IR-organs of *Merimna atrata* seem to have taken place.

2.6 Acknowledgements

Mike Cantelo and Brian Inglis from the Department of Environment and Conservation (DEC), Wanneroo, Western Australia, enabled us to visit bush fires and gave us generous support. The Wildlife Branch of DEC (Perth) issued collecting and export permits. We are indebted to Anke Schmitz for all her help on the burnt areas and for many valuable discussions. We thank Horst Bleckmann for his continuous interest in our work and for providing lab space. Supported by a grant from the German Science Foundation (DFG) to H.S.

2.7 Literature

Altman, J. S. and Tyrer, N. M. (1980). Filling selected neurons with cobalt through cut axons. in *Neuroanatomical techniques: insect nervous system*. N. J. Strausfeld and T. A. Miller. New York, Springer**:** 373-402.

Bellamy, C. L. (2002). "Zoological Catalogue of Australia, Vol. 29.5 Coleoptera: Buprestoidea". Melbourne, CSIRO Publishing.

Boyan, G. S. (1993). "Another look at insect audition: the tympanic receptors as an evolutionary specialization to the chordotonal system." *Journal of insect physiology* **39**: 187-200.

Bräunig, P. (1997). "The peripheral branching pattern of identified dorsal unpaired median (DUM) neurones of the locust." *Cell and Tissue Research* **290**(3): 641-654.

Davis, N. T. (1982). "Improved methods for cobalt filling and silver intensification of insect motor neurons." *Biotechnic & Histochemistry* **57**(4): 239-244.

Dowling, A. P. (1995). "The calculation of thermoacoustic oscillations." *Journal of Sound and Vibration* **180**(4): 557-581.

Eibl, E. (1978). "Morphology of the sense organs in the proximal parts of the tibiae of *Gryllus campestris* L. and *Gryllus bimaculatus* De Geer (Insecta, Ensifera)." *Zoomorphology (Berlin)* **89**(3): 185-205.

Evans, W. G. (1966). "Perception of infrared radiation from forest fires by *Melanophila acuminata* De Geer (Buprestidae, Coleoptera)." *Ecology* **47**(6): 1061-1065.

Ewing, A. W. (1978). "The antenna of *Drosophila* as a 'love song' receptor." *Physiological Entomology* **3**: 33-36.

Field, L. H. and Matheson, T. (1998). Chordotonal organs of insects. in *Advances in Insect Physiology*. P. D. Evans. San Diego, CA, Academic Press. **Volume 27:** 1-228.

Froggatt, W. W. (1907). "Australian insects". Sydney, William Brooks & Co.

Fullard, J. H. and Yack, J. E. (1993). "The evolutionary biology of insect hearing." *Trends in Ecology & Evolution* **8**(7): 248-252.

Göpfert, M. C. and Robert, D. (2002). "The mechanical basis of *Drosophila* audition." *Journal of experimental biology* **205**(9): 1199.

Hawkeswood, T. J. (2007). "Review of the biology of the genus *Merimna* Saunders, 1868 (Coleoptera: Buprestidae)." *Calodema* **9**: 12-13.

Hawkeswood, T. J. and Peterson, M. (1982). "A review of the larval host records for Australian jewel beetels (Coleoptera: Buprestidae)." *Victorian Naturalist (Blackburn)* **99**: 240-251.

Honegger, H. W. and Schürmann, F. W. (1975). "Cobalt sulphide staining of optic fibres in the brain of the cricket *Gryllus campestris*." *Cell and Tissue Research* **159**(2): 213-225.

Hoy, R. R. and Robert, D. (1996). "Tympanal hearing in insects." *Annual Review of Entomology* **41**: 433-450.

Kitchin, D. R. (2009). "Notes on the biology of *Merimna atrata*." *Australian Entomologist* **36**(1): 1-2.

Klocke, D. and Schmitz, H. (2012). "Material properties of photomechanical infrared receptors in pyrophilous *Melanophila* beetles and *Aradus* bugs." *Acta Biomaterialia* **8**(9): 3392-3399.

Luft, J. H. (1961). "Improvements in epoxy resin embedding methods." *The Journal of biophysical and biochemical cytology* **9**(2): 409-414.

Mainz, T., Schmitz, A. and Schmitz, H. (2004). "Variation in number and differentiation of the abdominal infrared receptors in the Australian 'fire-beetle' *Merimna atrata* (Coleoptera, Buprestidae)." *Arthropod Structure & Development* **33**(4): 419-430.

Mason, C. A. (1973). "New features of the brain-retrocerebral neuroendocrine complex of the locust *Schistocerca* (Scudder)." *Cell and Tissue Research* **141**(1): 19-32.

McIver, S. B. (1985). Mechanoreception. in *Comprehensive Insect Physiology, Biochemistry and Pharmacology*. G. A. Kerkut and L. I. Gilbert. Oxford, Pergamon Press. **6:** 71 - 132.

Meier, T. and Reichert, H. (1990). "Embryonic development and evolutionary origin of the orthopteran auditory organs." *Journal of Neurobiology* **21**(4): 592-610.

Mesce, K. A., Amos, T. M. and Clough, S. M. (1993). "A light insensitive method for contrast enhancement of insect neurons filled with a cobalt-lysine complex." *Biotechnic & Histochemistry* **68**(4): 222.

Metscher, B. (2009). "MicroCT for comparative morphology: simple staining methods allow high-contrast 3D imaging of diverse non-mineralized animal tissues." *BMC physiology* **9**(1): 11.

Michelsen, A. and Larsen, O. N. (1985). Hearing and sound. in *Comprehensive Insect Physiology, Biochemistry, and Pharmacology*. G. A. Kerkut and L. I. Gilbert. New York, Pergamon Press**:** 495-556.

Moulins, M. (1976). Ultrastructure of chordotonal organs. in *Structure and function of proprioceptors in the invertebrates*. P. J. Mill. London, Chapman and Hall**:** 387-426.

Mücke, A. and Lakes-Harlan, R. (1995). "Central projections of sensory cells of the midleg of the locust, *Schistocerca gregaria*." *Cell and Tissue Research* **280**(2): 391-400.

Niklaus, F., Vieider, C. and Jakobsen, H. (2007). "MEMS-based uncooled infrared bolometer arrays: a review". *Photonics Asia 2007*, International Society for Optics and Photonics.

Pitman, R. M., Tweedle, C. D. and Cohen, M. J. (1972). "Branching of central neurons: intracellular cobalt injection for light and electron microscopy." *Science* **176**(4033): 412-414.

Poulton, E. B. (1915). "The habits of the Australian buprestid "fire-beetle" *Merimna atrata*, (Laporte and Gory)." *Transactions of the Entomological Society of London* **Part 1. (Proceedings)**: iii-iv.

Sakai, M. and Yamaguchi, T. (1983). "Differential staining of insect neurons with nickel and cobalt." *Journal of insect physiology* **29**(5): 393-397.

Sandeman, D. and Okajima, A. (1973). "Statocyst-induced eye movements in the crab *Scylla serrata*." *Journal of experimental biology* **59**(1): 17-38.

Schmitz, A., Schätzel, H. and Schmitz, H. (2010). "Distribution and functional morphology of photomechanic infrared sensilla in flat bugs of the genus *Aradus* (Heteroptera, Aradidae)." *Arthropod Structure & Development* **39**(1): 17-25.

Schmitz, A., Sehrbrock, A. and Schmitz, H. (2007). "The analysis of the mechanosensory origin of the infrared sensilla in *Melanophila acuminata* (Coeloptera; Buprestidae) adduces new insight into the transduction mechanism." *Arthropod Structure & Development* **36**(3): 291-303.

Schmitz, H. and Bleckmann, H. (1997). "Fine structure and physiology of the infrared receptor of beetles of the genus *Melanophila* (Coleoptera: Buprestidae)." *International Journal of Insect Morphology and Embryology* **26**(3–4): 205-215.

Schmitz, H. and Bousack, H. (2012). "Modelling a historic oil-tank fire allows an estimation of the sensitivity of the infrared receptors in pyrophilous *Melanophila* beetles." *PLoS ONE* **7**(5): e37627.

Schmitz, H., Schmitz, A. and Bleckmann, H. (2000). "A new type of infrared organ in the Australian" fire-beetle" *Merimna atrata* (Coleoptera: Buprestidae)." *Naturwissenschaften* **87**(12): 542-545.

Schmitz, H., Schmitz, A. and Bleckmann, H. (2001). "Morphology of a thermosensitive multipolar neuron in the infrared organ of *Merimna atrata* (Coleoptera, Buprestidae)." *Arthropod Structure & Development* **30**(2): 99-111.

Schmitz, H. and Trenner, S. (2003). "Electrophysiological characterization of the multipolar thermoreceptors in the" fire-beetle" *Merimna atrata* and comparison with the infrared sensilla of *Melanophila acuminata* (both Coleoptera, Buprestidae)." *Journal of Comparative Physiology. A, Neuroethology, Sensory, Neural, and Behavioral Physiology* **189**(9): 715-722.

Shaw, S. R. (1994). "Re-evaluation of the absolute threshold and response mode of the most sensitive known "vibration" detector, the cockroach's subgenual organ: a cochlea-like displacement threshold and a direct response to sound." *Journal of Neurobiology* **25(9)**: 1167-1185.

Shimozawa, T., Murakami, J. and Kumagai, T. (2003). Cricket wind receptors: Thermal noise for the highest sensitivity known. in *Sensors and Sensing in Biology and Engineering*. F. G. Barth, J. A. C. Humphrey and T. W. Secomb. New York, Springer**:** 145-157.

Spangler, H. G. (1988). "Moth hearing, defense, and communication." *Annual Review of Entomology* **33**(1): 59.

Stumpner, A. and von Helversen, D. (2001). "Evolution and function of auditory systems in insects." *Naturwissenschaften* **88**: 159-170.

Tepper, J. G. O. (1887). "Common native insects of South Australia: a popular guide to South Australian entomology". Adelaide, E.S. Wigg & Son.

Thurm, U. (1982). Grundzüge der Transduktionsmechanismen in Sinneszellen. Mechano-elektrische Transduktion. in *Biophysik*. W. Hoppe, W. Lohmann, H. Markl and H. Ziegler. Berlin, Springer**:** 681-696.

Trimmer, B. A. and Weeks, J. C. (1989). "Effects of nicotinic and muscarinic agents on an identified motoneurone and its direct afferent inputs in larval *Manduca sexta*." *Journal of experimental biology* **144**(1): 303.

Tyrer, N. M. and Bell, E. M. (1974). "The intensification of cobalt-filled neurone profiles using a modification of Timm's sulphide-silver method." *Brain Research* **73**(1): 151-155.

Van Staaden, M. J., Rieser, M., Ott, S. R., Pabst, M. A. and Römer, H. (2003). "Serial hearing organs in the atympanate grasshopper *Bullacris membracioides* (Orthoptera, Pneumoridae)." *Journal of Comparative Neurology* **465**(4): 579-592.

VanDyke, E. C. (1926). "Buprestid swarming." *Pan-Pacific Entomologist* **3**: 41.

von Bohlen und Halbach, O. and Dermietzel, R. (1999). in *Methoden der Neurohistologie*. O. von Bohlen und Halbach and R. Dermietzel. Heidelberg, Spektrum Verlag.

Vondran, T., Apel, K. H. and Schmitz, H. (1995). "The infrared receptor of *Melanophila acuminata* De Geer (Coleoptera: Buprestidae): ultrastructural study of a unique insect thermoreceptor and its possible descent from a hair mechanoreceptor." *Tissue and Cell* **27**(6): 645-658.

Weyda, F. (1982). "Adaptation of Mallory's trichrome stain to insect tissue epoxy sections." *Zeitschrift für mikroskopisch-anatomische Forschung* **96**(1): 79-80.

Yack, J. E. (1992). "A multiterminal stretch receptor, chordotonal organ, and hair plate at the wing-hinge of *Manduca sexta*: unravelling the mystery of the noctuid moth ear B cell." *Journal of Comparative Neurology* **324**(4): 500-508.

Yack, J. E. (2004). "The structure and function of auditory chordotonal organs in insects." *Microscopy research and Technique* **63**(6): 315-337.

2.8 Appendix

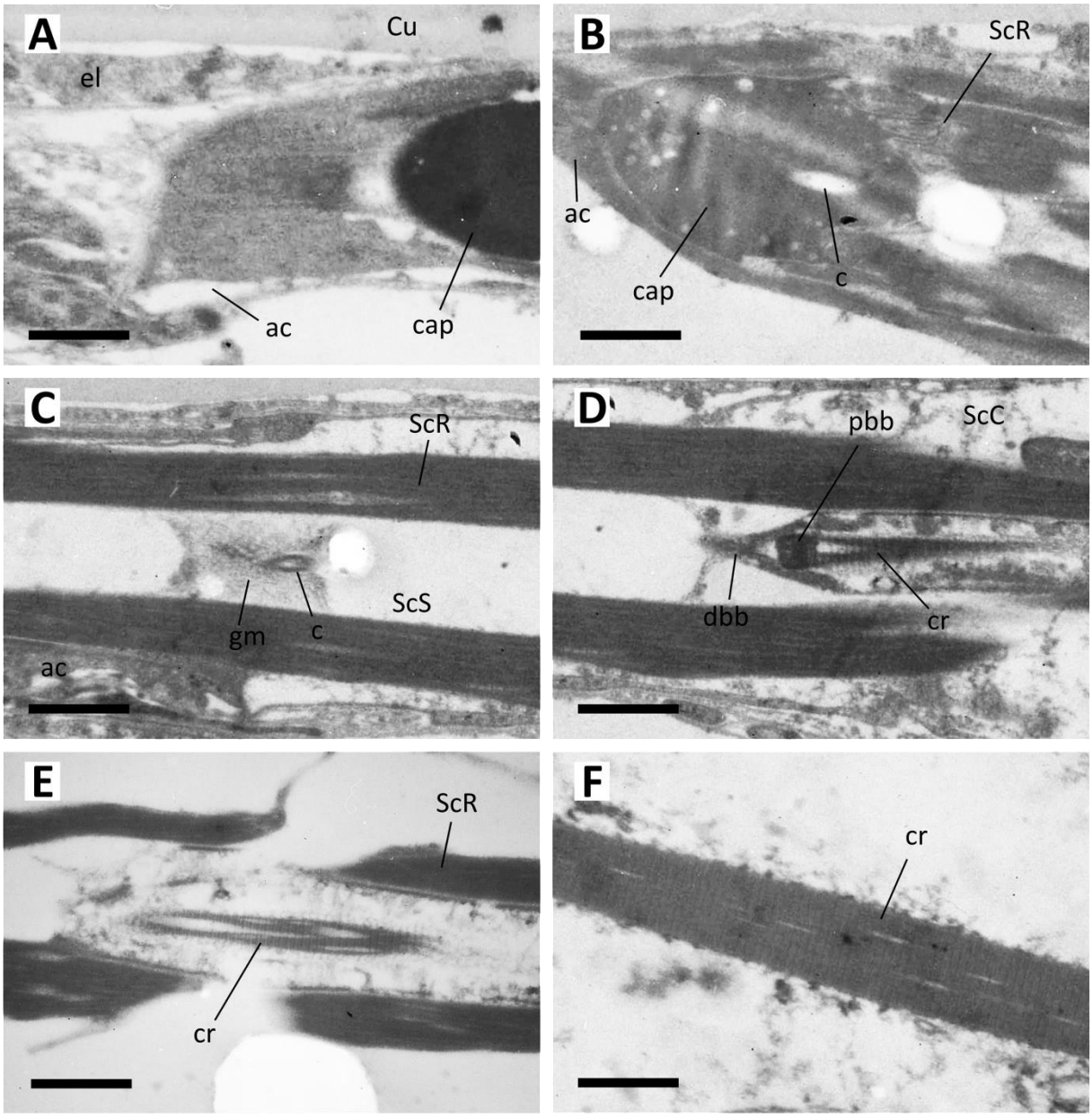

Fig. 2.A1 TEM-micrographs showing ultrastructural features of the scolopidia in the *Merimna* IR-organ. Preceding axonal filling and subsequent precipitation with ammonium sulphide resulted in poor preservation of the ultrastructure. However, relevant structures for the characterization of the present type of scolopidia could be identified. **A)** Connection of the scolopale cap to the cuticle via a subepidermal attachment cell. **B)** Detail of the scolopale cap showing its vacuolar consistence; dendritic cilium inserts distally into the cap. **C)** More proximal, the cilium is surrounded by the scolopale space and the scolopale rods. **D)** Transition zone between cilium and dendritic inner segment (ciliary constriction); from the distal basal body the cilium extends distally, and from the proximal basal body the cross-banded ciliary root extends proximally into the dendritic inner segment. **E)** Distal part of the dendritic inner segment showing ciliary rootlets enclosed by the scolopale rods. **F)** Proximal part of the dendritic inner segment showing densely packed ciliary rootlets. Bars in A – F: 1µm. Abbreviations: *ac:* attachment cell, *c*: dendritic cilium, *cap:* scolopale cap, *cr*: ciliary rootlets, *Cu*: cuticle, *dbb*: distal basal body, *el*: epidermal layer, *gm*: granular material, *pbb*: proximal basal body, *ScC*: scolopale cell, *ScR*: scolopale rods, *ScS*: scolopale space.

Tab. 2.A1 Dimensions and relative positions of the sensory components of n = 12 IR-organs from N = 10 *Merimna atrata* beetles. Measurements are based on two-dimensional projections of these components. The given values for the length of the scolopale (*ScR*) do not differentiate between the scolopale and the ciliary root (for detailed information see *2.3.1.1 Light microscopy*). Abbreviations: *MN*: multipolar neuron, *ScR*: scolopale/ scolopale rods, *SCSo*: soma of a scolopidium's sensory cell.

Sample/ position	IR-absorbing area [µm]	Multipolar neuron (MN)					Scolopidium 1 (Sc1)						Scolopidium 2 (Sc2)					
		relative position					relative position		SCSo		ScR		relative position		SCSo		ScR	
	diameter [µm]	x-axis	y-axis	length [µm]	width [µm]	angle between longitudinal axis of MN and sagittal axis [degree]	x-axis	y-axis	length [µm]	width [µm]	length [µm]	angle between longitudinal axis of scolopale and sagittal axis [degree]	x-axis	y-axis	length [µm]	width [µm]	length [µm]	angle between longitudinal axis of scolopale and sagittal axis [degree]
7/ 2.sternite	646	4.5	6.25	100	49	-145.7	5.25	5.5	31	18	41	33.9	5.0	5.25	27	18	50	51.5
8/ 2.sternite	529	5.0	6.0	94	47	-132.8	6.0	4.75	22	14	25	2.7	6.0	4.5	24	14	27	30.8
9/ 2.sternite	591	5.75	6.5	95	48	-133	6.5	5.5	28	18	51	-26.9	6.25	5.75	27	18	68	-20.9
10/ 2.sternite	758	6.0	6.0	127	62	-114.6	6.5	6.25	27	15	50	29.4	6.5	5.25	29	19	51	-1.9
11/ 2.sternite	698	5.0	7.0	116	57	-120.8	6.0	6.0	27	17	54	20.1	5.75	5.75	30	19	61	5.7
12/ 2.sternite	617	5.25	5.75	100	49	-135	5.75	4.75	28	19	43	-14.3	5.5	4.75	26	16	43	-5.7
mean (n=6)/ 2.sternite	639.8	5.3	6.3	105.3	52.0	-130.3	6.0	5.5	27.2	16.8	44.0	7.5	5.8	5.2	27.2	17.3	50.0	9.9
stdv (n=6)/ 2.sternite	80.7	0.5	0.4	13.2	6.1	11.0	0.5	0.6	2.9	1.9	10.5	24.6	0.5	0.5	2.1	2.0	14.3	26.5
1/ 3.sternite	682	4.5	5.25	126	63	-142.7	5.5	4.5	24	16	33	23.9	5.25	4.5	25	18	32	45.7
2/ 3.sternite	736	5.25	6.25	126	63	-132.2	6.0	5.25	30	20	37	-38.4	5.5	5.25	30	20	35	-10.4
3/ 3.sternite	492	4.25	6.25	100	50	-143	5.5	4.25	27	16	29	37.8	5.5	3.75	28	19	31	31.8
4/ 3.sternite	472	5.75	6.5	88	43	-114.8	6.25	5.5	23	15	56	15.9	6.0	5.5	24	13	50	15.2
5/ 3.sternite	520	6.25	6.0	99	48	-138	7.25	4.75	25	14	39	-13	7.0	4.75	25	16	35	-16.0
6/ 3.sternite	409	5.0	5.5	83	44	-103.7	5.75	4.75	24	16	38	-36.7	4.75	4.75	24	18	39	-5.9
mean (n=6)/ 3.sternite	551.8	5.2	6.0	103.7	51.8	-129.1	6.0	4.8	25.5	16.2	38.7	-1.8	5.7	4.8	26.0	17.3	37.0	10.1
stdv (n=6)/ 3.sternite	128.2	0.8	0.5	18.5	9.0	16.2	0.7	0.5	2.6	2.0	9.3	32.3	0.8	0.6	2.4	2.5	7.0	25.0
mean (n=12)/ 2.&3.sternite	595.8	5.2	6.1	104.5	51.9	-129.7	6.0	5.1	26.3	16.5	41.3	2.9	5.8	5.0	26.6	17.3	43.5	10.0
stdv (n=12)/ 2.&3.sternite	112.0	0.6	0.5	15.3	7.3	13.2	0.5	0.6	2.8	1.9	9.9	27.8	0.6	0.6	2.3	2.1	12.7	24.6

Kapitel 3

Vorwort

In Kapitel 2 konnten Anzahl, relative Position und Lagebeziehung der einzelnen sensorischen Komponenten im IR-Organ von *Merimna atrata* beschrieben werden. Dabei zeigte sich, dass der sensorische Komplex in direkter Nachbarschaft zu dem thermosensitiven multipolaren Neuron ein einzelnes Chordotonalorgan, bestehend aus zwei mononematischen monodynalen Skolopidien, beinhaltet. Die Position der Anheftungsstellen der Skolopidien in der Mitte der absorbierenden Fläche und erste Ergebnisse zu den dort vorliegenden strukturellen Anpassungen der Cuticula (z.B. Reduktion der Dicke) deuten auf eine Beteiligung des Chordotonalorgans bei der IR-Rezeption hin. Eine sich aus den Ergebnissen ergebene Hypothese ist, dass das Chordotonalorgan als photomechanische Komponente in die IR-Rezeption involviert ist und ggf. den Funktionsumfang des thermosensitiven multipolaren Neurons erweitert, z.B. durch Vergrößerung des Dynamikbereichs und der Sensitivität, oder durch Verringerung der Ansprechzeiten. Um dies zu testen, wurden vergleichende Untersuchungen zu strukturellen und mechanischen Eigenschaften der abdominalen Cuticula, insbesondere der absorbierenden Fläche, durchgeführt. Auf Grundlage dieser Ergebnisse wurden schließlich mit Hilfe von Finite-Element-Simulationen die thermomechanischen Eigenschaften der absorbierenden Fläche analysiert und in Hinblick auf die resultierende Performance der Skolopidien als potentielle photomechanische IR-Rezeptoren diskutiert.

Thermomechanical properties of the stimulus transducing cuticle in the infrared organ of *Merimna atrata* (Coleoptera, Buprestidae)

Erik S. Schneider and Helmut Schmitz

Published in Journal of Morphology
Accepted: 20 March 2014

3.1 Abstract

The pyrophilous Australian "fire-beetle" *Merimna atrata* strongly depends on the occurrence and localization of forest fires for its reproduction. As a special adaptation to its unusual biology, elaborate infrared (IR) organs have evolved in this species. The IR-organs consist of a specialized cuticular portion – the absorbing area – innervated by a sensory complex. The sensory complex contains a thermosensitive multipolar neuron with a specialized dendritic region – the terminal dendritic mass – and a mechanosensitive unit represented by a chordotonal organ.

Evidence for the IR-receptive function so far has only been provided for the multipolar neuron. Based on morphological data it has been speculated that the chordotonal organ could also be involved in IR-reception by measuring minute thermal deformations of the absorbing area.

To test this hypothesis we investigated structural features like cuticle thickness, reduced Young's modulus and hardness of the absorbing area. The results were used in finite element simulations to analyze the thermomechanical behavior and performance of the IR-organ. Our findings indicate that considerable thermal deformation of the absorbing area occurs, supporting the hypothesis that the chordotonal organ could function as photomechanical IR-receptor. Interestingly, at the innervation site of the chordotonal organ the lowest relative displacements of the absorbing area were found. This may indicate that the chordotonal organ as putative photomechanic IR-receptor has not been adapted according to the requirements of highest sensitivity. Probable benefits of the bimodal innervation by a thermo- and a mechanosensory unit and their possible interaction for an improved performance of the IR-organ are discussed.

3.2 Introduction

The “fire-beetle” *Merimna atrata* (Buprestidae) is the only known species within the buprestid genus *Merimna* and is endemic to Australia (Bellamy, 2002). This pyrophilous (fire-loving) jewel beetle is attracted by forest fires (Tepper, 1887; Froggatt, 1907; Poulton, 1915). *Merimna* has been reported to be highly dependent on the occurrence of forest fires for its reproduction: mating and oviposition exclusively take place on freshly burnt areas (Hawkeswood and Peterson, 1982). The eggs are deposited under the bark mainly at the base of trees and shrubs of the family *Myrtaceae* (Hawkeswood and Peterson, 1982; Hawkeswood, 2007; Kitchin, 2009). Larvae develop inside the burnt wood and the new generation of adult beetles emerges one, two or even more years later (Kitchin, 2009). Considering the great importance of forest fires for the reproductive cycle of *Merimna*, it seems not surprising that the beetle has developed unique IR-organs, not only for reliable and safe navigation on the freshly burnt area, but probably also for the detection of remote forest fires. As it has been proposed recently, IR-radiation seems to be the most suitable cue for the detection of forest fires over long distances (Schmitz and Bousack, 2012).

In *Merimna atrata* one pair of IR-organs is located ventrolaterally on the second, third and sometimes also on the fourth abdominal sternite each (Mainz et al., 2004) (Fig. 3.1). The IR-organs consist of an external cuticular portion – the radiation absorbing area – and an internal sensory complex innervating this area (Schmitz et al., 2001).

The absorbing area is a roundish invaginated area of the cuticle. Depending on the size of the beetle, the average diameter is about 500 µm and the depth is about 150 µm (Schneider and Schmitz, 2013). It is characterized by the following special features: i) a lack of dark pigments within the exocuticle resulting in a yellowish color of the IR-organ in contrast to the glossy dark brown color of ‘normal’ cuticle surrounding the absorbing area (Schmitz et al., 2001) (Fig. 3.1); ii) a honeycomb-like micro-structure in the central region of the absorbing area (Schmitz et al., 2000); iii) and a reduced thickness of the cuticle in the center (Schneider and Schmitz, 2013) under which the sensory complex is situated. It can be proposed that the lack of dark pigments in the cuticle of the absorbing area significantly reduces the absorption of visible light and subsequent heating, because dark pigments like melanins have their absorption maxima within the range of visible light (Stark et al., 2005). On the other hand IR-absorption is not reduced, because mid-IR-radiation in general is strongly absorbed by the biopolymers of the cuticle (proteins, chitin) (Vondran et al., 1995). Analysis of different cuticular regions in *Melanophila acuminata*, i.e. outer eye layer, wing vein, coxal capsule and

the IR-sensory pit organ, of which the latter also lacks dark pigments within the exocuticle, revealed similar IR-spectra with the same local minima and maxima. Absorption maxima were obtained in the range of 2.75 – 3.5 µm (Vondran et al., 1995; Sowards et al., 2001).

The sensory complex comprises a large multipolar Type1 neuron with a specialized dendritic region called TDM (terminal dendritic mass) and in close proximity to that a chordotonal organ (CO), represented by two scolopidia (Schneider and Schmitz, 2013). The thermoreceptive function of the multipolar neuron has been confirmed by electrophysiological recordings (Schmitz and Trenner, 2003). The experiments showed that the neuron responds in a phasic-tonic way with an increase of its spike frequency to increasing temperature. The thermoreceptive modality of the multipolar neuron has led to the technical classification of the *Merimna*-IR-organ as a bolometer: incoming IR-radiation is absorbed by the cuticle of the absorbing area and the resulting increase in temperature is measured by the underlying thermosensor. However, because of the rather low threshold sensitivity of 400 $W \cdot m^{-2}$, determined in the electrophysiological experiments mentioned above (Schmitz and Trenner, 2003), it has been concluded that the *Merimna*-IR-organ is not suitable for remote sensing of forest fires but rather for short-distance sensing, e.g. to prevent the beetle from landing on hot surfaces when flying over a freshly burnt area (Schmitz and Trenner, 2003). In comparison, threshold sensitivities reported for the photomechanic IR-receptors in *Melanophila acuminata*, which is thought to use IR-cues to approach fires over several kilometers, range between 50 $W \cdot m^{-2}$ (Schmitz and Bleckmann, 1998; Schmitz and Trenner, 2003) and $1.3 \cdot 10^{-4}$ $W \cdot m^{-2}$ (Schmitz and Bousack, 2012). More recent investigations have concentrated on the CO as a second, putative receptor system also involved in IR-perception, which could enable the beetle to detect also remote forest fires (Schneider and Schmitz, 2013). So far unambiguous electrophysiological recordings from the CO are missing. In some of the existing recordings (Schmitz and Trenner, 2003), potentials with much smaller amplitudes have been observed after stimulus onset apart from the large spikes generated by the multipolar neuron. These probably represented responses from the CO. However, due to the improper recording technique, i.e. inserting a metal electrode directly into the cuticle of the IR-organ, and the resulting unreliability in recording, the small potentials have not been further investigated.

The CO represents a mechanosensory unit, consisting of two mononematic monodynal scolopidia, located in direct proximity to the multipolar neuron in the center of the absorbing area (Schneider and Schmitz, 2013). Just like other scolopidia of this type, they are supposed to respond to axial stress or bending (Field and Matheson, 1998). In general scolopidia

function as proprioceptors or specialized mechanoreceptor organs, capable of detecting mechanical displacements over several orders of magnitude (Field and Matheson, 1998) down to 0.6 nm (Michelsen and Larsen, 1985). Therefore it has been proposed that the absorption of IR-radiation could also lead to minute deformations of the absorbing area with its highest extend in the central region, corresponding to the attachment site of the CO. The CO could perceive these mechanical events and thus probably extend the measuring range, thereby increasing the sensitivity of the IR-organ (Mainz et al., 2004; Schneider and Schmitz, 2013).
The aim of the present study is to test if maximum relative displacement of the absorbing area takes place at the attachment site of the CO. For that purpose we investigated the structural composition of the cuticle (thickness of the different cuticular layers) and its mechanical properties (reduced Young's modulus and hardness of the different cuticular layers) at the absorbing area and at normal cuticle. Based on these data we analyzed the influence of different geometrical and physical parameters on the thermomechanical behavior of the absorbing area by using finite element simulations and by testing an enlarged 3D model of the absorbing area.

3.3 Material and Methods

3.3.1 Animals

Adult *Merimna atrata* were collected on freshly burnt areas in Western Australia (near Perth) in January 2012 and 2013 (Collection permits issued by the Western Australian Department of Environment and Conservation: SF008424, SF009022). Animals were kept for several weeks in plastic boxes and fed with raisins and peanuts. Water was given ad libitum. Conducted experiments complied with the Principles of animal care of the National Institute of Health and also with the laws of Germany (Tierschutzgesetz).

3.3.2 Specimen preparation

After freezing overnight to about -18°C, beetles were air dried at room temperature. Afterwards IR-organs of the second and third abdominal sternites were carefully excised together with about 0.5 mm of surrounding cuticle. Residual tissue was removed from the cuticle manually and by sonicating in water for several minutes. Specimens were air dried again and embedded in Epoxy Resin L (Toolcraft Conrad Electronic SE, Germany) in standard embedding forms.

After curing for 24 hours at 60° C semithin sections (1µm thick) were cut from the embedded specimens using a diamond histo knife (Diatome AG, Switzerland) and an OM U3 microtome (C. Reichert, Austria). From samples intended for nanoindentation and scanning probe microscopy, several ultrathin sections with a thickness of about 100 nm were cut in order to obtain surfaces as smooth as possible.

3.3.3 Histological characterization

Characterization of the different cuticular layers was achieved by adopting Mallory's trichrome stain which has already been adapted to insect tissue by Weyda (1982). As result of the staining protocol the endocuticle appears blue, the mesocuticle red and because the exocuticle does not stain, it appears in faint yellow. In *Merimna* only the unpigmented cuticle could be stained. The normal dark pigmented exocuticle surrounding the IR-organs remained its dark brown color. Stained sections were examined with a Leitz DM RB/R microscope (Leica, Germany). Digital images were taken with a Nikon D5000 digital camera.

3.3.4 Stereological measurements

For stereological measurements of the different cuticular layers 5 IR-organs from 3 beetles were investigated. One organ was taken from the second sternite of a beetle with a body length of only 14 mm, another organ from the second sternite of an individual with a total length of 30 mm and three organs (one from the second and two from the third sternite) from a beetle with a body length of about 25 mm. For each organ a continuous series of semithin sections (1 µm thick) was cut. Sections were cut perpendicular to the anterior/posterior axis (cf. Fig. 3.1 B, C). Every 55µm, five consecutive sections were taken for further processing. After applying Mallory's trichrome stain, every fifth of the processed sections (or if damaged the preceding one) was photographed and the thickness of the different cuticular layers was measured. For every section two regions were analyzed, one in the center of the absorbing area ('IR'), the other one in the region of 'normal' cuticle ('Ref') surrounding the IR-organ either in medial ('Ref medial') or lateral position ('Ref lateral') serving as reference values (cf. Fig. 3.1 C). For regions 'IR' and 'Ref', cuticle thickness (d [µm]) was measured ten times (n=10) for exo-, meso- and endocuticle respectively. To achieve unbiased measurements, we used a systematic random sampling method (Howard and Reed, 1998). A grid with ten parallel lines with a spacing of 10 µm between each line was 'thrown' randomly onto the

regions of interest. Measurements of cuticular layer thickness were then exclusively made along the lines of the grid. For further analysis we calculated mean values of absolute cuticular layer thickness (*D*), the absolute differences of cuticular layer thickness (*⊿D*) between region 'IR' and 'Ref', mean values of relative cuticular layer thickness (*V*) and relative differences of the relative cuticular layer thickness (*⊿V*) between position 'IR' and position 'Ref', defined through the following equations:

$$\boldsymbol{D_x = \frac{1}{n}\sum_{i=1}^{n} d_{x_{(i)}}} \tag{3.1}$$

$$\boldsymbol{\Delta D_x = D_x(IR) - D_x(Ref)} \tag{3.2}$$

$$\boldsymbol{V_x = \frac{D_x}{D_{total}}} \tag{3.3}$$

$$\boldsymbol{\Delta V_x = \frac{[V_x(IR) - V_x(Ref)]}{V_x(Ref)}} \tag{3.4}$$

where subscript x represents the different cuticular layers exo-, meso-, endo- or total cuticle.

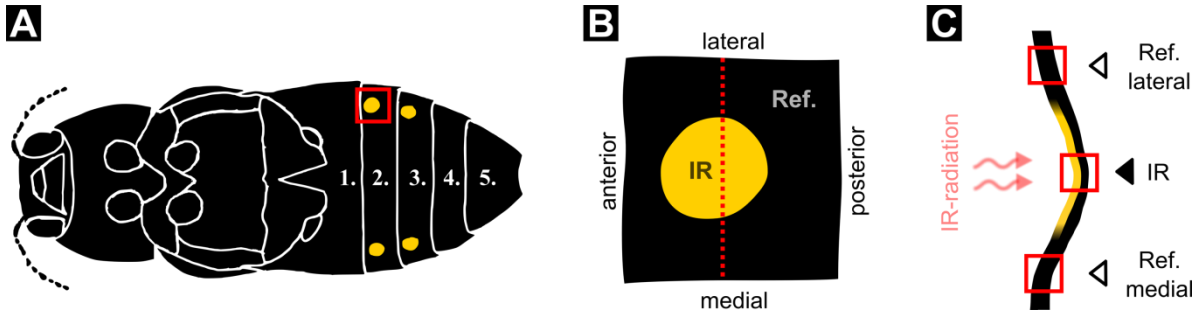

Fig. 3.1 Schematic drawing of *Merimna atrata* and its abdominal IR-organs. **A)** Habitus, ventral view, legs omitted; length of beetle about 25 mm; IR-organs are situated on the 2. and 3. abdominal sternites and can be identified by the yellowish cuticle of the absorbing area. **B)** Absorbing area ('IR') of a single IR-organ (diameter about 500 µm) at higher magnification, surrounded by 'normal' dark pigmented cuticle ('Ref'). Dotted line marks the position of cross-section shown in C. **C)** Cross-section through the absorbing area; red frames indicate the regions for which cuticular layer thickness (*d*), reduced Young's modulus (E_r) and hardness (*H*) were measured. Area 'IR' is situated in the center of the absorbing area, 'Ref medial' and 'Ref lateral' outside the IR-organ on normal cuticle respectively. Orientation: left = exterior; right = interior; top = lateral; bottom = medial.

3.3.5 Scanning probe microscopy (SPM) and mechanical testing by nanoindentation (NI)

High resolution SPM imaging was carried out in tapping mode using a Dimension 3100 (Digital Instruments, USA) atomic force microscope (AFM). Specimens were scanned in air. For mechanical testing, which was performed exclusively in pure water, the AFM was equipped with a nanomechanical test system (Triboscope, Hysitron, USA) capable of normal loading (nanoindentation, NI) and scanning probe microscopy (SPM). We used a three-sided Berkovich diamond tip with a total included angle of 142.3°, also suitable for testing in fluids. A proper area function covering all contact depths obtained during the measurements was generated by indenting in a polymethyl methacrylate test specimen with known hardness (*H*) and reduced Young's modulus (E_r). E_r is defined through the following equation, given by Oliver & Pharr (1992):

$$\frac{1}{E_r} = \frac{(1-\nu^2)}{E} + \frac{(1-\nu_i^2)}{E_i} \qquad (3.5)$$

where E and ν are Young's modulus and Poisson's ratio for the specimen and E_i and ν_i are the same parameters for the indenter used (E_i = 1141 GPa; ν_i = 0.17; manufacturer's information). E_r is subsequently just referred to as 'modulus'.

Contact depths ranged from 131 nm to 684 nm. Load during indentation was always adjusted to 500 µN with loading and unloading rates of 50 $\mu N \cdot s^{-1}$. To compensate for material creeping and to ensure that most of the plastic deformation was completed before unloading, a holding segment of 10 s was added to the load function at peak load (Klocke and Schmitz, 2011). The space between adjacent impressions was chosen to be always greater than 4 µm. *H* and E_r were calculated on basis of the unloading portion of the load-displacement curves following the method of Oliver and Pharr (1992). Indentation was performed in transverse direction (i.e. parallel to the surface of the cuticle). Data were obtained from samples under rewetted conditions (i.e. cuticle saturated with water) following the protocol of Klocke et al. (2011; Klocke and Schmitz, 2011, 2012). For mechanical testing regions 'IR' and 'Ref' of each specimen were analyzed (cf. Fig. 3.1 C).

3.3.6 Finite element simulations

To investigate the influence of different geometries and mechanical properties on the thermomechanical behavior of the absorbing area, various two-dimensional (2D) models were prepared using the CAD-software AutoCAD Mechanical 2011 (Autodesk). The geometries of the models corresponded to the profiles of sections through the centers of different absorbing areas along anterior-posterior direction. The projected length of all models was 720 µm. The *'model E'* (Fig. 3.5 E, J) represented the original architecture of the absorbing area in *Merimna atrata*. The shape of this model was traced from an original section through the center of the absorbing area of a third sternite including the different cuticular layers exo-, meso- and endocuticle. Regarding the mechanical properties we further differentiated between the regions 'Ref' and 'IR' in this model. The region 'IR' was set at the center of the absorbing area, extending for about 60 µm in anterior and posterior direction respectively. *'Model A'* (Fig. 3.5 A, F) was a plane plate with an overall thickness of 20 µm - corresponding to mean cuticle thickness of *'model E'* measured at region 'Ref'. *'Model A'* represented normal cuticle without any specializations. *'Model B'* (Fig. 3.5 B, G) was also a plate but exhibiting the same cuticular thickness like *'model E'*. *'Model C'* (Fig. 3.5 C, H) showed the same exterior pit-like shape like *'model E'* but had a constant cuticular thickness of 20 µm. *'Model D'* (Fig. 3.5 D, I) exhibited the same shape and cuticle thickness like *'model E'* but consisted of only one material (cf. Tab. 3.1). This basic condition also applied to *models A, B* and *C*. Mechanical properties of the different models and their cuticular layers used in the simulations are listed in Table 3.1 (Ishay and Pertsis, 2002; Combes and Daniel, 2003; Vincent and Wegst, 2004; Arenz, 2005; Galushko et al., 2005; Fabritius et al., 2009).

Finite element simulations were performed with Comsol Multiphysics (Version 4.2) using the 'thermal stress' module. The following assumptions were made for all models: they were linear elastic, isotropic, thermally insulated at all boundaries, and anterior as well as posterior boundaries were fixed (cf. Fig. 3.5). In the simulations a heat source with a total power of 0.1 W was applied to the exterior boundary layer of the 2D models. The reference temperature was set at 293.15 K. Cuticular displacement was measured after one second of applying heat. For better comparison of the different models we especially analyzed the total relative displacement at the region spanned by the CO in *Merimna atrata*, subsequently referred to as 'region of interest' *('ROI')* (cf. region between point 1 and 2 in Figure 3.5). A larger relative displacement at the *'ROI'* indicates a more excessive stretching of this specific region and could probably result in a stronger response of the underlying CO. Negative values of relative

displacement on the other hand would indicate a compression of the corresponding region. The projected length of the *'ROI'* was set to 60 µm corresponding to the mean length of scolopidia found in the IR-organ of *Merimna* (Schneider and Schmitz, 2013).

Tab. 3.1 Physical parameters used in finite element simulations. 'Ref_total' and 'IR_total' represent weighted average values for the region of 'normal' cuticle ('Ref') and the center of the absorbing area ('IR') regarding the relative proportion (V) of their different cuticular layers exo-, meso- and endocuticle respectively (cf. Tab. 3.3). Region 'IR' was set to the center of the absorbing area expanding over a distance of 60 µm in anterior and posterior direction each.

Cuticular layer	Relative cuticular layer thickness (V) [%]	Reduced Young's modulus (E_r) [GPa]	Young's modulus (E) [GPa]	Density (p) [kg/m^3]	Poisson's ratio (v)	Specific heat capacity (c) [J/g·K]	Thermal conductivity (λ) [W/m·K]	Thermal expansion coefficient (α) [1/K]·10^{-6}	Water content [%]
Ref_Exo	15.46	5.5	4.9 [h)]	1200 [a)]	0.33 [b)]	2.0 [d)]	0.204 [e)]	43.17 [c)]	12 [f)]
Ref_Meso	49.09	2.9	2.6 [h)]	1200 [a)]	0.33 [b)]	2.35 [d)]	0.267 [e)]	57.07 [c)]	26 [g)]
Ref_Endo	35.45	3.8	3.4 [h)]	1200 [a)]	0.33 [b)]	3.075 [d)]	0,3975 [e)]	50.73 [c)]	55 [f)]
Ref_total	100	3.62	3.2 [h)]	1200 [a)]	0.33 [b)]	2.55 [d)]	0.303 [e)]	51.81 [c)]	34
IR_Exo	27.93	6.45	5.8 [h)]	1200 [a)]	0.33 [b)]	2.0 [d)]	0.204 [e)]	40.27 [c)]	12 [f)]
IR_Meso	41.89	5.9	5.3 [h)]	1200 [a)]	0.33 [b)]	2.35 [d)]	0.267 [e)]	41.86 [c)]	26 [g)]
IR_Endo	30.18	5.1	4.6 [h)]	1200 [a)]	0.33 [b)]	3.075 [d)]	0,3975 [e)]	44.62 [c)]	55 [f)]
IR_total	100	5.81	5.2 [h)]	1200 [a)]	0.33 [b)]	2.55 [d)]	0.303 [e)]	42.15 [c)]	34

a) data given by Vincent & Wegst (2004) and Combes & Daniel (2003)

b) data given by Fabritius et al. (2009)

c) calculated on the basis of the empirical relation $E=4.5\alpha^{-2.3}$ given by Arenz (2005)

d) calculated from values for specific heat capacity of water and hornet cuticle given by Ishay & Pertsis (2002) in relation to the relative water content of the respective cuticle layer given by Vincent & Wegst (2004)

e) calculated from values for thermal conductivity of water and hornet cuticle given by Galushko et al. (2005) in relation to the relative water content of the respective cuticle layer given by Vincent & Wegst (2004)

f) value given by Vincent & Wegst (2004)

g) value assumed based on the data given by Vincent & Wegst (2004)

h) calculated from values of E_r (measured in this paper) and Poisson's ratio given by Fabritius et al. (2009) using equation 3.5

3.3.7 3D reconstruction and building of an artificial absorbing area

In a second approach to investigate the thermomechanical behavior of the absorbing area we reconstructed a 3D model of an IR-organ from a second sternite and fabricated it from acrylic-based resin. Measurements of the thermomechanical displacement and temperature at certain positions were performed by using two conventional strain gauges and a thermocouple.

The 3D model of the absorbing area was reconstructed on the basis of micro-CT images using the 3D visualization software Avizo (version 6.0.0 standard edition, Visualization Science Group). The micro-CT scan was carried out by RJL Micro & Analytic GmbH (Germany) using a Skyscan 1172 (Bruker-microCT, Belgium). After fixation in 70% ethanol and staining in 1% iodine metal dissolved in 100% ethanol (Metscher, 2009), the specimen was scanned in an ethanol saturated atmosphere mounted in an arrangement according to Metscher (2009). The 3D model was printed at the Steinmann institute (Department of Paleontology) of the University of Bonn by using the acrylic-based photopolymer FullCure 720 (Objet Ltd.) with an EDEN 260V (Objet Ltd.) 3D printer. The original model was scaled up by a factor of 145, so that the printed model had the following dimensions: length 138 mm, width 182 mm, height 46 mm. Two identical strain gauges (SGT-3E/350-FB13, Omega) sensitive to uniaxial stress and a thermocouple (5TC-GG-KI-30-1M, Omega) were mounted at specific positions onto the interior surface (cf. Fig. 3.5) along the anterior/posterior axis of the model (see Fig. 3.6 A). The position of the first strain gauge (SG_IR) and the thermocouple (TC_IR) at position 'IR' were chosen according to the positions of the 'ROI' and the multipolar neuron in the beetle respectively. The second strain gauge (SG_Ref) was fixed at the same position along the anterior/posterior axis like the first one but at a more medial position comparable to the region 'Ref'.

Signals of the strain gauges were amplified by an analog amplifier (GSV-1A4, ME-Meßsysteme GmbH) and fed into a CED (Micro 1401 mkII, Cambridge Electronic Design Ltd.); signals of the thermocouple were recorded via a custom made transducer (type K thermocouple-input to voltage-output) and fed into the CED. Data of all three sensors were recorded simultaneously and further analyzed using the software Spike2 (version 5.03, Cambridge Electronic Design Ltd.).

To check the strain gauges for proper performance after mounting onto the 3D model we recorded their response to mechanical load of 4N applied to their respective positions (perpendicular to the surface of the model). The results (not shown) confirmed that both strain gauges were fully functional, even though the strain gauge SG_IR showed a 54% higher signal amplitude than the strain gauge SG_Ref, which was most probably due to the reduced thickness of about 47% (cf. section 3.4.1) at the center of the absorbing area.

During the actual measurements the 3D model was fixed in an aluminium frame and exposed every 100 s for 100 s duration to infrared radiation emitted from a blackbody radiator (CS 500, DIAS infrared GmbH). The blackbody was set to a temperature (T_{rad}) of 773.15 K at a

distance (*r*) of 0.5 m to the 3D model, which corresponds to an intensity (*I*) of 220 $W \cdot m^{-2}$ at the position of the model. The intensity (*I)* was calculated based on the Stefan-Boltzmann law using the following equation:

$$\boldsymbol{I = \frac{\varepsilon \cdot \sigma \cdot T_{rad}^{4} \cdot A_{rad}}{r^{2}}} \qquad (3.6)$$

where ε is the emissivity of the blackbody radiator with 0.97; σ represents the Stefan-Boltzmann constant with $5.670373 \cdot 10^{-8}$ $W \cdot m^{-2} \cdot K^{-4}$; and A_{rad} is the surface area of the blackbody radiator with $2.8 \cdot 10^{-3}$ m^2. To compare the thermomechanical responses of the different sensors at their specific positions we measured the time required to reach a signal to noise ratio (SNR) of 2 after exposure to IR-radiation respectively. The SNR was defined as the ratio of signal mean to the standard deviation of noise.

3.3.8 Statistics

Data on the cuticular layer thickness of the different regions were analyzed using a one-way ANOVA and the least significant difference (LSD) test (Dytham, 2011) for post-hoc testing. The data have been checked previously for normal distribution (Kolmogorov-Smirnov test) and homogenity of variances (Levene test). Data on the mechanical properties of the cuticle including modulus and hardness were analyzed using the Mann-Whitney U-test (Dytham, 2011). For both tests the level of significance was set at $p < 0.05$.

3.4 Results

3.4.1 Composition and structure of the abdominal cuticle

In general the cuticle of the abdominal sternites of *Merimna atrata* is composed of endo-, meso-, exo- and epicuticle (from interior to exterior). The epicuticle was excluded from the following examination because of its very low thickness of about 50 nm. We could only identify the epicuticle as an outermost homogeneous layer by using transmission electron micrographs (not shown). The exocuticle consists of densely packed layers of chitin fibers oriented parallel to the surface. The distance between these layers of fibers is about 0.1 – 0.2 µm. The mesocuticle is characterized by a coarse lamellar structuring, most probably caused by a large number of pore channels passing the cuticle orthogonal to the plane of the

cuticle (Fig. 3.2 A). Distances between these pore channels varied between 0.5 µm and 1.5 µm (Fig. 3.2 A). The underlying endocuticle could be clearly divided into several sublayers (Fig. 3.2 A) differing from each other in thickness (between 0.5 µm and 9.0 µm) and structure (caused by the orientation of chitin layers). Depending on the size of the beetle and the position of cuticle investigated (‘Ref’ or ‘IR’; cf. Fig. 3.1) we could distinguish between 3 - 7 sublayers (Fig. 3.2). However, because of the staining result and for the sake of simplicity we subsumed all sublayers as endocuticle.

As can be seen in Figure 3.3, we found no sharp transition in layer thickness between the regions ‘Ref’ and ‘IR’ but a rather gradual decrease along the whole IR-organ, extending from the outer margin to the center of the absorbing area with the lowest overall thickness. Depending on the size of the beetle total thickness of the cuticle at position ‘Ref’ varied between 20.18 µm and 41.93 µm (cf. Fig. 3.3 A - E and Tab. 3.A1). The dark pigmented exocuticle had a relative proportion of 15%, the mesocuticle of 49% and the endocuticle of 35% (Tab. 3.2). At position ‘IR’ the exocuticle is characterized by a honeycomb-like micro-structure and a loss of dark pigments, clearly recognizable by the papillary surface structure and the yellowish color in the section shown in Figure 3.2 B. At position ‘IR’ total cuticle thickness is reduced to values between 14.11 µm and 19.88 µm; that is only 53% of the thickness of cuticle at position ‘Ref’. This lower cuticle thickness, however, was mainly related to a significant reduction of meso- and endocuticle of 55% and 56% respectively. The absolute thickness of the exocuticular layer, however, differed not significantly at the two regions. Looking at the relative proportions, the picture changes considerably. Due to the reduced thickness of the ‘IR’-region, the relative proportion of the exocuticle increased significantly from 15% (‘Ref’) to 28% (‘IR’), which is equivalent to a relative increase of about 86%. Relative proportions of meso- and endocuticle were reduced significantly from 49% and 35% to 42% and 30% respectively.

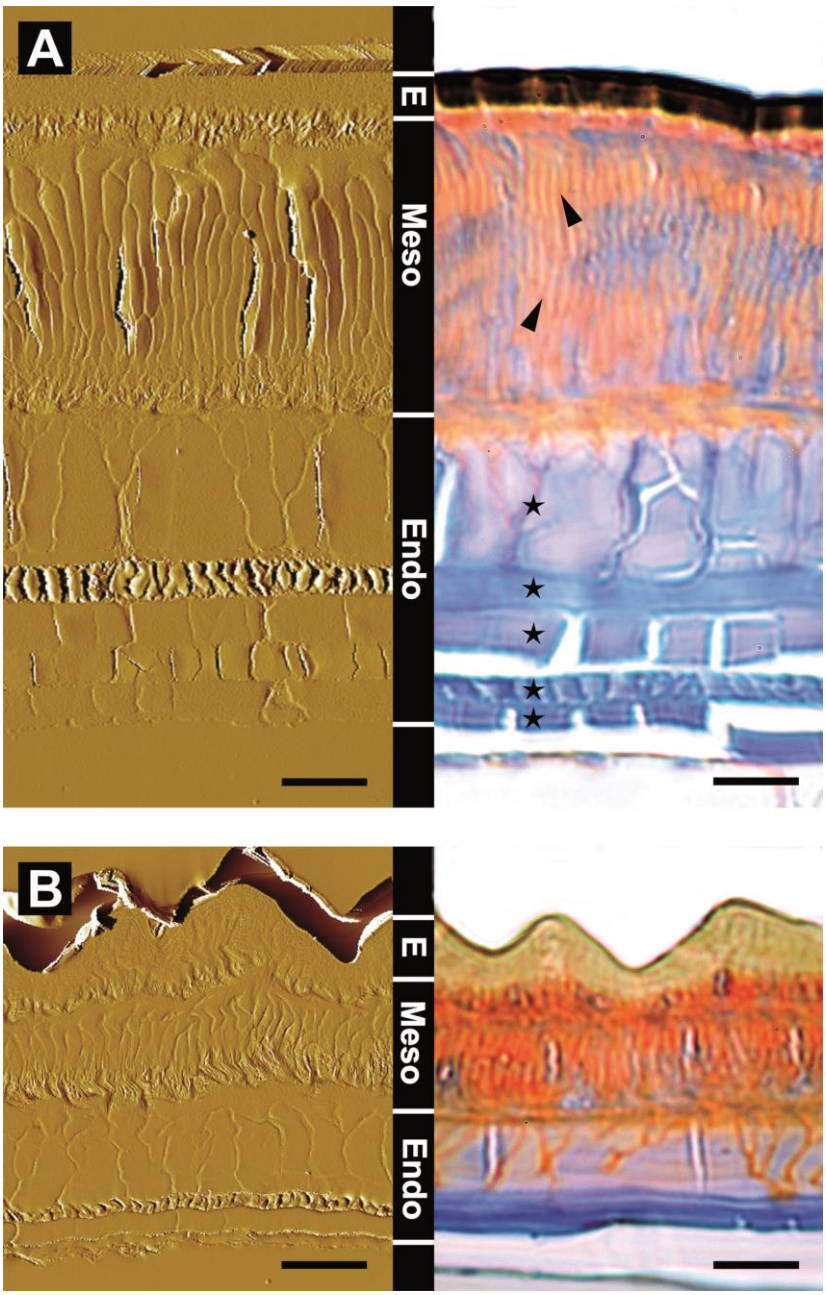

Fig. 3.2 Cross-sections through the abdominal cuticle of *Merimna atrata* including the IR-organ. The different cuticular layers exo- (E), meso- (Meso) and endocuticle (Endo) are shown. AFM-images (left); light microscope images of semithin sections stained with Mallory's Trichrome stain (right). Scale bars: 5 µm. **A)** Sections of 'normal' cuticle surrounding the IR-organ. Arrowheads and asterisks indicate pore channels passing the cuticle and distinctive sublayers of the endocuticle respectively. **B)** Sections of cuticle in the center of the absorbing area.

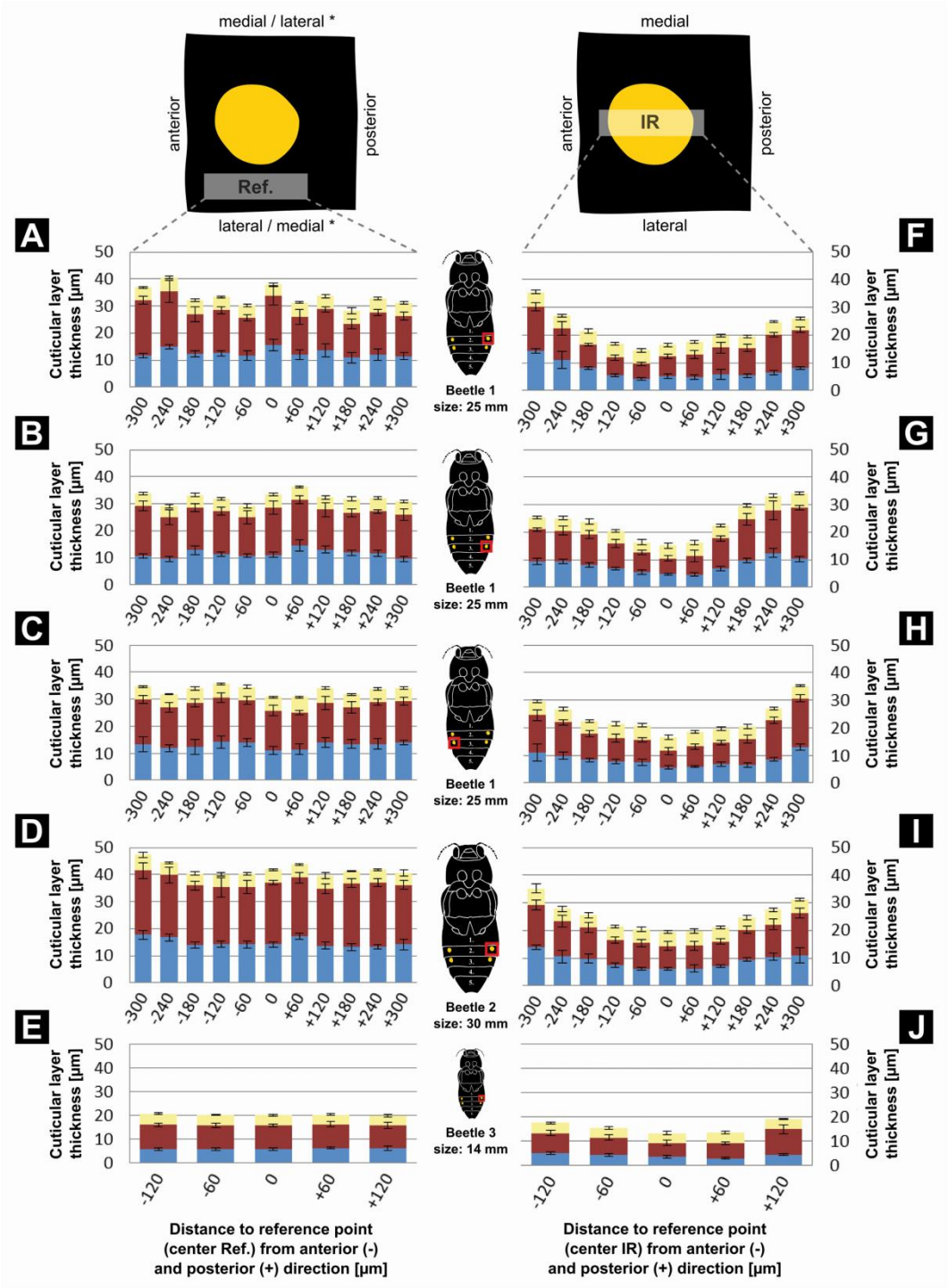

Fig. 3.3 Thickness of the different cuticular layers of 'normal' cuticle ('Ref'; **A - E**) compared to the absorbing area ('IR'; **F - J**). Endocuticle = blue; mesocuticle = red; exocuticle = yellow. Measurements were taken from 5 IR-organs of 3 beetles with different body sizes (given under the icons). Positions of investigated IR-organs are indicated by red frames within the beetle-icons. Bar plots show mean values ± standard deviations from n=10 measurements per layer and position respectively; measurements were taken from sections along a medial/lateral axis at the regions shown in Figure 3.1 C. Sections were made every 60 µm over a distance of 300 µm (120 µm in E, J) in anterior and posterior direction starting from a reference point (0 µm) i.e., the center of the absorbing area (center IR) and a corresponding point of normal cuticle next to it (center Ref.). * Refer to Figure 3.1 C.

Tab. 3.2 Mean thickness (*D*) of the different cuticular layers exo-, meso- and endocuticle at the center of the absorbing area ('IR') compared to 'normal' cuticle ('Ref'). Mean values ± standard deviations of 5 IR-organs from 3 beetles are given. Values for the region 'IR' only include measurements from sections within a distance of 60 µm to the center of the absorbing area from anterior and posterior direction respectively; values for region 'Ref' include all measurements shown in Figure 3.3 A - E. Mean values were regarded as significantly different (Sig. Diff.) at $p < 0.05$ (++ ≙ $p<0.01$; + ≙ $0.01 \leq p < 0.05$; n.s. ≙ $0.05 \leq p$). Additional calculated values: ΔD = absolute difference of cuticular layer thickness between 'IR' and 'Ref'; V = relative cuticular layer thickness; ΔV = relative difference of relative cuticular layer thickness between 'IR' and 'Ref' (cf. equations 3.1- 3.4 in section 3.3.4).

	Absolute values [µm]				Relative values [%]			
Cuticular layer	D (Ref)	Sig. Diff.	D (IR)	Δ D	V (Ref)	Sig. Diff.	V (IR)	ΔV
Exo	4.73 ± 0.33	n.s.	4.67 ± 0.46	-0.07 ± 0.28	15.46 ± 3.46	++	27.93 ± 1.36	86.05 ± 30.33
Meso	15.91 ± 4.42	++	7.11 ± 0.93	-8.79 ± 3.61	49.09 ± 2.88	++	41.89 ± 2.51	-14.59 ± 4.39
Endo	11.56 ± 3.31	++	5.14 ± 1.08	-6.42 ± 2.43	35.45 ± 3.46	+	30.18 ± 2.89	-14.75 ± 4.31
Total	32.20 ± 7.77	++	16.92 ± 2.30	-15.28 ± 5.83	100	n.s.	100	0

3.4.2 Mechanical properties

Comparison of the data obtained from mechanical testing of rewetted cuticle yields the following results: at region 'Ref' the exocuticular layer differed significantly from the meso- and endocuticular layers in being stiffer (mean $E_r = 5.5$ GPa) and harder (mean $H = 0.46$ GPa) (cf. Fig. 3.4, Tab. 3.3). We couldn't find any significant differences between the latter two layers. In comparison, the region 'IR' showed significant differences, particularly with regard to the meso- and endocuticle (Fig. 3.4). At position 'IR' meso- and endocuticle were approximately 100% and 30% stiffer and 100% and 50% harder than outside the IR-organ respectively. The exocuticle exhibited only a slight increase in modulus to 6.45 GPa, whereas no significant changes in hardness could be observed. Considering the relative proportion of the different layers, total cuticle at region 'IR' was about 61% stiffer and 71% harder than the cuticle surrounding the IR-organ (Tab. 3.3).

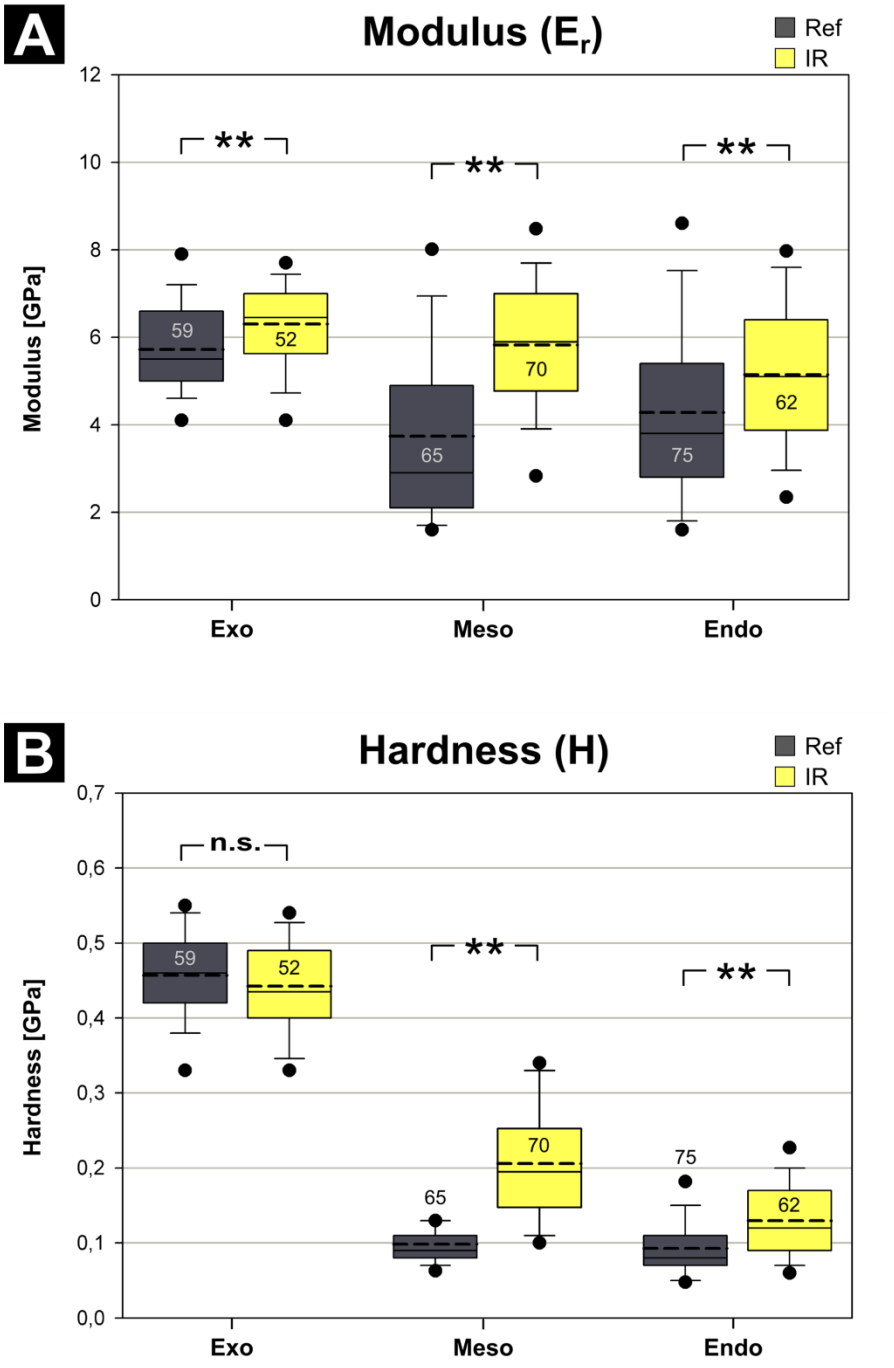

Fig. 3.4 A) Modulus and **B)** Hardness of rewetted cuticular layers exo- (Exo) meso- (Meso) and endocuticle (Endo), measured at the center of the absorbing area ('IR') compared to 'normal' cuticle ('Ref') surrounding the IR-organ (cf. Fig. 3.1). Box plots show distributions of the measured values (numbers of indentations are given within the boxes) with median, 10^{th}, 25^{th}, 75^{th}, and 90^{th} percentiles as boxes with error bars. Dots below and above error bars represent 5^{th} and 95^{th} percentiles. Dashed lines represent mean values. Significant differences are marked by asterisks (** ≙ $p < 0.01$; n.s. ≙ $0.05 \leq p$).

Tab. 3.3 Weighted average values of modulus (E_r) and hardness (H) at the center of the absorbing area ('IR') compared to 'normal' cuticle ('Ref'); calculated using median values of modulus and hardness of the different cuticular layers and their relative proportion (V) to the total cuticle (cf. Fig. 3.4 and Tab. 3.2).

			Ref			IR		
			Exo	Meso	Endo	Exo	Meso	Endo
E_r [GPa]	Median ± 95% Conf		5.5 ± 0.28	2.9 ± 0.50	3.8 ± 0.49	6.45 ± 0.27	5.9 ± 0.37	5.1 ± 0.42
H [GPa]	Median ± 95% Conf		0.46 ± 0.018	0.09 ± 0.012	0.08 ± 0.009	0.435 ± 0.018	0.195 ± 0.018	0.12 ± 0.013
V [%]	Mean ± std.dev		15.46 ± 3.46	49.09 ± 2.88	35.45 ± 3.46	27.93 ± 1.36	41.89 ± 2.51	30.18 ± 2.89
E_r [GPa]	Weighted average			3.6			5.8	
H [GPa]	Weighted average			0.14			0.24	

3.4.3 Thermomechanical behavior

3.4.3.1 Simulation

To analyze the influence of cuticular specializations found in the IR-organ of *Merimna atrata* on its thermomechanical behavior, we used finite element simulations of different 2D models. Cuticular specializations considered for the simulation were the pit-like geometry, thinning and changes in the mechanical properties at region 'IR'. We especially focused on the relative displacement (cf. section 3.3.6) of the 'ROI', corresponding to the innervation site of the CO.

We found that local thinning of the plate-like 'model A' (Fig. 3.5 A, F) as well as of the pit-like 'model C' (Fig. 3.5 C, H) generally led to faster heating and stronger deformation of the corresponding regions (cf. Fig. 3.5 F, G and Fig. 3.5 H, I). Lowest deformations occurred in the plane plate 'model A' with a total relative displacement at the 'ROI' of 2.8 nm. Largest deformations were found in the thinned plate 'model B' with a total relative displacement at the 'ROI' of 94.5 nm. If comparing the thinned plate 'model B' with the thinned pit-like 'model D', it can be stated that the pit-like geometry leads to considerable lower deformations. The total relative displacement at the 'ROI' in 'model D' was e.g. about 72.5% lower than in 'model B'. Taking into account the different mechanical properties measured for the cuticular layers at the regions 'IR' and 'Ref' (cf. Tab. 3.1) also resulted in a lower deformation of the 'ROI' (cf. Fig. 3.5 I, J). In all models investigated (except for 'model A') we found the lowest relative displacement between two points (not to be confused with the absolute displacement) to happen approximately in the center. In all pit-like models (model C, D and E; cf. Fig. 3.5) the region of the lowest relative displacement was not located exactly in

the center like in ‘model B’ but was shifted for about 30 µm in anterior direction, thus exactly matching with the ‘ROI’.

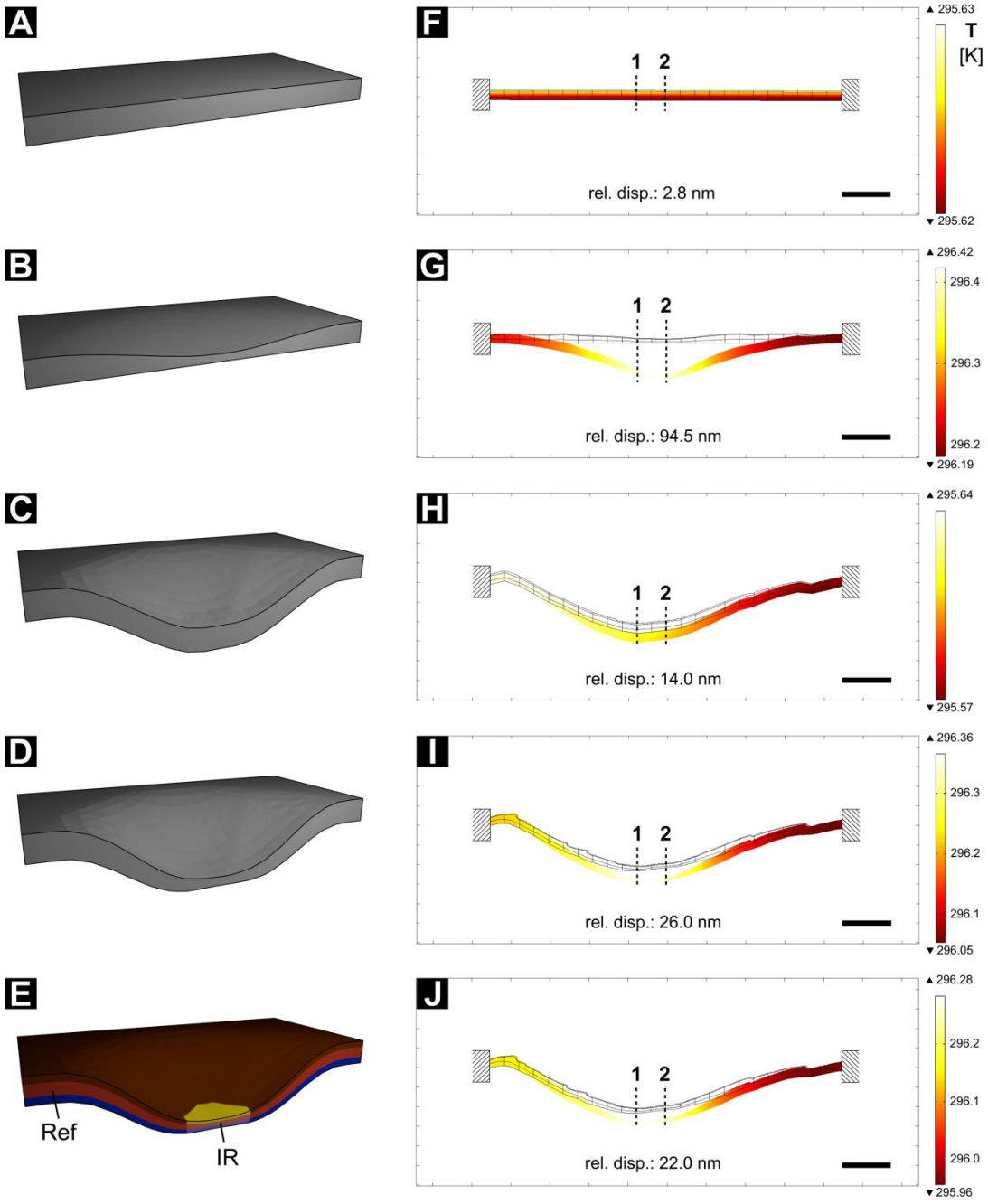

Fig. 3.5 Finite element simulation of the thermomechanical behavior of different 2D models. Orientation of the models: top = exterior, bottom = interior, left = anterior, right = posterior. **A) - E)** Schematic 3D representation of the different models. Different materials are color coded; IR = center of the absorbing area; Ref = ‘normal’ cuticle surrounding the IR-organ (cf. Tab. 3.1 and section 3.3.6). **F) – J)** Results of finite element simulations. Black line drawings show the different models at initial conditions with a temperature of 293.15 K. Colored drawings show the same models and their deformation (scaled up by a factor of 100) after applying heat for 1s with a total energy of 0.1 W to the upper surface; color tables show the resulting temperatures [K]. Total relative displacement (without scaling factor) between position 1 and 2, corresponding to the innervation site of the chordotonal organ, is given at the bottom respectively. Scale bars: 100 µm.

3.4.3.2 3D model

In a second approach to investigate the thermomechanical behavior of the absorbing area we tested a 3D reconstruction of the IR-organ of *Merimna*. We used identical strain gauges to measure the displacement at positions 'IR' and 'Ref' (Fig. 3.6 A) comparable to the 'ROI' in Figure 3.5 I and Figure 3.5 F respectively. The strain gauge at position 'IR' (SG_IR) responded to IR-radiation with amplitudes several times larger compared to those of the strain gauge (SG_Ref) at position 'Ref' (see Fig. 3.6 B). This indicates that region 'IR' was stronger deformed than region 'Ref'. Furthermore, the signs of the signals imply that the SG_IR was stretched whereas the SG_Ref was compressed. To compare the responsivities of the different sensors quantitatively we measured the time needed to reach a SNR of 2. The SG_IR did not only show the highest amplitude but with 1.34 ± 0.11 s also the shortest time to reach a SNR of 2. This is approximately four times faster than the signal of SG_Ref with 5.05 ± 0.29 s. The thermocouple mounted in the center of the absorbing area in direct proximity to the SG_IR showed the slowest response with 22.64 ± 2.51 s required to reach a SNR=2.

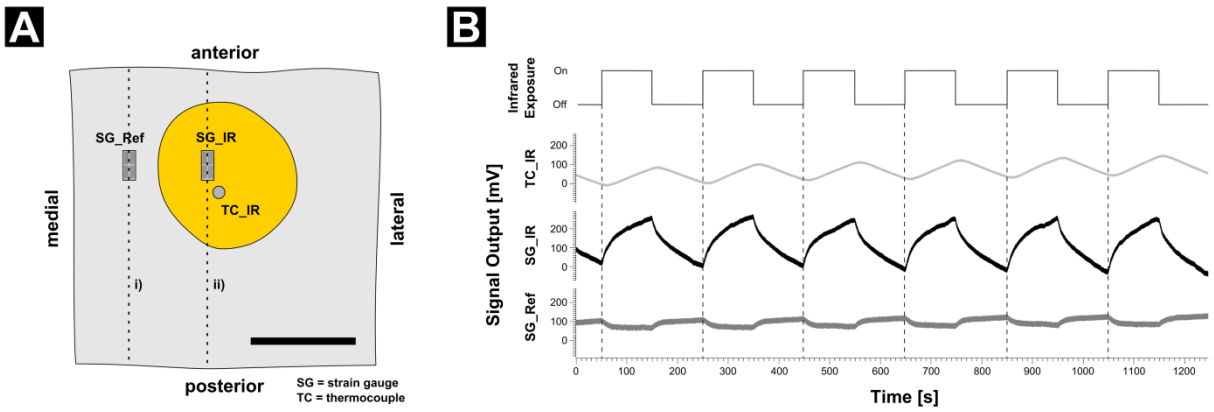

Fig. 3.6 Thermomechanical displacement and temperature change measured at specific regions on a 3D model of the absorbing area. **A)** Schematic drawing of the model showing the positions of the different sensors; interior view (opposed to the direction of incoming IR-radiation). SG = strain gauge; TC = thermocouple; IR = region of the absorbing area (yellow); Ref = region of normal cuticle surrounding the absorbing area. SGs respond to displacement along their anterior/posterior axes (dotted lines). A virtual section along the dotted line i) corresponds to the 2D model shown in Figure 3.5 F; section along the dotted line ii) corresponds to the model shown in Figure 3.5 I. The areas covered by the SGs correspond to the region between point 1 and 2 in Figure 3.5. Scale bar: 50 mm. **B)** Response of the different sensors to infrared radiation with an intensity of 220 $W \cdot m^{-2}$ (original recording). An increase in the signal amplitude of the SGs is correlated with an elongation/ stretching of the region covered by the SGs in anterior/ posterior direction, whereas a decrease in the signal amplitude is caused by compression of this region. An increase in the signal amplitude of the TC of 100 mV corresponds to an increase in temperature of about 1K. For details see section 3.3.7.

3.5 Discussion

At first our results do not support our initial hypothesis that the CO acts as highly sensitive photomechanic IR-receptor in the IR-organ of *Merimna atrata*. However, as will be discussed in the following, there is substantial evidence that the CO indeed serves as an additional IR-sensory unit.

3.5.1 Validity of finite element simulations

For the implementation of finite element simulations we made some assumptions about necessary physical parameters and boundary conditions. However, in some cases the real values were not known so far or have been chosen for the sake of simplicity. One of these somewhat critical conditions was e.g. to fix the anterior and posterior boundaries. The situation in the living animal for sure is more complex. In the beetle the absorbing area is surrounded by further cuticle, which is not completely fixed but will thermally expand in particular into the direction of the segment boundaries. In which manner and to what amount this happens is hard to estimate. Due to the clamping of our models at their anterior and posterior boundaries, the deformation in y-direction obtained in the simulations most probably was overestimated. Another condition that was set in the simulation is the thermal isolation of the models at all boundaries. Heat applied to the model was therefore accumulated and not emitted to the surroundings. This probably also resulted in an overestimation of the thermal deformation.

One of the physical parameters having a main influence on the thermal deformation in the finite element simulations is the thermal expansion coefficient α. We calculated this parameter from the measured values of modulus using the empirical relation $E=4.5\alpha^{-2.3}$, given by Arenz (2005). According to this relation there is a negative correlation between Young's modulus (E) and the thermal expansion coefficient (α); that means the higher the stiffness of a material is (higher value of E), the lower is its thermal expansion. Arthropod cuticle shows a highly anisotropic behavior caused by the inclusion of crystalline chitin fibers into a protein matrix. These fibers are oriented parallel to the outer surface and show a very high stiffness with a Young's modulus of at least 150 GPa (Vincent and Wegst, 2004). Depending on the direction of probing during indentation, results are either determined by the mechanical properties of the embedding protein matrix (when probing in normal direction, i.e. perpendicular to the cuticle surface) or influenced mainly by the mechanical properties of the chitin fibers (when probing parallel to the fiber orientation, i.e. in transverse direction), as

previously has been observed in the sternal cuticle of *Locusta* (Klocke and Schmitz, 2011). First measurements on dry cuticle from the IR-organ of *Merimna* also showed considerable higher values (not shown) of modulus when probing in normal direction. In the present study we only probed in transverse direction because of the much better accessibility of the different cuticular layers. Similarly, also the status of hydration strongly influences the mechanical properties of the cuticle (Klocke and Schmitz, 2011, 2012). In the present study we therefore exclusively tested rewetted cuticle, which we thought to reflect the real conditions in the living beetle much better than dried cuticle. But rewetted cuticle does not perfectly mirror the native conditions in the animal (Klocke and Schmitz, 2011). Both, the direction of indentation and the wetting status of the cuticle used in the present study, most probably resulted in a certain underestimation of stiffness and hardness, thus also leading to a general overestimation of thermal expansion in our finite element simulations.

3.5.2 Functional significance of cuticle structure and mechanical properties for the performance of the CO as putative IR-receptor

Results of the finite element simulations show that the specific geometry as well as the mechanical properties of the cuticle have a huge influence on the thermomechanical behavior of the absorbing area. For the putative function of the CO as highly sensitive photomechanic IR-receptor we would expect a maximum relative displacement of the absorbing area at the 'ROI' in response to heating. Finite element simulations revealed that the thinned plate 'model B' - consisting of normal cuticle thinned to a certain degree but without profound changes of its geometry or mechanical properties - represented the most effective configuration to obtain maximum relative displacement at the 'ROI'. Adding further structural features that are characteristic for the absorbing area of *Merimna* like the pit-like geometry and the changes of the mechanical properties at region 'IR', both resulted in considerable lower displacement of the 'ROI'. One explanation for this may be that the specializations found in *Merimna* are not a solution for a single demand but rather represent the best solution that meets multiple demands ensuring proper functioning of the whole IR-organ. The pit-like geometry for example may represent an adaptation to enable a certain directionality of the IR-organs, which in turn would be an essential feature for the localization of an IR-source. In contrast, with an IR-receptor situated under a plane cuticle (opening angle of 180°) the beetle would not be able to discriminate between stimuli coming from ahead or from behind. Similarly, the adaptations of the mechanical properties at region 'IR' may just

be a consequence of the cuticular thinning at this position to ensure structural integrity of the IR-organ. Thinning in turn would mean a reduction of the thermal mass resulting in stronger deformation and faster heating of the cuticle which may be beneficial for the performance of the CO as photomechanic IR-receptor as well as for the multipolar neuron as thermosensitive IR-receptor. However, the crucial point that contradicts the putative functionality of the CO as highly sensitive IR-receptor is its location within the IR-organ. According to the results of the finite element simulations, the 'ROI' exhibited the lowest relative displacement within the absorbing area. If the primary function of the CO would be IR-reception with the highest possible sensitivity, we could propose that it should have been shifted during evolution a certain distance into the periphery of the absorbing area, where the relative displacement was found to be a several times larger. A reason for the suboptimal position of the CO for IR-reception could be that the IR-sensory system in *Merimna* probably has not yet reached an evolutionary stable state, as had been hypothesized earlier by Mainz et al. (2004), who found considerable variation in number and arrangement of IR-receptors on the abdominal sternites. Thus we speculate that the integration of the CO into IR-reception currently is in progress. Consequently the maximum sensitivity has not been achieved.

3.5.3 Potential interaction of thermo- and mechanosensory units in IR-perception

If we assume 0.6 nm of total relative cuticular displacement at the 'ROI' as sufficient to stimulate the CO (Michelsen and Larsen, 1985), simulations of the performance of the biological model result in an intensity of 3.5 $W \cdot m^{-2}$ as minimum energy required to cause such a deformation. If we make the same simulation for the multipolar neuron and calculate the amount of energy required to increase the temperature of the cuticle at the 'ROI' by 0.08 K, which is the smallest increase in temperature that can be resolved by the multipolar neuron (Schmitz and Trenner, 2003), simulations also result in intensities of 3 - 3.5 $W \cdot m^{-2}$. According to these calculations, sensitivities of both units appear to be more or less equal. Together with the findings that the CO most probably has not been attached to the absorbing area to perceive maximum displacements (cf. section 3.4.3), an increase of sensitivity of the whole IR-organ due to the involvement of the CO in IR-perception appears unlikely.

This raises the question about the probable function of the bimodal innervation of the *Merimna* IR-organ. The position of its attachment site in the middle of the absorbing area clearly indicates the measurement of mostly local mechanical events. On the first abdominal

sternite, where no cuticular specializations can be found, a potential serial homologue of the sensory complex, also consisting of a multipolar neuron and two scolopidia, has been identified in a previous work (Mainz et al., 2004). Based on these findings, it has been proposed that the IR-sensory complex derived from a proprioceptive precursor (Mainz et al., 2004). Therefore, the possibility that the CO in the IR-organ remained unmodified and still functions as proprioceptor, measuring e.g. ventilatory movements of the abdomen, currently cannot be ruled out. An analogous scenario, which has been widely accepted, is the evolution of the tympanic hearing organs of noctuid moths from pre-existing proprioceptive organs. For the evolution of these organs, it has been proposed that the multipolar neuron remained unmodified while the chordotonal organ became sensitive to airborne vibrations (Yack, 1992).

However, calculations presented in this present study reveal that the CO at least could be able to receive IR-radiation with the same sensitivity as the multipolar neuron, even if its attachment site represents the region with the lowest relative displacement. Thus, a general involvement of the CO in IR-reception still seems to be likely, but the question about the additional benefit provided by this mechanosensory unit deserves further investigation. Enhanced temporal resolution could be a potential benefit of the bimodal innervation of the IR-organ. In general, mechanoreceptors show higher temporal resolutions than thermoreceptors. For the thermosensitive multipolar neuron in *Merimna* latencies of approximately 50 ms have been measured (Schmitz and Trenner, 2003), which corresponds to latencies of thermoreceptors in other species (Bullock and Diecke, 1956; Loftus, 1966; Kreiss et al., 2005; Ruchty et al., 2010). Values for latencies of mechanoreceptors range between 40 µs and 100 µs (Thurm, 1981), allowing responses approximately about three orders of magnitude faster than in thermosensitive neurons. Additionally, the multipolar neuron shows a phasic-tonic response pattern with ongoing activity in the absence of a stimulus, whereas the two scolopidia in the CO probably respond mostly phasic to a mechanical stimulus (McIver, 1985; Field and Matheson, 1998). Accordingly the thermosensitive unit could provide the CNS with more integrated information about the existence of an IR-source and general changes in IR-intensity with lower temporal resolution. In contrast, the CO could respond much faster to changes of the signal amplitude. In this way both units would complement each other and increase the overall performance of the IR-organ by extracting more information from a given input signal. Nevertheless, considerations about the probable interaction of the different sensory units remain hypothetic until the general IR-receptive

functionality and the specific response characteristics of the CO will be demonstrated by electrophysiological investigations. This should be the aim of future work.

3.6 Acknowledgements

Mike Cantelo and Brian Inglis from the Department of Environment and Conservation (DEC), Wanneroo, Western Australia, enabled us to visit burnt areas and gave us generous support. The Wildlife Branch of DEC (Perth) issued collecting and export permits. We thank Peter Göddertz at the Steinmann institute (Department Paleontology) of the University of Bonn for printing the 3D model. We are indebted to Anke Schmitz for her help on the burnt areas and Thilo Kahl for technical support. We thank Horst Bleckmann for his continuous interest in our work and for providing laboratory space. We also thank an anonymous referee for helpful comments. Supported by a grant from the German Science Foundation (DFG) to H.S., grant-no.: SCHM1161/10-1.

3.7 Literature

Arenz, R. J. (2005). "Relation of elastic modulus to thermal expansion coefficient in elastic and viscoelastic materials". *23rd Conference and exposition on structural dynamics, Orlando, Florida*.

Bellamy, C. L. (2002). "Zoological Catalogue of Australia, Vol. 29.5 Coleoptera: Buprestoidea". Melbourne, CSIRO Publishing.

Bullock, T. and Diecke, F. (1956). "Properties of an infra-red receptor." *Journal of Physiology* **134**(1): 47.

Combes, S. A. and Daniel, T. L. (2003). "Flexural stiffness in insect wings I. Scaling and the influence of wing venation." *Journal of experimental biology* **206**(17): 2979-2987.

Dytham, C. (2011). "Choosing and using statistics: a biologist's guide". Chichester, UK, Wiley-Blackwell.

Fabritius, H.-O., Sachs, C., Triguero, P. R. and Raabe, D. (2009). "Influence of structural principles on the mechanics of a biological fiber-based composite material with hierarchical organization: the exoskeleton of the lobster *Homarus americanus*." *Advanced Materials (Weinheim, Germany)* **21**(4): 391-400.

Field, L. H. and Matheson, T. (1998). Chordotonal organs of insects. in *Advances in Insect Physiology*. P. D. Evans. San Diego, CA, Academic Press. **Volume 27:** 1-228.

Froggatt, W. W. (1907). "Australian insects". Sydney, William Brooks & Co.

Galushko, D., Ermakov, N., Karpovski, M., Palevski, A., Ishay, J. and Bergman, D. (2005). "Electrical, thermoelectric and thermophysical properties of hornet cuticle." *Semiconductor science and technology* **20**: 286.

Hawkeswood, T. J. (2007). "Review of the biology of the genus *Merimna* Saunders, 1868 (Coleoptera: Buprestidae)." *Calodema* **9**: 12-13.

Hawkeswood, T. J. and Peterson, M. (1982). "A review of the larval host records for Australian jewel beetels (Coleoptera: Buprestidae)." *Victorian Naturalist (Blackburn)* **99**: 240-251.

Howard, C. V. and Reed, M. G. (1998). "Unbiased stereology: three-dimensional measurement in microscopy". Oxford, BIOS Scientific.

Ishay, J. S. and Pertsis, V. (2002). "The specific heat of the cuticle and the morphological differences between the brown and yellow cuticles of hornets." *Journal of electron microscopy* **51**(6): 401.

Kitchin, D. R. (2009). "Notes on the biology of *Merimna atrata*." *Australian Entomologist* **36**(1): 1-2.

Klocke, D., Schmitz, A., Soltner, H., Bousack, H. and Schmitz, H. (2011). "Infrared receptors in pyrophilous (“fire loving”) insects as model for new un-cooled infrared sensors." *Beilstein Journal of Nanotechnology* **2**(1): 186-197.

Klocke, D. and Schmitz, H. (2011). "Water as a major modulator of the mechanical properties of insect cuticle." *Acta Biomaterialia* **7**: 2935- 2942.

Klocke, D. and Schmitz, H. (2012). "Material properties of photomechanical infrared receptors in pyrophilous *Melanophila* beetles and *Aradus* bugs." *Acta Biomaterialia* **8**(9): 3392-3399.

Kreiss, E.-J., Schmitz, A. and Schmitz, H. (2005). "Morphology of the prothoracic discs and associated sensilla of *Acanthocnemus nigricans* (Coleoptera, Acanthocnemidae)." *Arthropod Structure & Development* **34**(4): 419-428.

Loftus, R. (1966). "Cold receptor on the antenna of *Periplaneta americana*." *Zeitschrift für vergleichende Physiologie* **52**(4): 380-385.

Mainz, T., Schmitz, A. and Schmitz, H. (2004). "Variation in number and differentiation of the abdominal infrared receptors in the Australian 'fire-beetle' *Merimna atrata* (Coleoptera, Buprestidae)." *Arthropod Structure & Development* **33**(4): 419-430.

McIver, S. B. (1985). Mechanoreception. in *Comprehensive Insect Physiology, Biochemistry and Pharmacology*. G. A. Kerkut and L. I. Gilbert. Oxford, Pergamon Press. **6:** 71 - 132.

Metscher, B. (2009). "MicroCT for comparative morphology: simple staining methods allow high-contrast 3D imaging of diverse non-mineralized animal tissues." *BMC physiology* **9**(1): 11.

Michelsen, A. and Larsen, O. N. (1985). Hearing and sound. in *Comprehensive Insect Physiology, Biochemistry, and Pharmacology*. G. A. Kerkut and L. I. Gilbert. New York, Pergamon Press**:** 495-556.

Oliver, W. C. and Pharr, G. M. (1992). "An improved technique for determining hardness and elastic modulus using load and displacement sensing indentation experiments." *Journal of materials research* **7**(06): 1564-1583.

Poulton, E. B. (1915). "The habits of the Australian buprestid "fire-beetle" *Merimna atrata*, (Laporte and Gory)." *Transactions of the Entomological Society of London* **Part 1. (Proceedings)**: iii-iv.

Ruchty, M., Roces, F. and Kleineidam, C. J. (2010). "Detection of minute temperature transients by thermosensitive neurons in ants." *Journal of neurophysiology* **104**(3): 1249-1256.

Schmitz, H. and Bleckmann, H. (1998). "The photomechanic infrared receptor for the detection of forest fires in the beetle *Melanophila acuminata* (Coleoptera: Buprestidae)." *Journal of Comparative Physiology A* **182**(5): 647-657.

Schmitz, H. and Bousack, H. (2012). "Modelling a historic oil-tank fire allows an estimation of the sensitivity of the infrared receptors in pyrophilous *Melanophila* beetles." *PLoS ONE* **7**(5): e37627.

Schmitz, H., Schmitz, A. and Bleckmann, H. (2000). "A new type of infrared organ in the Australian" fire-beetle" *Merimna atrata* (Coleoptera: Buprestidae)." *Naturwissenschaften* **87**(12): 542-545.

Schmitz, H., Schmitz, A. and Bleckmann, H. (2001). "Morphology of a thermosensitive multipolar neuron in the infrared organ of *Merimna atrata* (Coleoptera, Buprestidae)." *Arthropod Structure & Development* **30**(2): 99-111.

Schmitz, H. and Trenner, S. (2003). "Electrophysiological characterization of the multipolar thermoreceptors in the" fire-beetle" *Merimna atrata* and comparison with the infrared sensilla of *Melanophila acuminata* (both Coleoptera, Buprestidae)." *Journal of Comparative Physiology. A, Neuroethology, Sensory, Neural, and Behavioral Physiology* **189**(9): 715-722.

Schneider, E. S. and Schmitz, H. (2013). "Bimodal innervation of the infrared organ of *Merimna atrata* (Coleoptera, Buprestidae) by thermo- and mechanosensory units." *Arthropod Structure & Development* **42**(2): 135-142.

Sowards, L. A., Schmitz, H., Tomlin, D. W., Naik, R. R. and Stone, M. O. (2001). "Characterization of beetle *Melanophila acuminata* (Coleoptera: Buprestidae) infrared pit organs by high-performance liquid chromatography/mass spectrometry, scanning electron microscope, and Fourier transform-infrared spectroscopy." *Annals of the Entomological Society of America* **94**(5): 686-694.

Stark, K. B., Gallas, J. M., Zajac, G. W., Golab, J. T., Gidanian, S., McIntire, T. and Farmer, P. J. (2005). "Effect of stacking and redox state on optical absorption spectra of

melanins−Comparison of theoretical and experimental results." *The Journal of Physical Chemistry B* **109**(5): 1970-1977.

Tepper, J. G. O. (1887). "Common native insects of South Australia: a popular guide to South Australian entomology". Adelaide, E.S. Wigg & Son.

Thurm, U. (1981). "Mechano-electric Transduction." *Biophysics of structure and mechanism* **7**(4): 245-246.

Vincent, J. F. V. and Wegst, U. G. K. (2004). "Design and mechanical properties of insect cuticle." *Arthropod Structure & Development* **33**(3): 187-199.

Vondran, T., Apel, K. H. and Schmitz, H. (1995). "The infrared receptor of *Melanophila acuminata* De Geer (Coleoptera: Buprestidae): ultrastructural study of a unique insect thermoreceptor and its possible descent from a hair mechanoreceptor." *Tissue and Cell* **27**(6): 645-658.

Weyda, F. (1982). "Adaptation of Mallory's trichrome stain to insect tissue epoxy sections." *Zeitschrift für mikroskopisch-anatomische Forschung* **96**(1): 79-80.

Yack, J. E. (1992). "A multiterminal stretch receptor, chordotonal organ, and hair plate at the wing-hinge of *Manduca sexta*: unravelling the mystery of the noctuid moth ear B cell." *Journal of Comparative Neurology* **324**(4): 500-508.

3.8 Appendix

Tab. 3.A1 Thickness of the different cuticular layers (exo-, meso- and endocuticle) and the entire cuticle (Total) at the center of the absorbing area ('IR') compared to 'normal' cuticle ('Ref'). Mean values ± standard deviations are given. Values for the region 'IR' include measurements from sections within a distance of 60 µm to the center of the absorbing area from anterior and posterior direction respectively; values for the region 'Ref' include all measurements shown in Figure 3.3 A - E. *D* = absolute value of cuticular layer thickness. Δ*D* = absolute difference of cuticular layer thickness between 'IR' and 'Ref'; *V* = relative cuticular layer thickness; Δ*V* = relative difference of relative cuticular layer thickness between 'IR' and 'Ref' (cf. equations 3.1- 3.4 in section 3.3.4). Left (L) and right (R) IR-organs of the second (2) and third (3) sternite (S) of three different beetles (Beetle1-3) were measured (cf. Fig. 3.1).

		Absolute values [µm]			Relative values [%]		
Cuticular layer	Specimen	D (Ref)	D (IR)	Δ D	V (Ref)	V (IR)	ΔV
Exo	Beetle 1'_2S_L	4.89 ± 0.39	4.50 ± 0.50	-0.39	14.88	28.14	89.18
	Beetle 1'_3S_L	4.67 ± 0.32	4.41 ± 0.69	-0.26	14.55	27.86	91.42
	Beetle 1'_3S_R	5.11 ± 0.29	5.20 ± 0.13	0.09	15.50	28.22	82.09
	Beetle 2'_2S_L	4.78 ± 0.39	5.11 ± 0.16	0.33	11.41	25.82	126.29
	Beetle 3'_2S_L	4.23 ± 0.26	4.13 ± 0.28	-0.09	20.96	29.60	41.25
	Total	4.73 ± 0.33	4.67 ± 0.46	-0.07 ± 0.28	15.46 ± 3.46	27.93 ± 1.36	86.05 ± 30.33
Meso	Beetle 1'_2S_L	16.01 ± 2.65	6.95 ± 1.45	-9.06	47.51	42.67	-10.17
	Beetle 1'_3S_L	15.99 ± 1.27	6.51 ± 0.73	-9.48	49.63	40.76	-17.87
	Beetle 1'_3S_R	15.19 ± 1.05	7.13 ± 1.01	-8.07	45.69	38.12	-16.55
	Beetle 2'_2S_L	22.40 ± 1.06	8.67 ± 0.67	-13.74	53.43	43.40	-18.78
	Beetle 3'_2S_L	9.95 ± 0.21	6.32 ± 0.71	-3.63	49.22	44.52	-9.55
	Total	15.91 ± 4.42	7.11 ± 0.93	-8.79 ± 3.61	49.09 ± 2.88	41.89 ± 2.51	-14.59 ± 4.39
Endo	Beetle 1'_2S_L	12.57 ± 1.50	4.71 ± 0.46	-7.86	37.61	29.18	-22.42
	Beetle 1'_3S_L	11.53 ± 1.52	4.95 ± 0.51	-6.58	35.82	31.39	-12.38
	Beetle 1'_3S_R	12.95 ± 1.09	6.28 ± 1.08	-6.67	38.82	33.66	-13.29
	Beetle 2'_2S_L	14.75 ± 1.64	6.11 ± 0.09	-8.64	35.15	30.78	-12.45
	Beetle 3'_2S_L	6.01 ± 0.25	3.66 ± 0.71	-2.35	29.83	25.88	-13.22
	Total	11.56 ± 3.31	5.14 ± 1.08	-6.42 ± 2.43	35.45 ± 3.46	30.18 ± 2.89	-14.75 ± 4.31
Total	Beetle 1'_2S_L	33.47 ± 3.66	16.16 ± 1.51	-17.31	100.00	100.00	0.00
	Beetle 1'_3S_L	32.19 ± 2.05	15.87 ± 0.66	-16.32	100.00	100.00	0.00
	Beetle 1'_3S_R	33.25 ± 1.70	18.60 ± 2.13	-14.65	100.00	100.00	0.00
	Beetle 2'_2S_L	41.93 ± 2.34	19.88 ± 0.49	-22.05	100.00	100.00	0.00
	Beetle 3'_2S_L	20.18 ± 0.34	14.11 ± 1.14	-6.08	100.00	100.00	0.00
	Total	32.20 ± 7.77	16.92 ± 2.30	-15.28 ± 5.83	100 ± 0	100 ± 0	0 ± 0

Kapitel 4

Vorwort

Die in Kapitel 2 und 3 bezüglich ihrer Morphologie und Ultrastruktur beschriebenen IR-Organe von *Merimna atrata* stellten bislang die einzig bekannten abdominalen IR-Organe dar. Sie weisen eine einzigartige bimodale Innervation durch thermo- und mechanosensitive Einheiten auf. Des Weiteren konnten spezielle Anpassungen des reiztransduzierenden Cuticula-Apparates (absorbierende Fläche) identifiziert werden, die sehr wahrscheinlich im Dienste der IR-Rezeption stehen. Dazu gehört unter anderem eine Reduktion der Cuticula im Bereich der absorbierenden Fläche um bis zu 50%, was einer Reduktion der thermischen Masse entspricht und notwendig für die Funktion eines sensitiven IR-Rezeptors ist. Eine weitere Anpassung stellt die dreidimensionale Einbuchtung der absorbierenden Fläche dar. Diese resultiert in einer Richtungscharakteristik und scheint die räumliche Lokalisierung von IR-Quellen zu begünstigen.

Takàcs et al. (2009) beschrieben die Existenz von abdominalen IR-Rezeptoren bei der Amerikanischen Kiefernwanze *Leptoglossus occidentalis*. Die Autoren identifizierten kleine Bereiche auf den abdominalen Sterniten, die sich durch eine charakteristische Oberflächenstrukturierung auszeichnen und entfernt an die absorbierende Fläche der IR-Organe von *Merimna atrata* erinnern. Die Beschreibung der Funktion dieser Strukturen als vermeintliche IR-Rezeptoren basierte auf den Ergebnissen von Verhaltensversuchen und ersten qualitativen extrazellulären Ableitungen. Detaillierte morphologische Untersuchungen zu den genannten cuticulären Strukturen und ihrer für eine IR-rezeptive Funktion zu fordernden Innervation durch sensorische Komponenten fehlen jedoch bisher vollständig. Diese sind Gegenstand des folgenden Kapitels.

Presumed abdominal infrared receptors in the western conifer seed bug, *Leptoglossus occidentalis* turned out to be glandular fields

Erik S. Schneider, Anke Schmitz and Helmut Schmitz

Submitted to Arthropod Structure & Development

4.1 Abstract

The western conifer seed bug, *Leptoglossus occidentalis*, shows small spots of diverging surface structure on nearly all abdominal segments. The spots are characterized by a distinct micro-structured exterior surface. Because *L. occidentalis* feeds on pine cones, which show elevated temperatures when irradiated by the sun, it has been proposed that the abdominal spots serve as infrared (IR) receptors. Behavioral experiments indeed have indicated that bugs were able to approach IR-sources and occlusion of the proposed IR-receptors seemed to eliminate this ability. Although first extracellular recordings revealed changes of the electrophysiological signal due to IR-irradiation, an innervation of the spots has not been shown so far.

We investigated the proposed IR-receptive areas with morphological and neuroanatomical methods and were not able to find evidences for the existence of sensory cells. However, beneath the cuticle of the spots we found extended fields of at least two types of glandular cells suggesting that the micro-structured areas may serve for enhanced distribution of glandular secretions. Consequently pyrophilous insects like buprestid beetles of the genera *Melanophila* and *Merimna*, the "Little Ash beetle" *Acanthocnemus nigricans* and a few pyrophilous members of the bark bug family Aradidae still are the only insects with known extra-antennal IR-receptors.

4.2 Introduction

Adults of the diurnal western conifer seed bug, *Leptoglossus occidentalis* (Fig. 4.1), primarily feed on developing seeds in cones of various conifers (Bates et al., 2000; Strong et al., 2001). Consequently, *L. occidentalis* can be regarded as a serious forest pest (Koerber, 1963). Therefore, reliable localization of pine cones is a compelling task for the bugs. In addition to its visual appearance a pine cone shows a specific infrared signature and a characteristic olfactory bouquet during the day. Caused by good absorption of solar radiation and most probably also by production of endogenous metabolic heat a ripening cone exhibits a distinct

excess temperature which can be visualized by a thermal camera (Takács et al., 2009). Recently it has been established by behavioral and morphological investigations that *L. occidentalis* also uses infrared (IR) radiation for cone finding and for this purpose has evolved 4 pairs of IR-receptors on the abdomen (Takács et al., 2009).

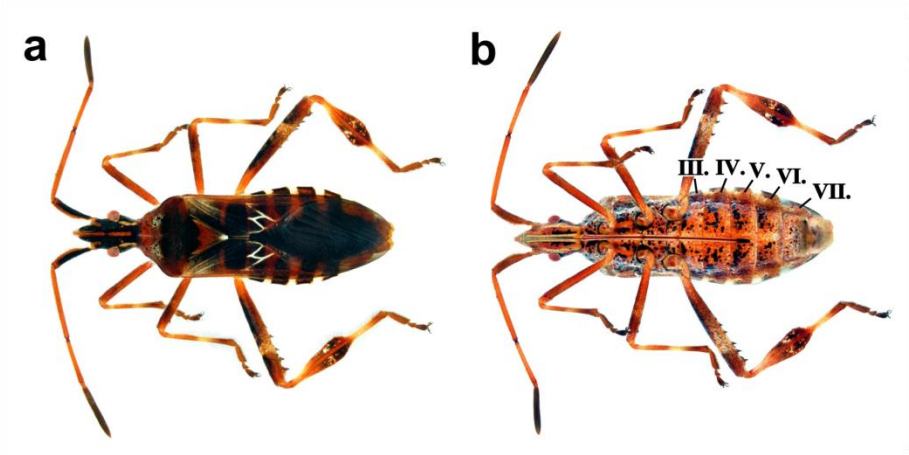

Fig. 4.1 a) Dorsal and **b)** ventral view of *Leptoglossus occidentalis*; body length about 18 mm. Numbers of abdominal sternites in b) are given in roman numerals.

At first this is a very interesting result. Although true IR-receptors existing in addition to the thermoreceptive sensilla on the antennae (Altner and Loftus, 1985) are very rare in insects, bugs (Heteroptera) appear to be predestined for developing IR-sensory capabilities. In particular a small group of pyrophilous flat bugs of the genus *Aradus,* which approaches forest fires, has groups of IR-receptors on the pleural regions of the prothorax (Schmitz et al., 2008). IR-receptors consist of tiny cuticular spheres which are innervated by ciliary mechanoreceptors (Schmitz et al., 2010) and, therefore, are similar to the photomechanic IR-receptors previously described in pyrophilous buprestid beetles of the genus *Melanophila* (Schmitz et al., 1997; Schmitz et al., 2007). Most probably pyrophilous *Aradus* bugs use their IR-receptors for localizing hot spots on a freshly burnt area in order to avoid to come too close to surfaces with harmful temperatures. In general, burning or glowing wood can be classified as an IR-source of high temperature showing a peak emission of IR-photons in the wavelength range between 2 and 5 µm which corresponds to surface temperatures between 1,180 and 300 °C (Budzier and Gerlach, 2010). IR-photons from those high temperature sources are well transmitted through an atmospheric "high temperature window" between 3 and 5 µm over large distances allowing fire detection with IR-sensors even from space (Vincent, 1990).

A second group of bugs with proven IR-sensory capabilities are blood-sucking triatomine bugs. These predatory insects search for a blood-meal at night. For close range orientation the bugs also use IR-radiation given off by their warm-blooded hosts (Lazzari and Núñez, 1989; Schmitz, Helmut et al., 2000; Guerenstein and Lazzari, 2009). This is promoted by another atmospherical window transparent for IR-radiation between 8 and 14 µm. This window can be termed as a "low-temperature window" because objects with surface temperatures between 90° C and - 66° C show their maximum of emission within this range (Vincent, 1990). Within the low temperature window all warm blooded creatures as well as objects, e.g. heated up by the sun, can be easily detected with appropriate IR-sensors against a cooler background. According to the current knowledge, however, IR-reception in triatomine bugs is accomplished by highly sensitive antennal thermoreceptors (Bernard, 1974; Lazzari and Wicklein, 1994; Insausti et al., 1999; Guerenstein and Lazzari, 2009). Additional extra-antennal IR-receptors so far have not been described morphologically and/or physiologically for blood-sucking bugs or any other insect supposed to use IR-radiation for the detection of low temperature IR-sources. Thus the first example for an insect with extra-antennal IR-receptors used for the detection of a low temperature IR-source like a slightly heated cone would be *Lepotglossus occidentalis*. The existence of IR-receptors in *L. occidentalis* would also encourage further attempts to search for IR-receptors in other blood-sucking insects like mosquitos or blood-sucking flies. It has to be stressed, however, that evidences for the existence of abdominal IR-receptors in *L. occidentalis* are relatively sparse. In the mentioned paper of Takács et al. (2009) only a SEM-micrograph depicting the outer morphology of an abdominal IR-receptor is provided together with a single potential trace from an extracellular electrophysiological recording from a supposed IR-organ. This trace shows some slow On /OFF amplitudes in response to IR-exposition but no action potentials. Thus a critical re-examination of the abdominal structures proposed to be IR-receptors deems necessary.

4.3 Material and Methods

4.3.1 Animals

Animals were collected between August and October 2013 in the surrounding areas of Bonn, Germany. Bugs were kept in plastic boxes for several days. Water, fresh pine cones and pine seeds were given ad libitum. All experiments complied with the Principles of Animal Care of the National Institute of Health and with the German Animal Welfare Act.

4.3.2 Axonal in vivo filling of neurons

For neuroanatomical studies of the putative abdominal IR-organs, abdomina of male and female adults were excised and transferred immediately dorsal side up into a Sylgard-lined dish filled with insect saline (140 $mM \cdot l^{-1}$ NaCl, 5 $mM \cdot l^{-1}$ KCl, 4 $mM \cdot l^{-1}$ $CaCl_2$, 28 $mM \cdot l^{-1}$ glucose, 5 $mM \cdot l^{-1}$ Hepes; pH 7.2 - 7.4; (Trimmer and Weeks, 1989)). Main nerves branching off the ganglia were carefully exposed. Right and left halves of the abdominal sternites were isolated and treated separately with particular attention not to damage or remove any nervous tissue. Main nerves of the III. up to the VI. sternite were cut close to the ganglion and isolated from the preparation by surrounding the proximal end of the nerve with a little cup of Vaseline (Mason, 1973). After a short exposure of the stump to distilled water, the Vaseline cup was filled with a drop of 0.2 - 0.5 M $CoCl_2$ (Pitman et al., 1972; Mason, 1973) and sealed with additional Vaseline to prevent leakage of the staining solution. Preparations were incubated in a moist chamber for 24 - 48 h at 4°C. Precipitation was achieved by transferring preparations to 1% ammonium sulphide for 15 min (Mücke and Lakes, 1988). After washing in fresh saline and fixation in Carnoy´s solution for 15 min (Sandeman and Okajima, 1973; Altman and Tyrer, 1980) specimens were dehydrated in a graded series of ethanol for 10 min each and finally cleared and stored in methyl salicylate (Mason, 1973; Honegger and Schürmann, 1975; Mücke and Lakes-Harlan, 1995) for several days. Backfills were conducted on a total of 27 abdominal sternites (7 x III. sternite, 9 x IV. sternite, 6 x V. sternite, 5 x VI. sternite) of 5 animals. In an attempt to enhance the staining intensity in some preparations, specimens were additionally silver intensified according to the light insensitive method introduced by Davis (1982) and further improved by Mesce et al. (1993) by adjusting the pH of the pretreatment and the intensification solution A to 10.5. It turned out, however, that the increase in quality of the staining was relatively small. Preparations were viewed using a Zeiss Stemi SV 11 binocular. Images were taken with a Nikon D5000 digital camera.

4.3.3 Light and transmission electron microscopy

Abdominal sternites were excised in iced glutardialdehyde fixative (3% glutardialdehyde in 0.05 $mol \cdot l^{-1}$ cacodylate buffer, pH 7.1; osmolarity 380 - 400 mosmol $\cdot$ l^{-1}) and fixed over night. Afterwards specimens were washed in buffer, postfixed with 1.5% OsO_4 in the same buffer, dehydrated through a graded series of ethanol and embedded via propylenoxide in Epon 812 (Luft, 1961). After identifying the abdominal regions supposed to contain IR-receptors, semi- and ultrathin sections of these specific regions were cut with an Om U3

microtome (C. Reichert, Austria) using a diamond knife (Diatome AG, Switzerland). Sections were cut parallel to the sagittal axis of the bugs. Semithin sections (0.5 – 1 µm) were stained with a 0.05% toluidine-blue/borax solution and examined with a Leitz DMRB/R light microscope. Ultrathin sections (100 nm) were double stained with uranyl acetate and lead citrate and examined with a Zeiss EM 109 transmission electron microscope. Images were taken with an integrated roll film camera and negatives were scanned and digitized with a resolution of 1200 dpi.

4.3.4 Scanning electron microscopy

Bugs fixed in 70% ethanol were cleaned after dissection for several minutes by sonication either in 70% ethanol or in a 2:1 mixture of chloroform and 100% ethanol. After drying in air, specimens were glued onto holders with carbon glue (Leit-C, Fa. Neubauer), sputter-coated with 10 - 25 nm gold (Balzers Union SCD 040 Sputter-Coater, Bal-Tec AG, Liechtenstein) and examined with a Cambridge Stereoscan 200 scanning electron microscope (Cambridge Instruments Ltd., Cambridge, UK) using a tungsten cathode and an accelerating voltage of 15 kV. Instead of drying in air, several specimens were dried according to the critical-point-drying method (Anderson, 1951) using a CPD 020 Critical-Point-Dryer (Balzers Union, Bal-Tec AG, Liechtenstein).

4.4 Results

4.4.1 Exterior morphology of the abdominal sternites

The description of the exterior morphology focuses on the five fully developed abdominal sternites III. to VII. (Figs. 4.1b, 4.2a) of adult *L. occidentalis*. Segments were determined according to Wagner (1966). Each of these sternites is characterized by a prominent stigma located at the lateral margins (cf. asterisks in Fig. 4.2a) and a specific number and arrangement of trichobothria in the medial region. On the third and fourth sternite we found a transverse row of three single trichobothria (Fig. 4.2d), on the fifth and sixth sternite three trichobothria arranged in a triad (Fig. 4.2e), and on the seventh sternite one pair of trichobothria. The triads of trichobothria on the fifth and the sixth sternites are located more laterally than the rows of trichobothria on the anterior segments (cf. position of boxes *d* and *e* in Fig. 4.2a).

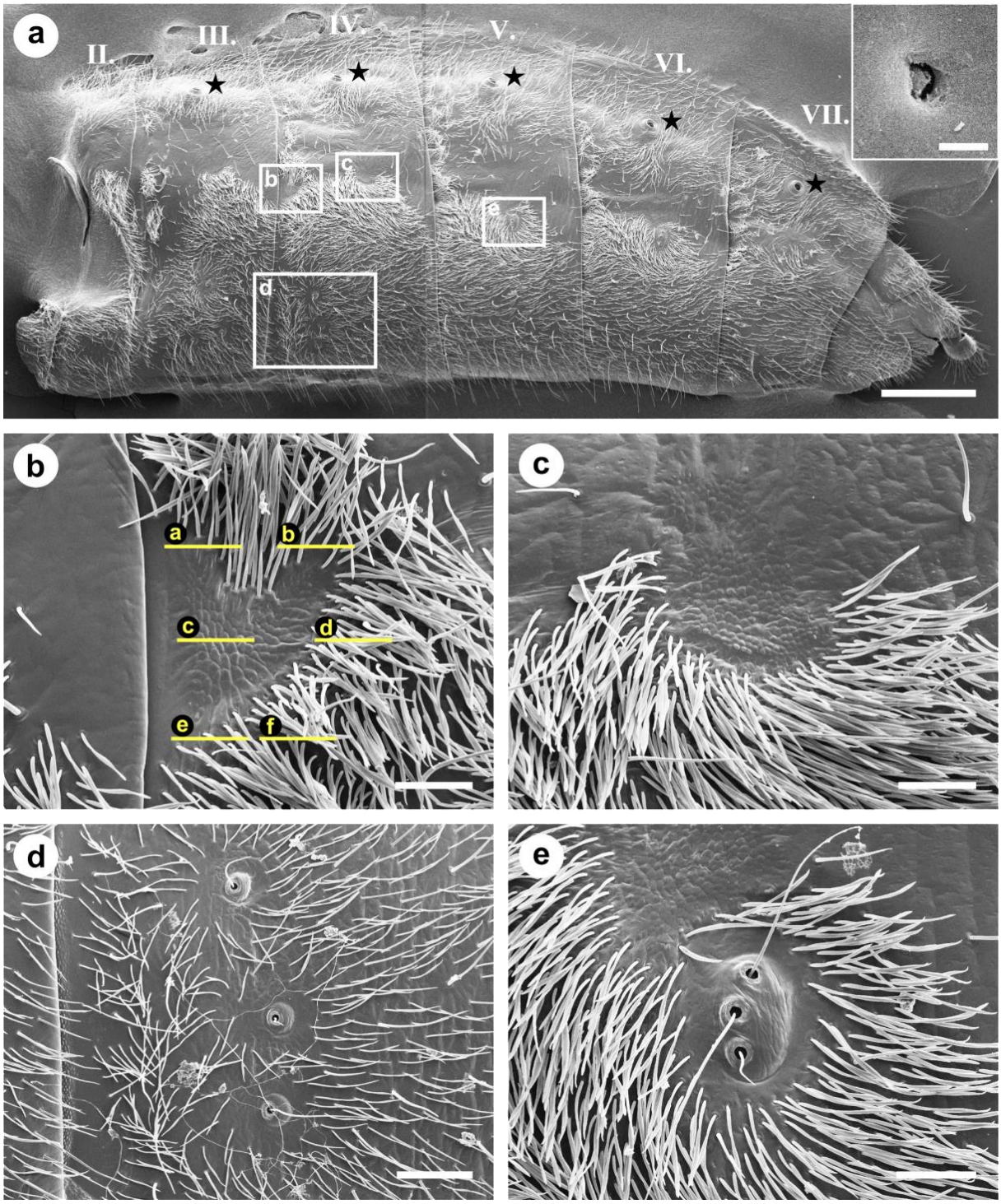

Fig. 4.2 SEM-micrographs showing the exterior surface of the ventral abdomen of *L. occidentalis* (only left half shown). Orientation: left = cranial, right = caudal, bottom = medial, top = lateral. **a)** Overview according to Figure 1b. II. to VII. indicate numbers of the respective abdominal sternites. White lettered boxes enclose specific regions shown in b) – e) at higher magnifications. Asterisks mark positions of stigmata. Bar: 1 mm. Inset at the upper right shows exterior opening of a Class 3 epidermal glandular cell (cf. Figs. 4.5 and 4.6). Bar: 2 µm. **b)** anterior micro-structured area (*aMSA*). Yellow lines (online version in color) indicate number, position and orientation of sections shown in Figure 4.3. Bar: 100 µm. **c)** posterior micro-structured area (*pMSA*). Bar: 100 µm. **d)** Three single trichobothria arranged in a transversal row on the fourth sternite. Bar: 200 µm. **e)** Three trichobothria arranged in a triad on the fifth sternite. Bar: 100 µm.

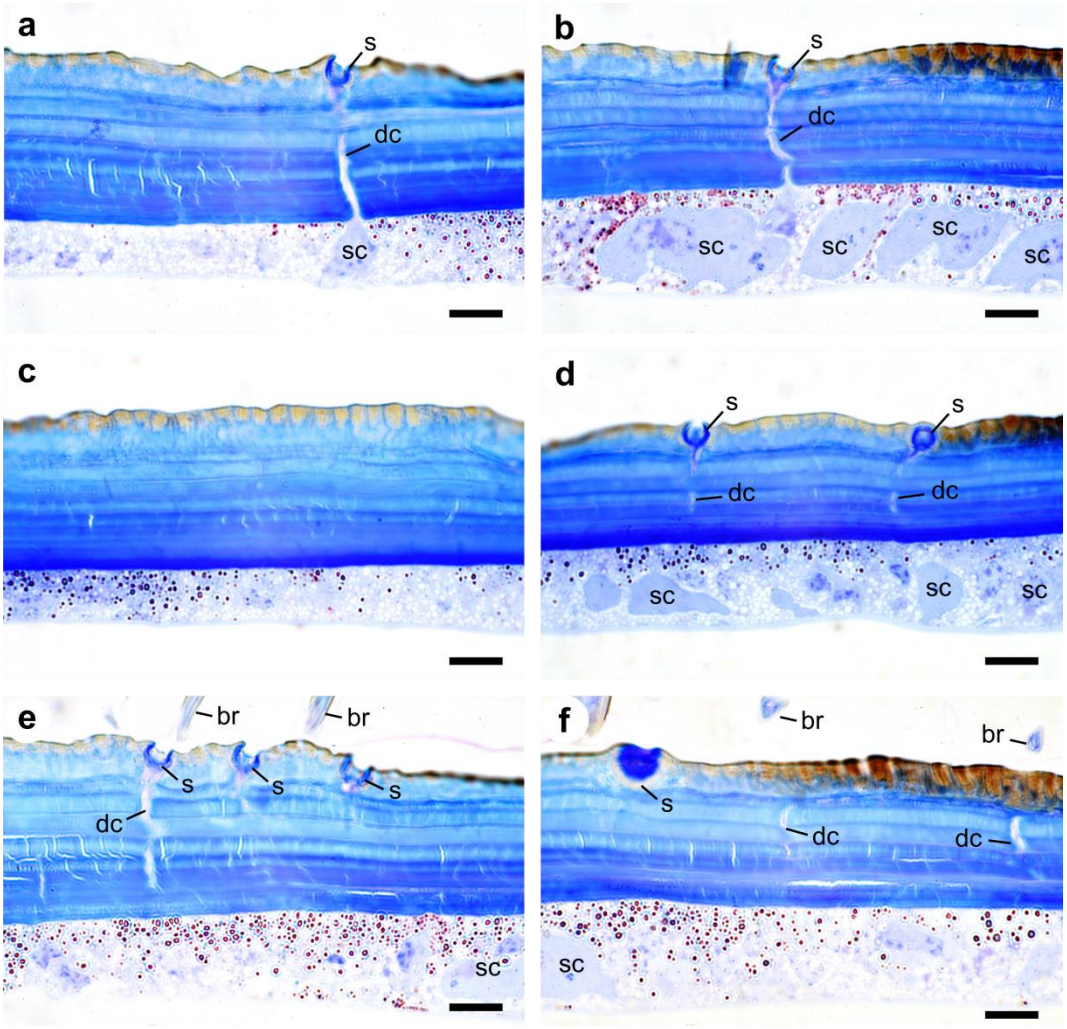

Fig. 4.3 Semithin sections through the anterior micro-structured area (*aMSA*) of a fifth sternite of *L. occidentalis* stained with toluidine-blue/ borax. Relative position and orientation of sections **a) – f)** is indicated by yellow lines (online version in color) and corresponding letters in Figure 4.2b. In a), b), and d) – f) various sections through hair mechanoreceptors (sensilla trichodea) are visible; br: bristle of hair mechanoreceptor; dc: dendritic canal; s: socket of mechanosensory hair; sc: soma of sensory cell. Bars: 10µm.

Generally, the abdominal sternites are densely covered with hairs. At the region between the stigmata and the groups of trichobothria, however, this covering becomes less dense and less regular. In this region also numerous little cuticular pores with a diameter of about 1.5µm (cf. inset in Fig. 4.2a) were found. Pores only became visible, if cleaning in chloroform was omitted and the critical-point drying method was used. Preliminary measurements on the IV sternite revealed an irregular distribution of the pores with a density of about 300 – 1000 pores/mm^2. Pores were not detectable at regions densely covered with hairs and were also missing at two distinct areas, subsequently referred to as micro-structured areas (*MSA*s). These *MSAs* exhibit a more or less roundish shape and are further characterized by a scaly surface structure (Fig. 4.2b, c). The *MSA* situated at the anterior margin (*aMSA*) of each

sternite (Fig. 4.2a, b) was identified as the one that has been described by Takács et al. (2009) as IR-receptive area. Its distinct surface structure, however, is limited to the outermost cuticular layers (cf. Fig. 4.3c). More profound structural specializations of the three-dimensional shape of the cuticle (e.g. indentations or bulges extending deeper into the cuticle) within the *aMSAs* were not found. A further difference between the *aMSA* and normal abdominal cuticle apart from the surface structure, if any, was a slight increase in cuticle thickness at the *aMSA* (cf. Fig. 4.A1). In general, the restrictions and the surface structure of the *aMSA*s revealed considerable variations throughout the different sternites and between different individuals. Posterior from the *aMSA*, about in the middle of each half of a sternite (Fig. 4.2a), we found a second *MSA* (*pMSA*), which looked very similar with respect to its size, shape and surface structure (cf. Fig. 4.2c).

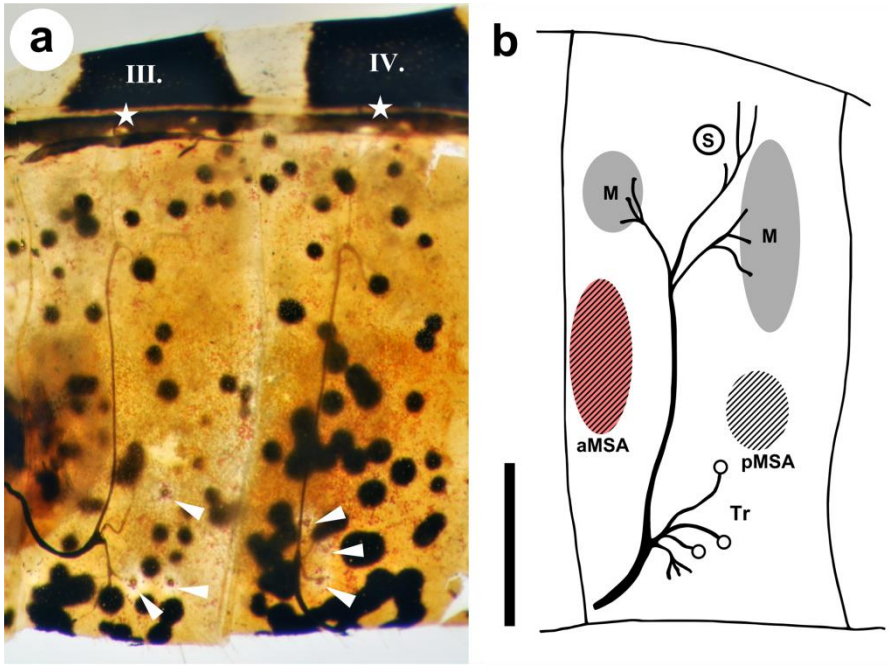

Fig. 4.4 a) Interior view of the right half of a third (III) and fourth (IV) abdominal sternite of *L. occidentalis*. Nervous tissue stained black after axonal filling with 0.2M $CoCl_2$ and subsequent sulphide precipitation. Asterisks and arrowheads indicate positions of stigmata (covered by connexivum) and trichobothria respectively. **b)** Schematic drawing of the innervation of the right half of an abdominal sternite of *L. occidentalis* reconstructed on the analysis of 27 backfills. *aMSA* = anterior micro-structured area (striped area colored in red; cf. Fig. 4.2b) represents the 'IR-receptive region' proposed by Takács et al. (2009). M = dorsoventral muscles (gray areas); *pMSA* = posterior micro-structured area (striped area; cf. Fig. 4.2c); S = stigma; Tr = trichobothria (marked by small circles). Orientation in both subfigures: left = cranial, right = caudal, bottom = medial, top = lateral. Bar: 1mm.

4.4.2 Innervation of the ventral abdomen

Each half of the abdominal sternites (III.–VII.) is innervated by a prominent main nerve branching off from the respective abdominal ganglion. Basally some smaller nerves already branch off, innervating the trichobothria while the main nerve extends laterally into the periphery (Fig. 4.4). In the last third of its way to the lateral margin of the sternite the nerve branches again to innervate two dorsoventral muscles; one muscle is located anterior to the stigma, the second one posterior to the stigma (Fig. 4.4b). Distally from the stigma the nerve ramifies again and from this point on could not be tracked further. Nerves branching off from the main nerve between the trichobothria and the two dorsoventral muscles, which might innervate the *aMSA* or the *pMSA* indicated in *Figure 4.4b* by striped areas, could not be tracked in our preparations.

4.4.3 Histology of epithelia below the anterior micro-structured cuticular areas

Combined series of semi- and ultrathin sections through several *aMSA*s revealed a distinctive layer of underlying epithelial cells (Figs. 4.3, 4.5, and 4.6). In the regions densely covered with hairs, directly bordering on the *aMSA* (Fig. 4.2b), we could identify hair mechanoreceptors (sensilla trichodea) by the existence of cuticular socket-structures and dendritic canals extending through the cuticle down to the appendant somata of the sensory cells (Fig. 4.3a, b, d - f). Directly below the *aMSA*s, however, we could not find any evidence for an innervation (Figs. 4.3c and 4.5) that might point to a sensory function of the area.

However, our findings clearly prove the existence of glandular cells (Figs. 4.5 and 4.6). According to the classification scheme of Noirot and Quennedey (1974), at least two different types of epidermal glandular cells were identified. Most frequently Class 1 glandular cells were found, which were characterized by large accumulations of intracellular vacuoles with a diameter of 0.5 – 1.5 µm and small electron dense granules (diameter: 50 – 250 nm). Many vacuoles appear empty in the gland cells shown in Figures 4.5 and 4.6, because most probably their former lipid content was washed out during the embedding process by propylenoxide. Dark staining of the content of other vacuoles also points to lipid compounds, which were stained black by osmium (Figs. 4.3 and 4.5). Two different subsets of Class 1 gland cells could be identified histologically by a lucid or a dark cytoplasm, respectively (cf. Figs 4.5b, e, 4.6a). Surrounded by the numerous Class 1 gland cells, we also found Class 3 glandular cells recognizable by inner reservoirs (cavities) filled with dark secretions (Figs. 4.5c, d and 4.6a). The cavities of the glandular cells and probably also the lumina of their associated ductule-

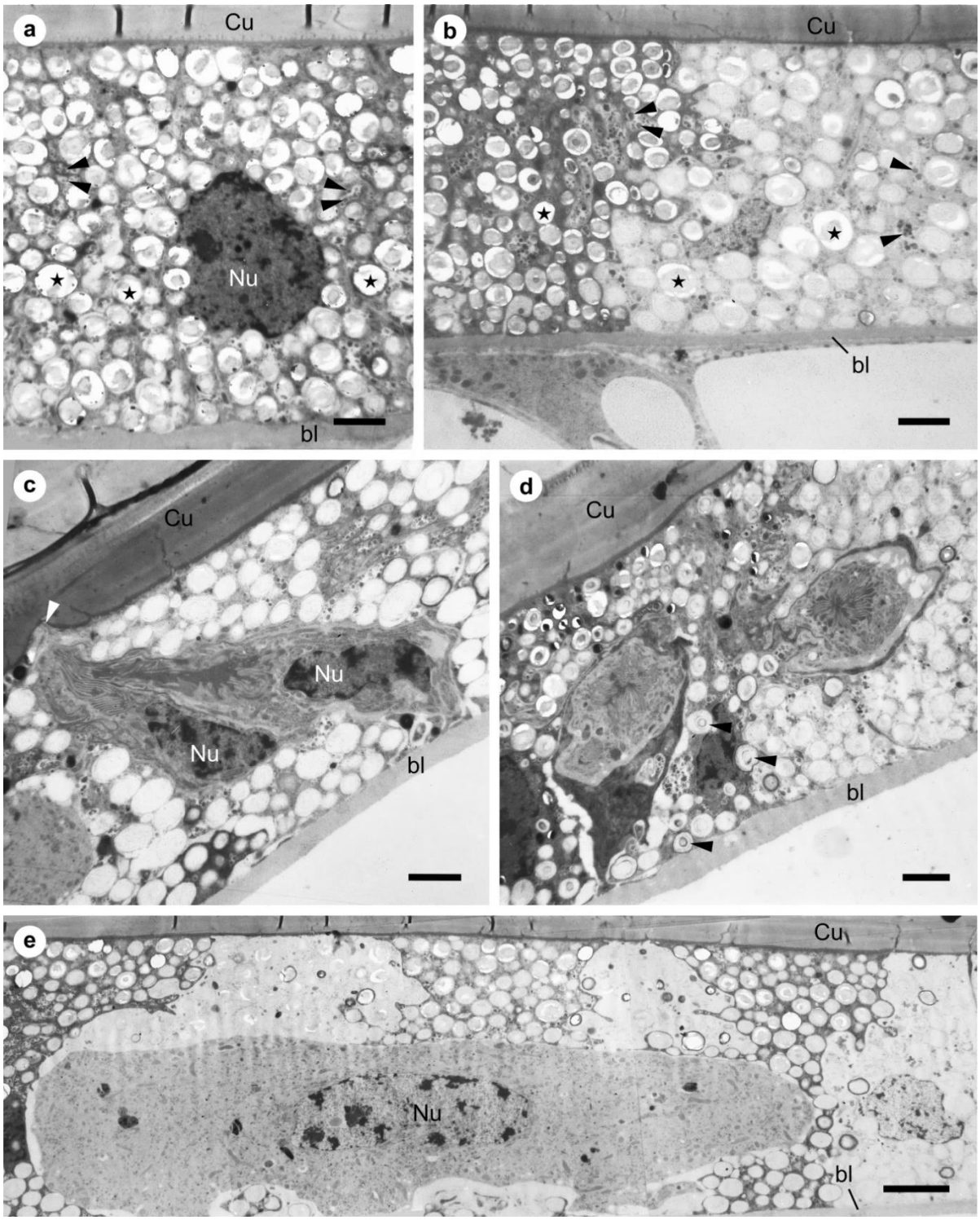

Fig. 4.5 TEM-micrographs through the fifth abdominal sternite of *L. occidentalis* at the *aMSA* showing different types of epidermal glandular cells (classified after Noirot and Quennedey (1974)). Abbreviations: bl = basal lamina; Cu = cuticle; Nu = nucleus. **a)**, **b)** Class 1 gland cells densely packed with vacuoles (asterisks); electron dense granules (arrowheads) are abundant. Bars: 2µm. **c)** Longitudinal section through two single Class 3 gland cells surrounded by highly vacuolated tissue. Arrowhead indicates basal part of a cuticular ductule. Note the extensive mazelike foldings of the cell membranes bordering the inner reservoir of the gland cells. Bar: 2µm. **d)** Cross-sectional profile of two single Class 3 gland cells. Inner reservoirs are well visible by dark staining of their content. Arrowheads mark lamellar bodies in neighboring Class 1 gland cells. Bar: 2µm. **e)** Large cell type, most probably representing an oenocyte or Class 2 glandular cell, surrounded by Class 1 gland cells as shown in a) and b). Bar: 4µm.

cells are bordered by numerous microvilli (Figs. 4.5c, d and 4.6a). The ductules extend through the cuticle and open to the exterior most probably by the small pores shown in the inset in Figure 4.2a. The third cell type we found, apparently a Class 2 glandular cell or oenocyte, is clearly distinguishable from the others. It is represented by a relative large elongated cell that has no direct contact with the cuticle and the basal lamina (Figs. 4.5e and 4.6b) but is embedded in the surrounding Class 1 glandular cells. Finally it has to be emphasized that the three types of gland cells were not restricted to the *aMSA* but were also found about 1 mm into medial direction (Fig. 4.6) and also extending over the segment boundaries in anterior-posterior direction.

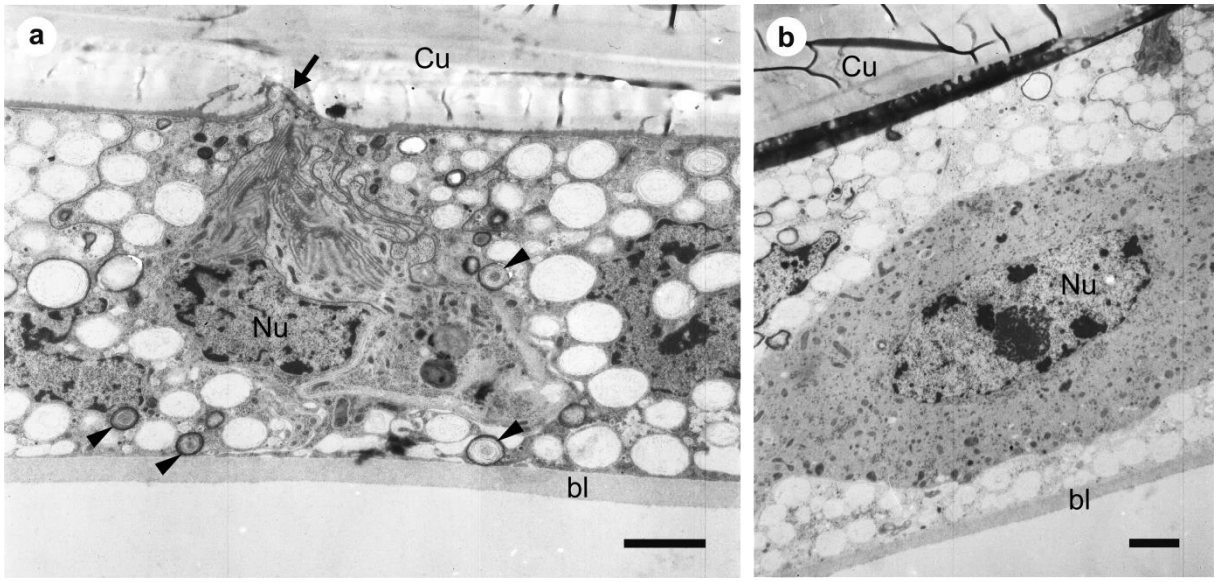

Fig. 4.6 TEM-micrographs through the fifth abdominal sternite of *L. occidentalis* at a reference region, i.e. about 1mm distant from the *aMSA* in medial direction (cf. Fig. 4.2a), showing different types of epidermal glandular cells (classified according to Noirot and Quennedey (1974)). Abbreviations: bl = basal lamina; Cu = cuticle; Nu = nucleus. **a)** Longitudinal section through a single Class 3 gland cell with basal part of its cuticular ductule (arrow) surrounded by highly vacuolated Class 1 gland cells. Arrowheads indicate lamellar bodies. Bar: 2µm. **b)** Large cell type, probably representing an oenocyte or Class 2 glandular cell, surrounded by Class 1 glands (cf. Fig. 4.5). Bar: 2µm.

4.5 Discussion

4.5.1 Extra-antennal IR-receptors in insects

Based on morphological as well as on electrophysiological investigations, extra-antennal IR-receptors that have developed in addition to thermoreceptors located on the antennae (Altner and Loftus, 1985), so far have been established only in a small group of so-called pyrophilous

insects, which approach ongoing forest fires: namely jewel beetles of the genus *Melanophila* (Evans, 1966; Schmitz et al., 2007), the Australian "fire-beetle" *Merimna atrata* (Schmitz et al., 2001) (both from the family Buprestidae), the "little ash beetle" *Acanthocnemus nigricans* (Kreiss et al., 2007) (family Acanthocnemidae), and very few pyrophilous members of the bark bug genus *Aradus* (Schmitz et al., 2010) (family Aradidae). The pyrophilous insects most probably use their IR-receptors for the detection of fires and subsequently for orientation on freshly burnt areas. A look onto the IR-receptors reveals that receptors can be very different from each other. Whereas in *Melanophila* beetles and in pyrophilous *Aradus* species thoracic IR-sensilla consist of little cuticular spherules, which are innervated by ciliary mechanoreceptors (Vondran et al., 1995; Schmitz et al., 2010), the abdominal IR-receptors of the Australian "fire-beetle" *Merimna atrata* consist of shallow round depressions of the cuticle, characterized by a honeycomb-like micro-structure (Schmitz, H. et al., 2000). From inside the IR-absorbing areas are innervated by a prominent sensory complex consisting of a thermosensitive multipolar neuron and a small chordotonal organ (Schmitz et al., 2001; Schneider and Schmitz, 2013). Again different from these two types of receptors are the prothoracic IR-organs of *Acanthocnemus nigricans*. Each organ consists of a little cuticular disc held in place by a small stalk over an air filled cavity. On its anterior surface the disc contains about 90 tiny sensilla which most probably act as thermoreceptors (Kreiss et al., 2005; Kreiss et al., 2007).

According to their external appearance the *MSA*s on the abdominal sternites of *L. occidentalis* in some respects are similar to the abdominal IR-receptors of *Merimna atrata*. On the outer surface of the *Merimna* IR-organ as well as on the surface of the *MSA*s in *L. occidentalis,* no cuticular apparatuses of sensilla except those of surrounding hair mechanoreceptors (sensilla trichodea) are visible. Thus it has to be requested that internal sensory neurons are in contact with the absorbing cuticular surfaces of the receptors. In contrast to the IR-receptors of *Merimna atrata* (Schmitz et al., 2001; Schneider and Schmitz, 2013) sensory neurons could not be found in the proposed abdominal IR-receptors of *L. occidentalis*. Our neuroanatomical staining protocol did not allow depiction of single hair mechanoreceptors that surround the *MSA*s in *L. occidentalis*. Most probably the single axons running to the somata of the mechanosensory cells were too small to take up sufficient amounts of dye. On the other hand it was no problem to stain the larger somata of the trichobothria and - with the same protocol - the neurons of the sensory complex in the IR-organ of *Merimna atrata* (Schneider and

Schmitz, 2013). Furthermore, the systematic histological search for neurons of sensory cells under the cuticle of the *aMSA* yielded no results.

4.5.2 Cone detection by *Leptoglossus occidentalis*

Like other phytophagous insects *L. occidentalis* has to find a specific plant part, a cone. Commonly, the detection of leaves, flowers or fruits is accomplished by visual or olfactory cues. Because *L. occidentalis* is diurnal, both cues can be used and a need for additional IR-sensory capabilities deems not mandatory. For close range orientation it may be possible that *L. occidentalis* also uses thermal cues to walk towards a cone heated up by the sun. Like in blood-sucking triatomine bugs (Lazzari and Núñez, 1989; Insausti et al., 1999; Guerenstein and Lazzari, 2009; Lorenzo Figueiras et al., 2013) sensitive antennal thermoreceptors could enable an approach by walking towards a warm object from a distance of some centimeters. However, in the paper of Takács et al. (2009) it is implied that bugs use their proposed abdominal IR-receptors also in flight for long range detection of cones from distances of many meters (Takács et al., 2009). This, however, would require a sensitivity by far exceeding that of the sophisticated IR-organs of rattlesnakes. With its pinhole camera-like IR-organs *Crotalus atrox* is able to detect a mouse - roughly having the same size as a cone - up to a distance of 1 m. An outstanding sensitivity of only 3 - 4 µW/cm² of the uncooled IR-receptors is necessary to allow this sensory performance (Ebert and Westhoff, 2006). Even if the *MSA*s on the abdomen of *L. occidentalis* would be richly innervated by highly sensitive thermoreceptors, it seems questionable if this uncooled IR-receptor could outperform such sensitivity without any special adaptations of its radiation absorbing cuticle, e.g. i) a radiation concentrating apparatus, ii) elaborate protection against wind convection, iii) reduction of the thermal mass, etc.

4.5.3 Possible function of the gland cells and suggestions for future work

The missing innervation precludes a sensory function of the *aMSA*s in *L. occidentalis*. Most probably, the nerve fibre shown in *figure 6* of Takács et al. (2009) is a part of the main nerve running into the periphery (cf. Fig. 4.4b of this paper) and, therefore, is not suitable to demonstrate an innervation of the *aMSA*. Our histological results clearly point to the existence of extended glandular fields under most of the abdominal cuticle, including both *MSA*s. These fields mostly consist of Class 1 epidermal glandular cells, which are often involved in

pheromone production (Noirot and Quennedey, 1974). In our study two morphologically distinct types were found as revealed by differential staining of their cytoplasm (cf. Figs. 4.5b, e). In principle, secretions of Class 1 gland cells reach the cuticular surface via pore canals and epicuticular filaments. Based on our morphological results it is not possible to decide which specific kinds of secretions are produced by the gland cells. As mentioned in the *Results* the possible leaching of the vacuolar content by propylenoxide and the dark staining of other vacuoles after osmium treatment indicate a lipidic content in the Class 1 cells. This is in line with a production of lipophilic hydrocarbons which are used as pheromone components in many insects; e. g. short-chain aldehydes have been described to function as aggregation pheromones in pentatomid bugs (Chapman, 1998). All bugs used in our study were caught in fall when insects sought sheltered places for overwintering. Aggregations of more than 2,000 *L. occidentalis* had been observed at overwintering sites and there is strong evidence that aggregation is mediated by pheromones (Blatt, 1994).

Class 3 gland cells are easily identifiable by a duct extending through the cuticle and an inner cavity confined by microvilli (cf. Figs. 4.5c, d, 4.6a). Class 3 cells usually produce the cement on the outer surface of the cuticle and also are involved in the synthesis of defensive secretions (Chapman, 1998).

The oenocytes found between the other gland cells often are responsible for lipid processing and detoxification (Martins and Ramalho-Ortigão, 2012). Hydrocarbons and other lipids synthesized are used to constitute the epicuticle. The lipids can be transported directly to the epidermal cells by cytoplasmatic strands (Wigglesworth, 1988). This may explain that we did not found appreciable accumulations of vacuoles in the oenocytes: a need for prolonged storage in intracellular vacuoles appears not necessary.

Thus we conclude that most probably, also the a*MSA* serve for the distribution of glandular secretions. This is supported by the finding that a second, more posterior field with the same surface structuring was found on each abdominal segment.

As mentioned in the *Introduction* the extracellular electrophysiological recording presented in the paper of Takács et al. (2009) reveals no action potentials. The large but rather slow inverted ON / OFF changes of the potential may have been caused by thermo-mechanical effects at the contact zone between the cuticle and the electrode. According to the behavioral data presented in the paper of Takács et al. (2009) the covering of the *aMSA*s with acrylic paint impaired the ability of bugs to approach an IR-source. This may have several reasons,

one of which is that the procedure may have irritated and / or inactivated the bugs so that they were not longer motivated to approach a thermal source.

In summary the behavioral experiments described in the paper of Takács et al. (2009) demonstrate that *L. occidentalis* is able to use thermal cues for orientation. However, to what extend IR-radiation is used for this capability has to be further investigated by additional experiments carefully excluding any transfer of heat by convection of air. For this purpose slightly cooled filters should be interposed between the IR-source and the bug like it has been done in the study of Schmitz et al. (2000) with the bloodsucking bug *Rhodnius prolixus*. Furthermore it has to be prevented that IR-radiation is absorbed by parts of the experimental setup accessible for the bug. IR-absorption e.g. by plastic material will inevitably cause generation of warm air at the surfaces of the material. If it should turn out that *L. occidentalis* can perceive weak IR-radiation, an approach should be made to identify and characterize the antennal thermoreceptors allowing IR-reception in the near field.

4.6 Acknowledgements

We thank Monika Goldammer, Rolf Kaiser, Heinz Löhrer, Sabine Nöbel, Robert Schallehn and Frank Täufer for the supply of animals. We are grateful to the NEES Institute of the University of Bonn for the use of the scanning electron microscope and to Hans-Jürgen Ensikat for technical support. We are indebted to Horst Bleckmann for his interest in our work and for providing lab space. Supported by a grant of the DFG to H. S.

4.7 Literature

Altman, J. S. and Tyrer, N. M. (1980). Filling selected neurons with cobalt through cut axons. in *Neuroanatomical techniques: insect nervous system*. N. J. Strausfeld and T. A. Miller. New York, Springer**:** 373-402.

Altner, H. and Loftus, R. (1985). "Ultrastructure and function of insect thermo-and hygroreceptors." *Annual Review of Entomology* **30**(1): 273-295.

Anderson, T. F. (1951). "Techniques for the preservation of three-dimensional structure in preparing specimens for the electron microscope." *Transactions of the New York Academy of Sciences* **13**(4 Series II): 130-134.

Bates, S. L., Borden, J. H., Kermode, A. R. and Bennett, R. G. (2000). "Impact of *Leptoglossus occidentalis* (Hemiptera: Coreidae) on Douglas-fir seed production." *Journal of Economic Entomology* **93**(5): 1444-1451.

Bernard, J. (1974), "Etude électrophysiologique de récepteurs impliqués dans l'orientation vers l'hote et dans l'acte hématophage chez une Hémiptère: *Triatoma infestans*", University of Rennes

Blatt, S. (1994). "An unusually large aggregation of the western conifer seed bug, *Leptoglossus occidentalis* (Hemiptera: Coreidae), in a man-made structure." *Journal of the Entomological Society of British Columbia* **91**.

Budzier, H. and Gerlach, G. (2010). "Thermische Infrarotsensoren: Grundlagen für Anwender". Weinheim, Germany, Wiley-VCH Verlag.

Chapman, R. F. (1998). "The insects: structure and function". Cambridge, UK, Cambridge University Press.

Davis, N. T. (1982). "Improved methods for cobalt filling and silver intensification of insect motor neurons." *Biotechnic & Histochemistry* **57**(4): 239-244.

Ebert, J. and Westhoff, G. (2006). "Behavioural examination of the infrared sensitivity of rattlesnakes (*Crotalus atrox*)." *Journal of Comparative Physiology A* **192**(9): 941-947.

Evans, W. G. (1966). "Morphology of the infrared sense organ of *Melanophila acuminata* (Buprestidae: Coleoptera)." *Annals of the Entomological Society of America* **59**: 873-877.

Guerenstein, P. G. and Lazzari, C. R. (2009). "Host-seeking: How triatomines acquire and make use of information to find blood." *Acta Tropica* **110**: 148 - 158.

Honegger, H. W. and Schürmann, F. W. (1975). "Cobalt sulphide staining of optic fibres in the brain of the cricket *Gryllus campestris*." *Cell and Tissue Research* **159**(2): 213-225.

Howard, C. V. and Reed, M. G. (1998). "Unbiased stereology: three-dimensional measurement in microscopy". Oxford, BIOS Scientific.

Insausti, T. C., Lazzari, C. R. and Campanucci, V. A. (1999). Neurobiology of behaviour. A: morphology of the nervous system and sense organs. in *Atlas of Chagas Disease Vectors in America*. C. e. al. Rio de Janeiro, Editoria Fiocruz. **3:** 1017-1051.

Koerber, T. W. (1963). "*Leptoglossus occidentalis* (Hemiptera, Coreidae), a newly discovered pest of coniferous seed." *Annals of the Entomological Society of America* **56**(2): 229-234.

Kreiss, E.-J., Schmitz, A. and Schmitz, H. (2005). "Morphology of the prothoracic discs and associated sensilla of *Acanthocnemus nigricans* (Coleoptera, Acanthocnemidae)." *Arthropod Structure & Development* **34**(4): 419-428.

Kreiss, E.-J., Schmitz, H. and Gebhardt, M. (2007). "Electrophysiological characterisation of the infrared organ of the Australian "Little Ash Beetle" *Acanthocnemus nigricans* (Coleoptera, Acanthocnemidae)." *Journal of Comparative Physiology. A, Neuroethology, Sensory, Neural, and Behavioral Physiology* **193**(7): 729-739.

Lazzari, C. and Wicklein, M. (1994). "The cave-like sense organ in the antennae of Triatominae bugs." *Memórias do Instituto Oswaldo Cruz* **89**(4): 643-648.

Lazzari, C. R. and Núñez, J. (1989). "The response to radiant heat and the estimation of the temperature of distant sources in *Triatoma infestans*." *Journal of insect physiology* **35**(6): 525-529.

Lorenzo Figueiras, A. N., Flores, G. B. and Lazzari, C. R. (2013). "The role of antennae in the thermopreference and biting rersponse of haematophagous bugs." *Journal of insect physiology* **59**(12).

Luft, J. H. (1961). "Improvements in epoxy resin embedding methods." *The Journal of biophysical and biochemical cytology* **9**(2): 409-414.

Martins, G. and Ramalho-Ortigão, J. (2012). "Oenocytes in insects." *Invertebrate Survival Journal* **9**: 139-152.

Mason, C. A. (1973). "New features of the brain-retrocerebral neuroendocrine complex of the locust *Schistocerca* (Scudder)." *Cell and Tissue Research* **141**(1): 19-32.

Mesce, K. A., Amos, T. M. and Clough, S. M. (1993). "A light insensitive method for contrast enhancement of insect neurons filled with a cobalt-lysine complex." *Biotechnic & Histochemistry* **68**(4): 222.

Mücke, A. and Lakes-Harlan, R. (1995). "Central projections of sensory cells of the midleg of the locust, *Schistocerca gregaria*." *Cell and Tissue Research* **280**(2): 391-400.

Mücke, A. and Lakes, R. (1988). "Das Experiment: Darstellung von Sinnesorganen und peripheren Nerven bei Insekten." *Biologie in unserer Zeit* **18**(2): 58-61.

Noirot, C. and Quennedey, A. (1974). "Fine structure of insect epidermal glands." *Annual Review of Entomology* **19**(1): 61-80.

Pitman, R. M., Tweedle, C. D. and Cohen, M. J. (1972). "Branching of central neurons: intracellular cobalt injection for light and electron microscopy." *Science* **176**(4033): 412-414.

Sandeman, D. and Okajima, A. (1973). "Statocyst-induced eye movements in the crab *Scylla serrata*." *Journal of experimental biology* **59**(1): 17-38.

Schmitz, A., Gebhardt, M. and Schmitz, H. (2008). "Microfluidic photomechanic infrared receptors in a pyrophilous flat bug." *Naturwissenschaften* **95**(5): 455-460.

Schmitz, A., Schätzel, H. and Schmitz, H. (2010). "Distribution and functional morphology of photomechanic infrared sensilla in flat bugs of the genus *Aradus* (Heteroptera, Aradidae)." *Arthropod Structure & Development* **39**(1): 17-25.

Schmitz, A., Sehrbrock, A. and Schmitz, H. (2007). "The analysis of the mechanosensory origin of the infrared sensilla in *Melanophila acuminata* (Coeloptera; Buprestidae) adduces new insight into the transduction mechanism." *Arthropod Structure & Development* **36**(3): 291-303.

Schmitz, H., Bleckmann, H. and Mürtz, M. (1997). "Infrared detection in a beetle." *Nature* **386**(6627): 773-774.

Schmitz, H., Schmitz, A. and Bleckmann, H. (2000). "A new type of infrared organ in the Australian" fire-beetle" *Merimna atrata* (Coleoptera: Buprestidae)." *Naturwissenschaften* **87**(12): 542-545.

Schmitz, H., Schmitz, A. and Bleckmann, H. (2001). "Morphology of a thermosensitive multipolar neuron in the infrared organ of *Merimna atrata* (Coleoptera, Buprestidae)." *Arthropod Structure & Development* **30**(2): 99-111.

Schmitz, H., Trenner, S., Hofmann, M. H. and Bleckmann, H. (2000). "The ability of *Rhodnius prolixus* (Hemiptera; Reduviidae) to approach a thermal source solely by its infrared radiation." *Journal of insect physiology* **46**(5): 745-751.

Schneider, E. S. and Schmitz, H. (2013). "Bimodal innervation of the infrared organ of *Merimna atrata* (Coleoptera, Buprestidae) by thermo- and mechanosensory units." *Arthropod Structure & Development* **42**(2): 135-142.

Strong, W. B., Bates, S. L. and Stoehr, M. U. (2001). "Feeding by *Leptoglossus occidentalis* (Hemiptera: Coreidae) reduces seed set in lodgepole pine (Pinaceae)." *The Canadian Entomologist* **133**(06): 857-865.

Takács, S., Bottomley, H., Andreller, I., Zaradnik, T., Schwarz, J., Bennett, R., Strong, W. and Gries, G. (2009). "Infrared radiation from hot cones on cool conifers attracts seed-feeding insects." *Proceedings of the Royal Society B: Biological Sciences* **276**(1657): 649.

Trimmer, B. A. and Weeks, J. C. (1989). "Effects of nicotinic and muscarinic agents on an identified motoneurone and its direct afferent inputs in larval *Manduca sexta*." *Journal of experimental biology* **144**(1): 303.

Vincent, J. D. (1990). "Fundamentals of infrared detector operation and testing", John Wiley & Sons.

Vondran, T., Apel, K. H. and Schmitz, H. (1995). "The infrared receptor of *Melanophila acuminata* De Geer (Coleoptera: Buprestidae): ultrastructural study of a unique insect thermoreceptor and its possible descent from a hair mechanoreceptor." *Tissue and Cell* **27**(6): 645-658.

Wagner, E. (1966). "Die Tierwelt Deutschlands und der angrenzenden Meeresteile. Wanzen oder Heteropteren. I. Pentatomorpha.". Jena, Fischer Verlag.

Wigglesworth, V. B. (1988). "The source of lipids and polyphenols for the insect cuticle: the role of fat body, oenocytes and oenocytoids." *Tissue and Cell* **20**(6): 919-932.

4.8 Appendix

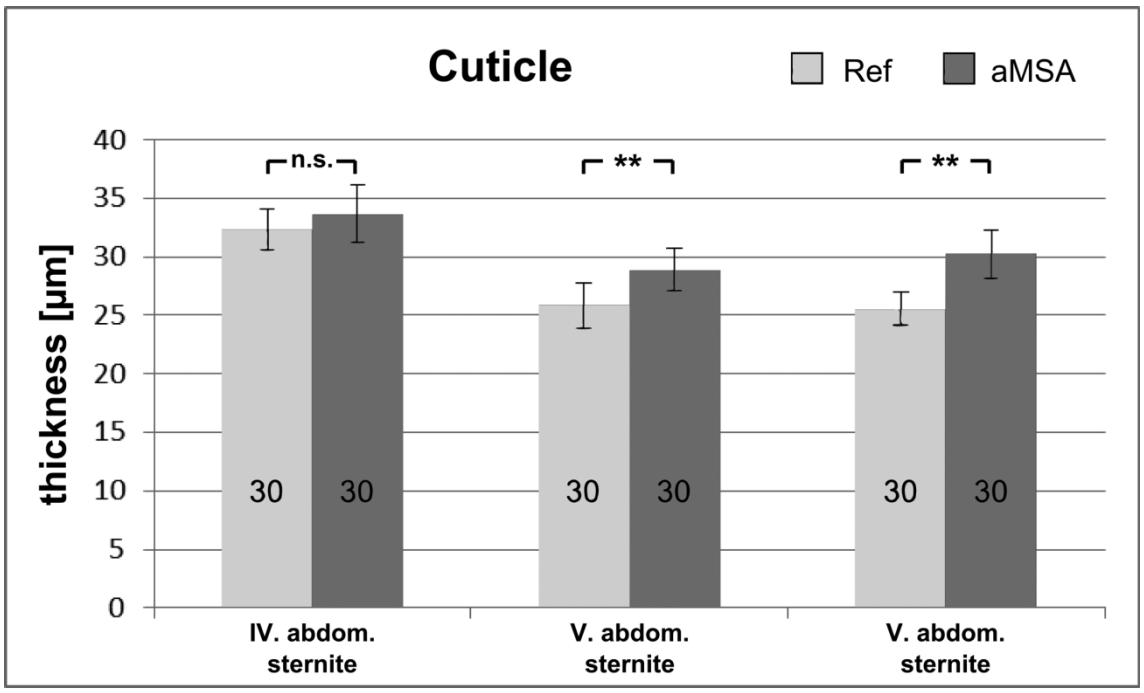

Fig. 4.A1 Cuticular thickness of the anterior micro-structured area (*aMSA*) and of unspecialized cuticle (*Ref*) several hundred micrometers in medial direction measured on three individual sternites. For both regions (*aMSA* and *Ref*) six different sections were analyzed. From each section five measurements were taken respectively. To achieve unbiased measurements we used a systematic random sampling method (cf. Howard and Reed 1998). Bars and whiskers indicate mean values and standard deviations respectively. Numbers of measurements are given within the bars. Significant differences (analyzed with Mann-Whitney U-test) are marked with asterisks (**≙ $p < 0.01$).

Kapitel 5

Diskussion

5.1 IR-Rezeption bei *Leptoglossus occidentalis*

Die in Kapitel 4 dargestellten Ergebnisse widerlegen eine IR-rezeptive Funktion der von Takács et al. (2009) beschriebenen abdominalen Strukturen bei der Amerikanischen Kiefernwanze, *Leptoglossus occidentalis*. Das Vorkommen von extra-antennalen IR-Rezeptoren innerhalb der Klasse der Insekten bleibt somit nach derzeitigem Erkenntnisstand beschränkt auf Spezies mit pyrophiler Lebensweise. Takács et al. (2009) hatten postuliert, dass *L. occidentalis* die von ihrer Nahrungsquelle (Zapfen verschiedener Koniferen-Arten) emittierte IR-Strahlung zur Fernortung verwendet. Da jedoch entsprechend dem Stefan-Boltzmann-Gesetz (vgl. Gleichung 1.2, Abschnitt 1.1) die emittierte Strahlungsleistung einer IR-Quelle proportional zur vierten Potenz ihrer Oberflächentemperatur (Einheit Kelvin) und näherungsweise umgekehrt proportional zur zweiten Potenz ihres Abstandes ist, scheint eine Eignung zur Fernortung generell unwahrscheinlich; insbesondere in Anbetracht der geringen Temperatur und Oberfläche eines Zapfens als IR-Quelle. Geht man z.B. von einem Zapfen mit einer Fläche von 5 x 10 cm, einer Temperatur von 40°C und einer Emissivität von 0,97 (entsprechend eines herkömmlichen Schwarzkörperstrahlers) aus, so könnte eine Wanze, die im Besitz von IR-Rezeptoren mit einer Sensitivität von 50 $W \cdot m^{-2}$ ist (entsprechend der in elektrophysiologischen Untersuchungen ermittelten Sensitivität eines IR-Sensillums von *Melanophila acuminata* (Schmitz and Bleckmann, 1998; Schmitz and Trenner, 2003)), diesen maximal nur auf eine Entfernung von 23 cm wahrnehmen. Hierzu müssten jedoch bereits spezielle Anpassungen der IR-absorbierenden Cuticula vorhanden sein, die eine entsprechende Sensitivität ermöglichen. Anpassungen könnten z.B. eine Reduktion der thermischen Masse, Schutz vor Windkonvektion, oder die Ausbildung eines strahlungs-konzentrierenden Apparates sein (vgl. Abschnitt 1.3.2).

Ein mittelgroßer Waldbrand mit einer Fläche von 100.000 m^2 und einer Temperatur von 700°C hingegen wäre unter gleichen Bedingungen auf eine Entfernung von bis zu 10 km detektierbar. Insbesondere die im Vergleich zu verschiedenen Nahrungsquellen, wie z.B. Zapfen (bei *L. occidentalis*) oder endothermen Beutetieren (bei Schlangen, vgl. Abschnitt 1.3.1.1), relativ große Fläche von Waldbränden stellt somit eine Grundvoraussetzung für die potentielle Fernortung durch IR-rezeptive Tiere dar.

Das Vorhandensein von IR-Rezeptoren zur Ferndetektion von Zapfen bei *L. occidentalis*, an anderer Stelle als der in der vorliegenden Arbeit Untersuchten (abdominale Sternite), erscheint daher ebenfalls unwahrscheinlich.

Bei tagaktiven Insektenspezies wird das Auffinden und die Auswahl der Wirtspflanzen vor allem durch olfaktorische und visuelle Reize bestimmt (Finch and Collier, 2000). Es ist anzunehmen, dass Ähnliches auch für *L. occidentalis* gilt. Anders als bei pyrophilen Spezies, liegt bei *L. occidentalis* kein ersichtlicher Vorteil durch die Nutzung von IR-Reizen und die Entstehung entsprechender Rezeptoren beim Auffinden von Zapfen vor.

Es soll an dieser Stelle darauf hingewiesen werden, dass *L. occidentalis* durchaus über empfindliche Thermorezeptoren an Antennen oder Beinen verfügen mag, durch die selbst geringe Temperaturunterschiede wahrgenommen werden können. Ob diese jedoch am Auffinden der Zapfen als Nahrungsquelle beteiligt sind, bleibt aus oben dargestellten Gründen ebenfalls fraglich.

5.2 Bimodale Innervation des IR-Organs von *Merimna atrata*

In der vorliegenden Arbeit wurden die abdominalen IR-Rezeptoren von *Merimna atrata* mit Hilfe von histologischen, neuroanatomischen und materialwissenschaftlichen Methoden funktionsmorphologisch charakterisiert. Die Ergebnisse belegen eine Innervation des IR-Organs durch eine zusätzliche mechanosensitive Einheit in Form eines Chordotonalorgans, bestehend aus zwei einzelnen mononematischen, monodynalen Skolopidien. Finite Element Simulationen zu den ermittelten thermomechanischen Eigenschaften der absorbierenden Fläche bestätigen, basierend auf den in Kapitel 2 und 3 dargestellten Ergebnissen zur Geometrie und den gemessenen Materialeigenschaften der abdominalen Cuticula, eine potentielle Funktion der Skolopidien als photomechanische IR-Rezeptoren. Darüber hinaus deuten die Ergebnisse der Simulationen an, dass ein möglicher Vorteil der zusätzlichen Innervation durch das Chordotonalorgan, neben dem multipolaren Neuron, nicht in einer gesteigerten Sensitivität des IR-Organs zu suchen ist, sondern z.B. in der Erweiterung des Dynamikbereichs oder einem höheren zeitlichen Auflösungsvermögen (siehe Abschnitt 3.5.3). Eine Erweiterung des Dynamikbereichs könnte z.B. aus einer größeren Steigung der Rezeptorkennlinie resultieren. Das würde bedeuten, dass innerhalb eines bestimmten Intensitätsbereichs eintreffender IR-Strahlung, geringere Temperaturunterschiede vom Rezeptor aufgelöst werden könnten. Gleichzeitig könnte auch die Lage des Sättigungs-bereichs einer der beiden sensorischen Einheiten zu höheren Intensitäten hin verschoben sein.

Ob das Chordotonalorgan jedoch tatsächlich an der IR-Rezeption beteiligt ist und welches seine speziellen Antwortcharakteristika sind, kann nur über elektrophysiologische Ableitungen eindeutig bestimmt werden. Dies sollte das Ziel zukünftiger Arbeiten darstellen.

5.3 Technisches Potential des IR-Organs von *Merimna atrata*

Die Natur ist nicht nur Ideengeber, sondern besitzt mit geschätzt rund 10 Millionen unterschiedlichen Arten (Barthlott et al., 2014) (davon über 90% unbekannt, (Mora et al., 2011)) einen schier unermesslichen Fundus an raffinierten und ausgefeilten Lösungen für verschiedenste Aufgaben. Diese Lösungen sind entsprechend der jeweiligen Anforderungen des Lebensraumes an den Organismus in höchstem Maße optimiert, da sie i.d.R. bereits einen Jahrmillionen andauernden Entwicklungsprozess vollzogen haben.

Die Wissenschaftsdisziplin der Bionik hat dieses Potential erkannt und versucht, die Funktionsprinzipien biologischer Vorbilder zu verstehen, zu abstrahieren und in die Technik zu übertragen.

Die Funktionsprinzipien der beiden im IR-Organ von *Merimna atrata* vorhandenen sensorischen Einheiten entsprechen im Falle des thermosensitiven multipolaren Neurons, dem eines Mikrobolometers (vgl. Abschnitt 1.2.2.3) und im Falle des Chordotonalorgans, dem photo- oder thermomechanischen Prinzip wie es z.B. in Mikrotragarm-Sensoren (vgl. Abschnitt 1.2.2.5) Verwendung findet. Bezüglich des Letzteren kann die Cuticula der absorbierenden Fläche aufgrund ihres Aufbaus aus verschiedenen Schichten mit unterschiedlichen thermischen Ausdehnungskoeffizienten als Bimorph angesehen werden. Die Kombination aus der dreidimensionalen Gestalt und der Anordnung der einzelnen Cuticula-Schichten der absorbierenden Fläche führt bei Erwärmung zu einer mechanischen Deformation in eine bestimmte Vorzugsrichtung (vgl. Abschnitt 3.4.3). Diese thermomechanische Deformation der Cuticula wird schließlich vom darunter liegenden Chordotonalorgan, einem Mechanorezeptor, gemessen.

Beide Funktionsprinzipien sind bekannt und werden in abstrahierter Form in der technischen IR-Sensorik bereits erfolgreich angewandt. Die technologische Entwicklung beider Sensor-Typen ist dabei bereits so weit fortgeschritten, dass diese höhere Sensitivitäten erreichen, als für das IR-Organ von *Merimna atrata*, mit einer Sensitivität von 400 $W \cdot m^{-2}$ und einem noch wahrzunehmenden Temperaturunterschied von 0,08 K (Schmitz and Trenner, 2003), beschrieben wurde. Mikrobolometer können nach aktuellem Stand der Technik Temperatur-

unterschiede von 0,03 K, Mikrotragarmsensoren sogar von 0,005 K auflösen (Amantea et al., 1997; Rogalski, 2011, 2012).

Das Potential zur Entwicklung eines IR-Sensors mit neuartigem Funktionsprinzip, sowie zur Optimierung existenter technischer Sensoren hinsichtlich einer reinen Sensitivitätssteigerung, auf Grundlage der im IR-Organ von *Merimna atrata* vorliegenden Funktionsprinzipien, ist nach derzeitigem Ergebnisstand nicht gegeben. Dies ist zumindest der Fall hinsichtlich der isolierten Betrachtung der einzelnen Sensor-Typen.

Eine potentielle Verbesserung technischer Sensoren könnte sich jedoch möglicherweise aus der bimodalen Innervation des IR-Organs von *Merimna* ableiten lassen, z.B. durch Integration zweier unterschiedlicher Sensor-Typen mit verschiedenen Antwortcharakteristika zu einem Sensor-System. Vorteile könnten sich dann nicht nur durch die bloße Addition der Sensorantworten (größerer Dynamikbereich, kürzere Ansprechzeiten, höhere Ausfallsicherheit) ergeben, sondern eventuell auch durch die Art und Weise der Integration beider Signale innerhalb des Sensor-Systems (Filtereigenschaften).

Hierzu sind jedoch weiterführende Untersuchungen am IR-Organ von *Merimna atrata* notwendig. Für zukünftige Arbeiten wird daher zunächst vorgeschlagen, die Antworteigenschaften des Chordotonalorgans bei der IR-Rezeption mit Hilfe elektrophysiologischer Ableitungen detailliert zu charakterisieren.

5.4 Literatur

Amantea, R., Knoedler, C., Pantuso, F. P., Patel, V., Sauer, D. J. and Tower, J. R. (1997). "Uncooled IR imager with 5mK NEDT". *Infrared Technology and Applications XXIII (Proceedings of SPIE), Orlando, Florida, USA.*

Barthlott, W., Erdelen, W. R. and Rafiqpoor, M. D. (2014). Biodiversity and technical innovations: bionics. in *Concepts and values in biodiversity*. D. Lanzerath and M. Friele. London & New York, Routledge**:** 300-315.

Finch, S. and Collier, R. H. (2000). "Host-plant selection by insects – a theory based on 'appropriate/inappropriate landings' by pest insects of cruciferous plants." *Entomologia Experimentalis et Applicata* **96**(2): 91-102.

Mora, C., Tittensor, D. P., Adl, S., Simpson, A. G. B. and Worm, B. (2011). "How many species are there on earth and in the ocean?" *PLoS Biology* **9**(8): e1001127.

Rogalski, A. (2011). "Infrared detectors". Boca Raton, Florida, USA, CRC Press.

Rogalski, A. (2012). "History of infrared detectors." *Opto-Electronics Review* **20**(3): 279-308.

Schmitz, H. and Bleckmann, H. (1998). "The photomechanic infrared receptor for the detection of forest fires in the beetle *Melanophila acuminata* (Coleoptera: Buprestidae)." *Journal of Comparative Physiology A* **182**(5): 647-657.

Schmitz, H. and Trenner, S. (2003). "Electrophysiological characterization of the multipolar thermoreceptors in the" fire-beetle" *Merimna atrata* and comparison with the infrared sensilla of *Melanophila acuminata* (both Coleoptera, Buprestidae)." *Journal of Comparative Physiology. A, Neuroethology, Sensory, Neural, and Behavioral Physiology* **189**(9): 715-722.

Takács, S., Bottomley, H., Andreller, I., Zaradnik, T., Schwarz, J., Bennett, R., Strong, W. and Gries, G. (2009). "Infrared radiation from hot cones on cool conifers attracts seed-feeding insects." *Proceedings of the Royal Society B: Biological Sciences* **276**(1657): 649.

Abkürzungsverzeichnis

ac - attachment cell
AFM - atomic force microscope
as - air sack
aMSA - anterior micro-structured area
bl - basal lamina
br - bristle
c - dendritic cilium
CAD - computer-aided design
cap - scolopale cap
CNS - central nervous system
CO - chordotonal organ
cr - ciliary rootlets
CT - computed tomography
Cu - cuticle
dbb - distal basal body
dc - dendritic canal
DIS - dendritic inner segment
DOS - dendritic outer segment
el - epidermal layer
FIR - fernes Infrarot
gc - glial cell
gm - granular material
IR - Infrarot, *engl.: infrared*
LM - light microscopy
LTTD - lateraler absteigender Ast und Kern des Nervus trigeminus
M - dorsoventral muscles
MIR - mittleres Infrarot
MN - multipolar neuron
MNSo - soma of multipolar neuron
MSA - micro-structured area
N - nerve
NI - nanoindentation
NIR - nahes Infrarot
Nu - nucleus
pbb - proximal basal body
pMSA - posterior micro-structured area
REM - Rasterelektronenmikroskop
ROI - region of interest
s - socket
S - stigma
sc - soma of sensory cell
Sc - scolopidium
ScC - scolopale cell
ScR - scolopale rods
ScS - scolopale space
SCSo - soma of the sensory cell of a scolopidium
SEM - scanning electron microscope
SNR - signal to noise ratio
SPM - scanning probe microscopy
TDM - terminale dendritische Masse, *engl.: terminal dendritic mass*
TEM - transmission electron micro-scope
TNM - terminale Nervenmasse, *engl.: terminal nerve mass*
tr - trichobothria
UFIR - ultra-fernes Infrarot
ZNS - zentrales Nervensystem
2D/3D - two-/ three-dimensional

Abbildungsverzeichnis

Tabellenverzeichnis

Danksagung

An erster Stelle danke ich PD Dr. Helmut Schmitz für seine hervorragende Betreuung und fortwährende Unterstützung. Für anregende Diskussion, konstruktive Kritik, Vermittlung von Wissen und Erfahrung, eine ausgezeichnete Anleitung zum selbständigen wissenschaftlichen Arbeiten, und kontinuierliches Vertrauen in meine Fähigkeiten, bin ich überaus dankbar.

Prof. Dr. Horst Bleckmann danke ich für die freundliche Aufnahme in seiner Abteilung, für die Breitstellung von Labor und Gerätschaften, und für die Übernahme des Korreferats.

Der Deutschen Forschungsgemeinschaft (DFG) danke ich für die Förderung (SCHM1161/10-1) der vorliegenden Arbeit.

Bei PD Dr. Anke Schmitz bedanke ich mich für die Einweisung in vielfältige Methoden, ihre Unterstützung und ihren fachlichen Rat.

Thilo Kahl und Dr. David Klocke danke ich für Diskussion, Unterstützung bei technischen und fachlichen Fragestellungen, für eine angenehme Arbeitsatmosphäre und eine schöne Zeit.

Der Abteilung Vergleichende Sinnes- und Neurobiologie (Prof. Bleckmann) und seinen Mitarbeitern danke ich für Diskussion, Hilfsbereitschaft und eine spannende Zeit.

Für die Möglichkeit der Nutzung des Rasterelektronenmikroskops am Nees-Institut der Universität Bonn danke ich Prof. emer. Dr. Wilhelm Barthlott und Prof. Dr. Maximilian Weigend. Hans-Jürgen Ensikat gebührt besonderer Dank für die technische Unterstützung während dieser Zeit.

Ganz besonders möchte ich mich bei meiner Familie für ihren Rückhalt, ihre grenzenlose Unterstützung und ihre Liebe bedanken.

Erklärung

Hiermit versichere ich an Eides statt, die vorliegende Arbeit persönlich, selbständig und ohne Benutzung anderer als der angegebenen Hilfsmittel angefertigt zu haben. Die aus anderen Quellen direkt oder indirekt übernommenen Daten und Konzepte wurden unter Angabe der Quelle kenntlich gemacht. Für die Erstellung dieser Arbeit oder die Gelegenheit zur Promotion wurde keine fremde (entgeltliche) Hilfe in Anspruch genommen. Die vorliegende Arbeit wurde nicht an anderer Stelle als Dissertation eingereicht. Sie wurde auszugsweise an den nachstehend aufgeführten Quellen veröffentlicht:

- **Schneider, E. S. and Schmitz, H.** (2014). "Thermomechanical properties of the stimulus transducing cuticle in the infrared organ of *Merimna atrata* (Coleoptera, Buprestidae)." *Journal of Morphology* **275**(9): 991-1003. DOI: 10.1002/jmor.20276.

- **Kahl, T., Bousack, H., Schneider, E. S. and Schmitz, H.** (2014). "Infrared receptors of pyrophilous jewel beetles as model for new infrared sensors." *Sensor Review* **34**(1): 123 - 134. DOI: 10.1108/SR-10-2012-716.

- **Schneider, E. S. and Schmitz, H.** (2013). "Bimodal innervation of the infrared organ of *Merimna atrata* (Coleoptera, Buprestidae) by thermo- and mechanosensory units." *Arthropod Structure & Development* **42**(2): 135-142. DOI: 10.1016/j.asd.2012.11.001.

Bonn, den